TRANSIENT BOILER HEAT EXCHANGER THERMAL BEHAVIOUR ANALYSIS

Prepared by:

Excellent Zibhekele Gwebu

GWBEXC001

Department of Mechanical Engineering

University of Cape Town

Supervisor:

Professor Louis Jestin

September 2014

Submitted to the Department of Mechanical Engineering at the University of Cape Town in partial fulfilment of the academic requirements for a Master's of Science degree in Mechanical Engineering

Key Words: Aging, conduction, transient, thermal stresses, analytical, numerical, Flownex.

Abstract

Coal fired power plants that were built in the past four decades are aging. The main aging mechanisms are creep and thermal fatigue. Creep results from the high temperatures at which the components operate. Thermal fatigue is due to thermal stresses and these stresses result from temperature gradients within the material. Cycling of these thermal stresses accelerate the creep in a process called creep-fatigue aging. The boiler and its final heat exchangers and headers are the main components that are affected by these mechanisms. The aging of these components results in high maintenance costs, reduction of the plant reliability and availability, and contribute to increased safety risks for the plant and personnel. Therefore, there is a need to understand the steady state and dynamic behaviour of the components of these plants in order to predict the stresses that the material experience.

This report discusses an investigation to the possibility of modelling the thermal dynamic behaviour of typical boiler heat exchanger components which have to withstand the highest temperature of a Pulverised Fuel Rankine cycle power plant. Thus, illuminating the issues that need to be addressed in modelling such heat exchangers. Modelling approaches of heat exchangers are systematically presented, starting with the use of exact analytical solutions. This is followed by the application of finite volume numerical method. Finishing off with the use of the Flownex software.

The exact analytical solutions are used to characterise the transient temperature distribution in solid materials with simplified heat transfer, highlighting the dependence of the solutions on the Fourier number and Biot number. These solutions are further used to calculate thermal stresses generated in the material, illustrating the relationship between thermal stresses and temperature gradients. Furthermore, a finite volume solution is applied to modelling an infinitely long tube. It is illustrated that for transient conduction heat transfer problems, the solution depends on both physical space discretisation and time-wise discretisation. The numerical solution is verified against the exact analytical solution.

Finally, the Flownex software is used to illustrate the issues that need to be addressed when modelling the transient behaviour of a heat exchanger. For this purpose only the average area discretisation scheme is used since it allows for any generic solid structure to be modelled, provided that the appropriate level of discretization is applied. The Flownex modelling starts by modelling transient conduction heat transfer within an infinitely long tube. The Flownex solution is verified against the finite volume numerical solution. The Flownex solution depends on thickness discretisation, especially for thick cylindrical components. Finite tubes are also modelled on Flownex including axial discretisation and layout simplification of the tubes. Flownex is also used to model a heat exchanger bundle using two methods; a tube by tube method and a method that involves the combination of all

the tubes into one tube. The product of the thermal resistance and the capacitance of the system governs the transient simulations for both methods.

Declaration

I, *Excellent Zibhekele Gwebu*, hereby declare the work contained in this dissertation to be my own. All information which has been gained from various journal articles, text books or other sources has been referenced accordingly. I have not allowed, and will not allow, anyone to copy my work with the intention of passing it off as their own work or part thereof.

Signed by candidate

_____ _____

Signature Date

Acknowledgements

Firstly, I would like to thank my supervisor Professor Louis Jestin for his assistance, support and guidance throughout the course of this project.

Secondly, I would like to thank my co-supervisor Dr Wim Fuls for his assistance and follow up throughout the course of this project.

I would also like to thank Professor Pieter Rousseau who consistently helped me throughout the project despite the fact that I was not directly being supervised by him. I respect him for that.

I would like thank the relevant parties in the Eskom Energy Efficiency Specialisation centre, the National Research Foundation (NRF) and the University of Cape Town for funding my project.

I would also like to appreciate my colleagues at the Eskom Energy Efficiency Specialisation centre for a welcoming and awesome working environment.

Lastly, I would like to dedicate this work to my family and my close friends for their consistent support and love. They have been my strength throughout the project.

Table of Contents

List of Figures

List of Tables

Nomenclature

General symbols

$\dot{E}$	Rate of energy	V	Volume
q	Heat conducted	h	Heat transfer coefficient or enthalpy
$\dot{q}$	Energy generated per unit volume	a	Radius for a rod or inner radius for a tube
c	Specific heat of the material	b	Outer radius for a tube
k	Thermal conductivity	$\dot{m}$	Mass flow rate
t	time	v	Velocity
T	Temperature	$\dot{Q}$	Heat input
r	Radius or radial coordinate direction	$\dot{W}$	Work done
x, y, z	Cartesian coordinate system	g	Acceleration due to gravity
L	Thickness or length	z	Elevation from the ground
A	Area	C	Capacitance
P	Perimeter/ circumference	R	Resistance

Greek symbols

ρ	Density	λ	Eigenvalue
κ	Thermal diffusivity	τ	Time constant, dimensionless time
θ	Theta direction on cylindrical coordinates	α	Integration weighting factor

Acronyms and Abbreviations

PF	Pulverised fuel	FDM	Finite difference method
PV	Photovoltics	FEM	Finite element method
LTI	Linear time invariant	FVM	Finite volume method
Bi	Biot number	SA	Surface Area
Fo	Fourier number	OD	Outer diameter
HT	Heat transfer element	ID	Inner diameter
IPCM	Implicit Pressure Correction Method	ODE	Ordinary differential equation
RKTD	Runge Kutta method with Trapezoidal Damping	CM	Condition Monitoring

Subscripts and superscripts

st	Stored	or	Original
gen	Generated	0	Initial or total
i	Initial or inlet	∞	Stream or infinity
e	Exit	s	Surface
a	Radius for a rod or inner radius for a tube	d	Dimensionless
th	Thermal		

Functions and Series

$J_0(x)$	Bessel function of the zero order
$J_1(x)$	Bessel function of order one
$Y_0(x)$	Bessel function of the second kind zero order
$V_0(x)$	Specific combination of the Bessel series

Chapter 1

1 Introduction

Fossil fuel power plants which were built in the last four decades produce more than 70% of the global electricity, with pulverised coal boilers connected to a water-steam Rankine Cycle producing about 40% of the global electricity. These plants are aging. The key aging mechanisms affecting the large coal fired plants are creep, thermal fatigue and the combined creep-fatigue interactions in the high pressure and high temperature components of these plants. This situation is worsening when these large plants are operated in swinging modes e.g. to complement the electricity produced by less predictable renewable energy sources that are connected to the grid. Aging of these plants results in high maintenance costs, reduces their reliability and availability, and leads to safety risks as well.

1.1 General project background

A pulverised fuel (PF) power plant is a system that generates electricity from burning pulverised coal. During combustion, the energy of the coal is first transferred into flue gas that then transfers its thermal energy to the water-steam circuit to run a Rankine cycle. The system contains several components which include the boiler, turbine, generator, condenser, feedwater heaters, cooling tower, pumps, valves and pipes, as shown in Figure 1-1 and are all connected together by the water-steam circuit.

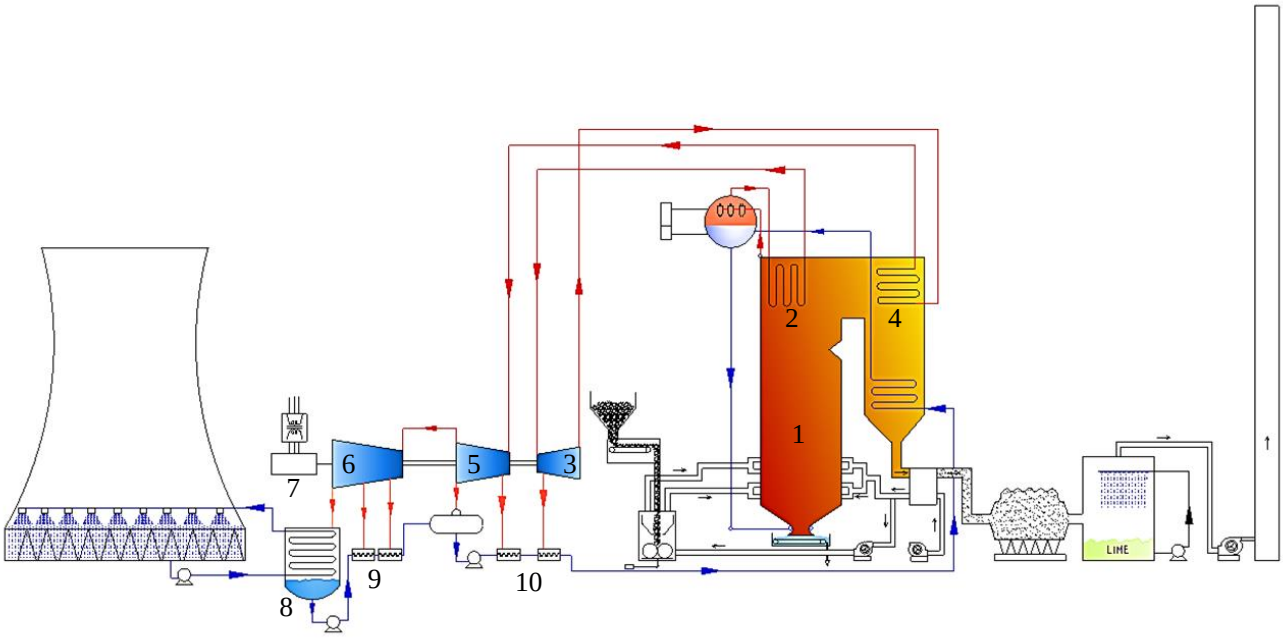

Figure 1-1. Complete Coal fired Power Station with a Drum Boiler Schematic Diagram [1].

Figure 1-1 shows that combustion takes place in the furnace, 1, and the hot flue gas from the combustion heats pressurised water through heat exchangers to produce steam and superheat the steam, 2. The superheated steam is ducted from the boiler to the high pressure turbine, 3, where it expands and rotate the turbine. The steam or water-steam mixture at the exhaust of the high pressure turbine is ducted back to the boiler to be reheated, 4. Thereafter, this reheated steam is ducted to the intermediate pressure turbine, 5, then the low pressure turbine, 6. Usually, the turbines are connected to the same shaft which rotates and turns a generator, 7, which produces electricity. The water-steam mixture at the turbine exhaust is transferred to the condenser, 8, to fully condense the steam to water. Then the water is pumped back to the boiler to complete a cycle. Along the way back to the boiler, feedwater heaters, 9 & 10, use bled steam from the turbines to raise the temperature of the boiler feedwater and so increase the whole cycle efficiency. In the process, the amount of steam having to be condensed in the main condenser is reduced, hence less heat is ejected to the atmosphere. However, this has to be a trade-off with the work done by the turbine, since bleeding steam from the turbines reduces the amount of steam that passes the later stages of the turbine.

From a water-steam thermo-hydraulic circulation perspective, there are two types of industrial boilers, namely; the drum boiler, shown in Figure 1-1 and the once-through or tower type boiler. The drum boiler design is for subcritical conditions, yet the once through boiler is for high water-steam pressure conditions typically above 170 bar. The once through boiler can operate both under subcritical and supercritical conditions allowing pressure to change with the boiler load. The boilers consist of a number of different water-steam heat exchangers. These heat exchangers transfer the heat energy from the combustion gases into the water-steam circuit, hence heating water, vaporising it to steam and superheating the steam. In the transfer of energy, the hot flue gas passes over numerous boiler tubes, transferring heat by radiation and convection to these water-steam tubes. The heat is conducted through the walls of these tubes into the water-steam side.

The tubes of the heat exchanger are connected to inlets and outlets headers with the length of the tubes making passes within the flue gas pass in the boiler, hence increasing the surface area for heat transfer. These tubes and their associated headers, which distribute or collect the water or steam from many individual tubes, work under pressures of tens MPa from the inside of the tubes. All these tubes and headers are so called “boiler pressure parts” and are made of relatively thick steel materials. These “pressure parts” tube thicknesses are usually in the range of a few tens in percentage compare to the internal tube diameter. The thick components (headers/ tubes) of the pressure parts are very sensitive to thermal stresses and creep, especially those that operate at high temperatures in the final superheater and reheater before steam goes to the turbine. Thermal stresses and creep reduce the lifespan of the components.

1.2 Problem statement

Most of the large coal fired power plants which are still in operation presently were built in the last four decades. In these plants, the high temperature components in the boiler, i.e. the final superheaters, reheaters and their respective headers and control valves as well as the steam pipes and high temperature parts of the turbines, have been designed according to international codes to operate under creep for 200,000 hours at the design operating temperature and pressure. From a creep point of view only, a large part of this worldwide power production fleet has already exhausted its lifespan, while thermal fatigue that has not really been taken into account in the design of the components is adding up to the creep aging mechanism. Aging is more accelerated when thermal fatigue cycling is present, in a mechanism known as creep-fatigue aging. Thermal fatigue cycling results from continuous cycling of thermal stresses. Continuous dynamic operation of the plants initiates temperature transients that causes these thermal stresses. Unfortunately, nowadays the situation is worsening when these large coal fired plants are operated in intermittent or cycling modes. This is required to complement the electricity produced by less predictable renewable energy sources such as wind and photo-voltaics or, as the case in France for example, to complement hydro and nuclear power generation which operates mainly as base load plants.

These aging mechanisms could result in plant safety issues as these components contain high energy steam at high pressure and temperatures in excess of 150 bar and 550 °C, respectively. To ensure safety from these high energy components, inspections and controls have to be in place during outages to make a decision in agreement with authorities whether to allow operation of the plant to resume for a next period or not. This maintenance method is based on risk assessment and management strategy which comes at a cost that has to be traded off with the cost of component replacement.

Therefore, there is a need to understand the steady state and dynamic behaviour of the components of these plants to predict the local stresses that the materials experience. The most critical operating condition is the local temperature of the material which is driven by the flow conditions that the material experience on both sides of the component, i.e. the velocity, temperature and pressure. This understanding should at least help in identifying the most critical areas to be inspected and controlled, and to optimise the operation and control of these plants to keep the stresses within acceptable limits. It should also help in designing new plants with less stresses for the most critical components either in steady state or dynamic operation. This is achieved through understanding and modelling of the thermal dynamic behaviour of the different components such as heat exchangers, pumps, valves, etc. that make up the power plant. As the water-steam dynamic behaviour is transmitted from one component to the

next, the global dynamic behaviour of the plant with its own instrumentation and control system can only be studied by coupling all these components together within a numerical process flow model.

1.3 Project objectives

The overall objective of this project is to investigate the possibility of modelling the dynamic thermal behaviour of typical boiler heat exchangers encountered in coal-fired power plants and to illustrate the issues that need to be addressed when modelling such heat exchangers in the Flownex thermal-fluid process modelling software tool. This aims to serve as a basis for future studies on boiler heat exchanger modelling using Flownex, under which a full power plant simulator will be developed to serve as an engineering tool.

The enabling objectives of the project are:

1. **A review and application of known exact analytical solutions of simplified transient conduction heat transfer problems.** These will illustrate the fundamentals of the transient conduction problems and serve as reference cases for further work.
2. **Preliminary calculations of thermal stresses in these simplified problems** based on the transient conduction results to demonstrate the relationship between temperature gradients and thermal stresses.
3. **The development and application of finite volume numerical solutions of transient conduction heat transfer problems** to account for more complex boundary conditions for which exact solutions cannot be obtained or are harder to obtain. The results of the numerical solutions are to be verified against the exact solutions for simplified cases and will also serve as reference cases for the Flownex solutions.
4. **Application of the Flownex software for solving problems** that approximate real boiler heat exchangers with finite lengths, complex layouts, etc. This entails investigating and comparing different levels of simplifications and illuminating the issues that need to be addressed in modelling such heat exchangers. For this purpose only the average area discretisation scheme is used since it allows for any generic solid structure to be modelled, provided that the appropriate level of discretization is applied.

1.4 Project scope

The scope of this project is to demonstrate the approach for modelling typical boiler heat exchangers using Flownex and highlighting aspects that need to be looked at during the modelling process. Only the average area discretisation scheme is used since it allows for any generic solid structure to be modelled, provided that the appropriate level of discretization is applied.

The purpose of this study is **not** to produce a final validated model of any specific heat exchanger or a generic model that can be used to model any boiler heat exchanger, or to provide an exhaustive analysis of sources of errors encountered in numerical modelling techniques.

1.5 Format of the Report

In the subsequent chapter, an understanding of the problem is established through the practical background and modelling approaches to transient conduction heat transfer analysis are briefly introduced. In chapter 3, a brief survey on previous work done in modelling heat exchangers and the errors that rises in the modelling is presented. Chapter 4 presents the application of the boiler heat exchanger modelling approaches, highlighting the issues that need to be addressed during the modelling process. Chapter 5 presents the conclusions of the study and future work that will follow this study.

Chapter 2

2 Practical and theoretical background

In this chapter, practical and theoretical background of this project is presented. The practical background focuses on the boiler design, operation, maintenance and aging mechanism, thus clarifying the problem being analysed. The theoretical background presents analyses of transient conduction heat transfer using available literature as an introductory step to solving transient heat conduction into solids.

2.1 Practical background

The components operating at the highest temperature and pressure in a PF power plant are the final heat exchangers within the boiler. The temperature transient behaviour of these components depend on the overall plant system behaviour. Therefore, in order to understand the dynamic behaviour of these components, the overall design of the plant components and their operation needs to be understood. However, this work only focus on the boiler side, especially the high temperature and high pressure heat exchangers, keeping in mind that the other components including pipes, pumps, steam turbines, valves, etc. are also being studied in parallel by other researchers in the Eskom Energy Efficiency Specialisation centre at the University of Cape Town.

2.1.1 The boiler – an overview

The steam generator, normally called a boiler, is a system in the coal fired power plant that generates pressurised steam from heating pressurised water using hot flue gas from the combustion of coal, as explained in chapter 1. The boiler water-steam circuit comprises of various heat exchangers which are systematically arranged such that heat from combustion products is efficiently absorbed to produce steam at the rated temperature, pressure and flow rate. These heat exchangers are sequentially arranged along the flue gas path from the furnace waterwalls (evaporators), the superheaters and reheaters, the economizer and finally the air heater [2]. In addition, the boiler's water-steam circuit also include systems for water-steam separation and steam temperature controls. The system for water-steam separation is usually made of cyclones situated in the boiler drum for the drum-type boilers and the water-steam separator for once through boilers. Attemperators are used to control the superheater and reheater steam outlet temperature by injection of water in the steam. Other technologies can also be used to control the steam temperature such as flue gas by-pass or burner tilting.

The boiler can either have two passes from a flue gas side: one pass from the bottom of the furnace to the top and the other from the top to the bottom also called the back-pass, as shown in Figure 1-1

(chapter 1) or be a tower type as shown in Figure 2-1. There are several other external components which are attached to the boiler, connecting it to the whole power unit. These include the mills, the fans, the burners, a network of connecting pipes and ducts, and the support structures. The mills pulverise the coal which ignites at the burner tip, then the flame propagates into the boiler. In most of the recent technologies, the whole boiler is hanging from the top support structures allowing for expansion and contraction of the metal that makes up the boiler pressure parts during heating up and cooling down of the boiler system.

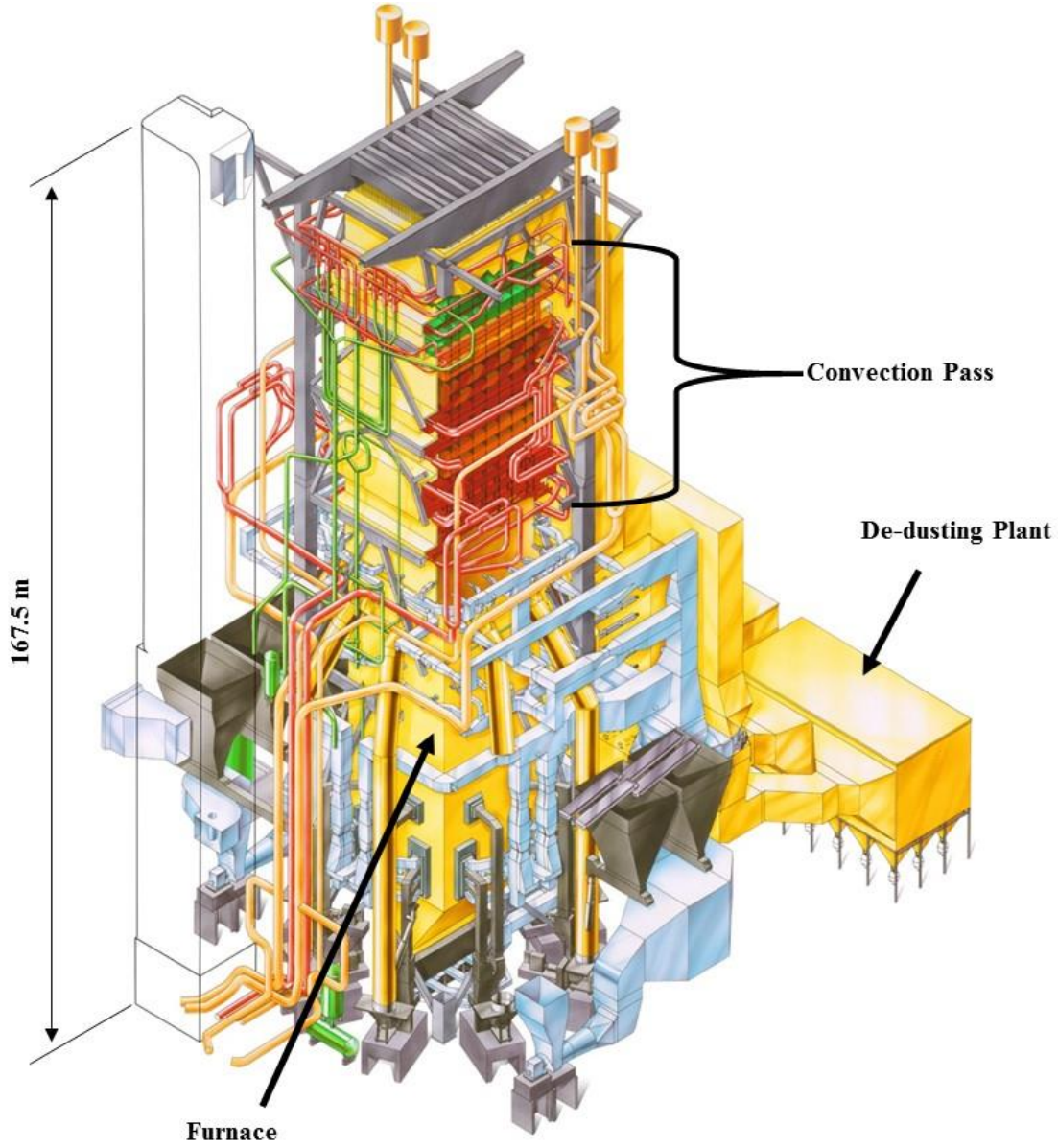

Figure 2-1. A 3D schematic view of a tower - type once through 1000MWe Class boiler system, lignite fired boiler, Niederaussem Power Plant.

From a heat transfer point of view, the boiler consists of two general sections: the furnace and the convection pass [2]. The furnace is a large volume enclosed by water-cooled wall tubes which are connected together. Combustion occurs inside the furnace and the combustion products (flue gas) are

cooled to an appropriate furnace exit gas temperature (FEGT) through exchanging heat with the furnace walls. The boiler should be sized in such a way that the FEGT is lower than the ash melting temperature, in order to prevent slagging on the heat exchangers located in the flue gas path downstream of the furnace. The convection pass consists of tube bundles which make up the superheater, reheater and economiser as shown in Figure 2-1. The temperature of the flue gas decreases as the gas moves towards the exit of the boiler.

The boiler is the part of the Rankine cycle that generates steam, starting at the economiser inlet until the outlet of the superheaters and the reheaters. The contribution of the boiler system to the Rankine cycle is represented by the Temperature vs entropy graph shown in Figure 2-2, for both subcritical and supercritical pressure conditions. As it can be seen in Figure 2-2, for supercritical plants the reheat should be at a higher pressure to avoid the formation of water droplets at the outlet of the high pressure turbine, as that would quickly erode the steam turbine blades.

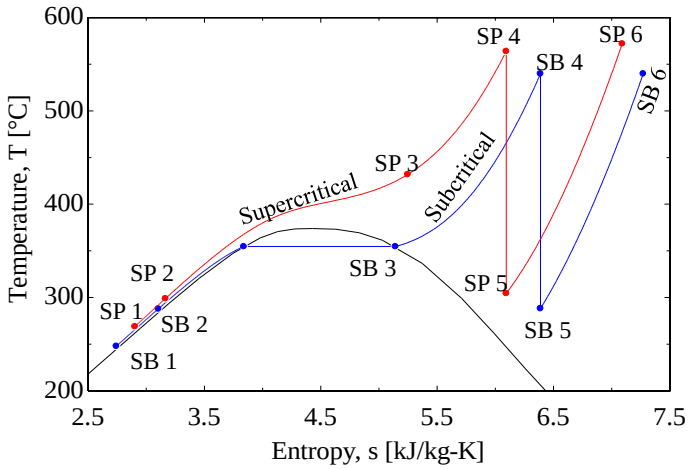

Key:

SP: Supercritical	SB: Subcritical
SP 1: Economizer inlet	SB 1: Economizer inlet
SP 2: Economizer outlet	SB 2: Economizer outlet
SP 3: Superheater inlet	SB 3: Superheater inlet
SP 4: HP Turbine inlet	SB 4: HP Turbine inlet
SP 5: Reheater inlet	SB 5: Reheater inlet
SP 6: Reheater outlet	SB 6: Reheater outlet

Figure 2-2. T-s diagram for a boiler for both subcritical and supercritical pressure conditions.

After exiting the furnace at the FEGT, the flue gas enters the convection pass where a large part of the heat transfer is still due to radiation, especially in the hottest superheaters and reheaters regions. This pass consists of tube bundles making the superheaters, reheaters and economiser, as shown in Figure 2-3, which are systematically arranged to achieve the design water and steam temperatures while keeping the metal temperatures at a sustainable level. These sophisticated heat exchanger arrangements as well as the choices of metals used are aimed at minimizing the capital expenditures while keeping the maintenance costs at acceptable levels. The corresponding design margins are dictated by the knowledge and expertise of the manufacturers. In the water-steam circuit, the first superheater inlet is either connected to the outlet of the water-steam separating system or to the outlet of the furnace wall tubes.

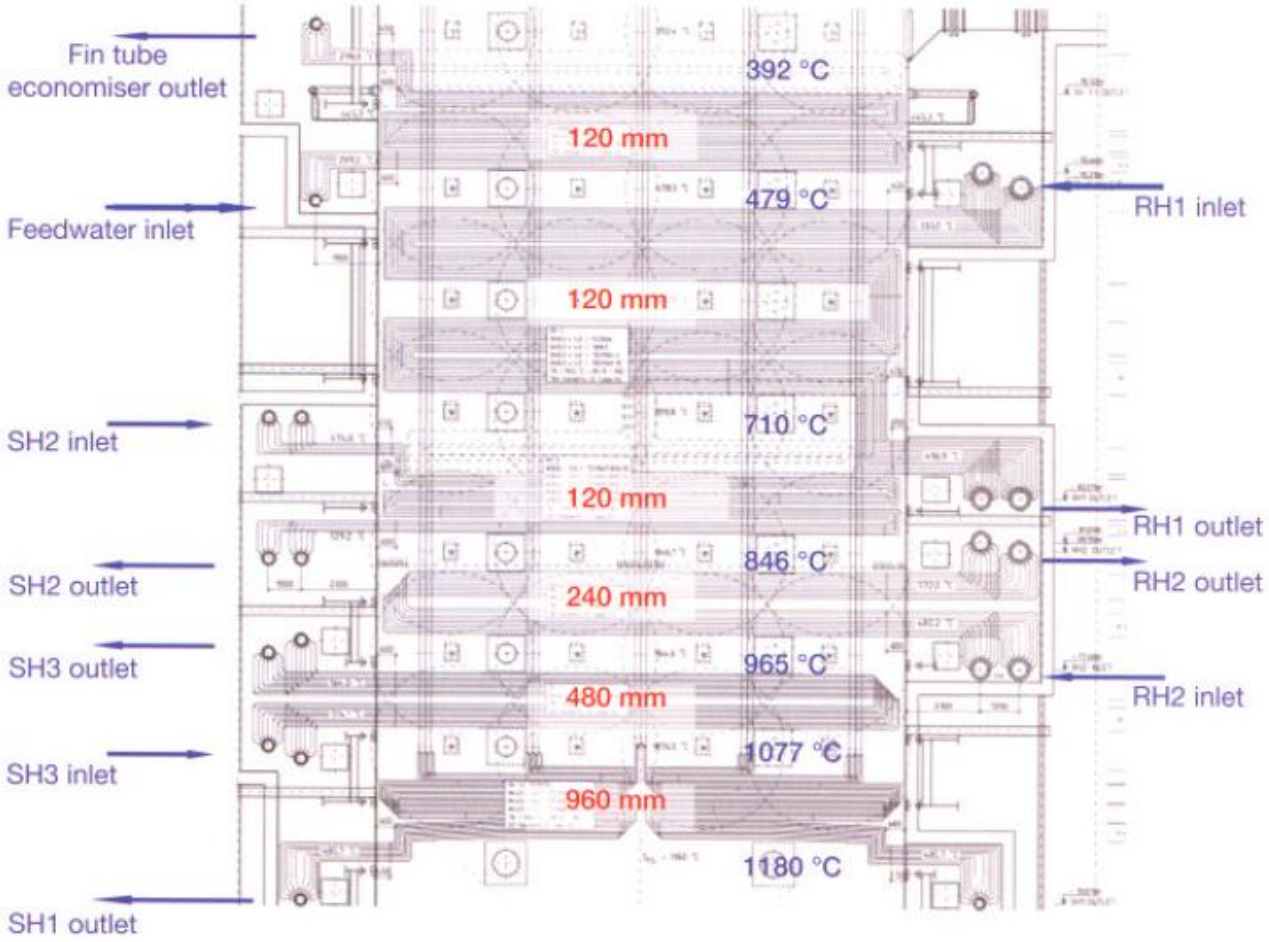

Figure 2-3. Superheaters and reheaters arrangements in a once through type 800MWe coal fired power plant, Medupi and Kusile units [3].

There are two basic types of superheaters depending on the dominant mode of heat transfer from flue gas in the region around the superheater. These are the radiant superheater and the convection superheater. The radiant superheater primarily receives energy through thermal radiation from the flue gas in the furnace with minimal convection from the flue gas passing the tube bundles. Since thermal radiation mainly depends on temperature, the radiant superheater is also highly dependent on the temperature of the flue gas. In addition, the radiant superheater steam outlet temperature is lower at higher boiler loads mainly because at high loads there is more steam to cool the heat exchanger tube walls. On the other hand, the convective superheater primarily receives energy from convection from the flue gas passing over the tube bundles, with minimal radiation since the flue gas is at a relatively low temperature. The performance of the convective superheater is highly dependent on the characteristics of the flue gas flow and mainly its velocity. At maximum boiler load, the convection heat transfer in this superheater is higher. Thus, higher heat absorption result in high boiler steam outlet temperature [2].

Extra caution is required in the design of the radiant and convection superheaters to avoid a mass flux difference in steam and flue gas distribution that could result in tube overheating. In general, superheaters are made of tube elements that are stacked one after the other by connecting them on two headers: the inlet and outlet headers. The tube element is made up of a bare tube that has been bent several times depending on the design of the superheater, as shown in Figure 2-4. The parameters considered in a superheater design include the following: the specified maximum exit steam temperature, the boiler load range over which steam outlet temperature has to be controlled, the material to be used to make the superheater and support structures, the type of the superheater [2], etc.

Figure 2-4. Tube banks for the superheaters and reheater in a once through 800 MWe boiler system.

As demonstrated in Figure 2-2, after the last superheater, the steam is ducted to the high pressure turbine. After doing work in the turbine it is returned back to the boiler to be reheated to a higher temperature before being ducted to the intermediate and low pressure turbines. The tube bundles that are used to reheat the steam in the boiler are called the reheaters. Their governing fundamental design principles are the same as that of the superheaters [2]. However, the pressure drop in the reheater design is considered with added caution because a high pressure drop through the reheater can nullify the advantage of heating the steam again before sending it to the turbines at lower pressures.

The last tube bundles at the end of the convection pass make up the economiser. The economiser heats up the boiler feedwater before it is sent to the steam drum for a drum boiler or the evaporators for a once through boiler. Its key function is to improve the boiler overall thermal efficiency through the recovery of low level energy from the flue gas that is at a low temperature before it is sent to the air heater [2]. Similar to the superheater and reheater, the economiser is made of tube elements that are connected to an inlet and outlet header. However, contrary to superheaters and reheaters, economiser's tubes can have fins to increase the surface area for heat transfer as well as reduce the size and cost of the heat exchanger.

The materials used to make the tubes in the convection pass are determined by the material's resistance to oxidation, allowable stress and economics. This material selection criteria is carefully implemented in the design process of a superheater or reheater system to develop an economical and reliable configuration as well as to provide the required surface area [2]. In general, for an economically feasible boiler system the tubes nearer to the furnace are made of the most expensive material and only a few bundles of tubes are located in that region. As the temperature decreases in the convection pass, less expensive materials are used with more tubes.

In general, the number of tubes in the heat exchangers on the convection pass compared to the headers demonstrate that most of the dynamic behaviour in the heat exchanger is dominantly due to the tubes. For the final superheater of a 600MWe unit in an Eskom power station the mass of tubes is about 137 860 kg compared to the mass of the headers which is about 14 617 kg.

2.1.2 Boiler operation and boiler transients

The operation of a coal fired power station is dependent on the grid power demand. Some power stations are operated as base load stations, while some as peaking stations (on/off cycling) to control the supply and demand of power in the grid. During the operation of these plants, the power produced varies with time. The boiler system experiences two general transients, namely: major transients and minor transients. Major transients introduce a large temperature change in the boiler metal components per given unit time. These transients include unit start-up, shut-down and trips. However, minor transients introduce a smaller temperature differential in the metal components but they occur frequently. These include load variation, soot blowing, attemperation for temperature control, change of fuel quality, etc.

2.1.2.1 Major boiler transients

During boiler start-up, different software and control philosophies are used to optimise the process as well as to protect thick metal components such as the steam drum from thermal stresses. Li et al. [4]

states that boiler start-ups can be classified into three categories, which are cold, warm and hot start-ups. A hot start-up is typically when the boiler has been down for less than 8 hours [5], for warm start-up the boiler has been down for a time between 8 hours and 36 hours and lastly, cold start-up is for a boiler that has been down for more than 36 hours [4]. These classification can change, for example according to the cooling which happens during the shut-down time as well as the way the boiler has been boxed-up.

Start-ups should be carefully monitored to prevent increases of thermal stresses due to temperature differentials which in turn might shorten the lifespan of the boiler. Start-up times differs with the categories; for hot start-up the start-up time is approximately from 1 to 2 hours, for warm start-up it is from 2 to 3 hours and for cold start-up it can vary from 2 to 10 hours. Boiler start-up operation procedures differ with the boiler designs and boiler manufacturers. However, there are certain objectives to which each operation procedure should conform to. The Babcock & Wilcox (B & W) Company [2] specifies that these objectives should include protection of the boiler pressure parts from corrosion, overheating and thermal stresses, avoiding furnace explosions, producing steam of the desired temperature, pressure and purity, and complying with the environmental regulations.

During boiler shutdown, control philosophies are used to control the boiler as it was with boiler start-up. However, boiler shutdown is not as complex as the start-up process. As with start-up, boiler safety and the protection of the metal making the components is emphasised. There are two shutdown situations that can occur, namely; the controlled shutdown and the emergency shutdown (unit trip) [2].

2.1.2.2 Typical small boiler transient operation regimes

The boiler operators should consistently strive for efficient boiler operation through minimising fuel consumption and maximising steam production. However, there are many operating variables that affect the steam production, especially the steam temperature. These variables are constantly adjusted to maintain the output steam temperature, thus introducing frequent (minor) transients in the system. These variables include fuel variations, load variations amongst others. A summary of such transients is presented in Table 2-1.

For example, burning different types of fuel or fuel with differing characteristics on a daily basis introduces variations in the heat flux generated, thus affecting the outlet steam temperature. Then, this variation is compensated by adjusting parameters such as the fuel flow rate, air flow rate amongst others in order to produce steam at the rated temperature, pressure and flow rate. Another important minor transient is an increase in load. This requires an increase in the quantity and temperature of the flue gas, which yield an increase in steam temperature for a convection superheater. As for a convection

superheater, steam temperature increase with load, and the increase becoming lesser for superheaters near the furnace. However, an increase in load yield a decrease in steam temperature for a radiant superheater. Thus, generally the superheater arrangement includes both radiant and convection superheaters connected in series, as mentioned in the subsections above, to maintain the steam temperature as constant as possible over the load range [2].

Table 2-1. A summary of small boiler transient operating regimes.

Minor (frequent) Transients			
1.	Fuel variation	7.	Feedwater heater out for service
2.	Variation of burner operation	8.	Load variation
3.	Variation in amount of excess air	9.	Variation of operating pressure
4.	Sootblowing	10.	Attemperation
5.	Blowdown	11.	Gas proportioning using a damper
6.	Use of saturated steam on auxiliaries	12.	Flue gas recirculation

2.1.3 Boiler maintenance

In the process of operating the boiler system, the operator also has to ensure that the boiler is operable. Operability is ensured by maintaining the system. Maintenance ensures reliability and also control costs [6]. The reliability of the boiler plant is ensured by preventing oxidation, vibration, corrosion, breakdown, etc. Maintaining and operating the boiler properly has the potential of preventing failures of equipment with significant repair costs [6]. Faulty operation, excessive temperatures, boiler transients, or abnormal conditions result in the safety limits of the material of the components being exceeded, hence increasing the rate of failure as well as reducing the life of the component [7]. Conducting routine maintenance which include activities such as monitoring, testing and physical equipment repairs, can optimise the production, availability, safety and life of the component as well as minimize operation cost.

In general, there are three maintenance categories; which are breakdown, preventive and predictive maintenance [6]. The maintenance option that is implemented depends on the reliability required and the costs of that maintenance option compared to potential loss. Breakdown maintenance is the traditional method based on physical repairs of damaged components, which generates costs due to the

maintenance as well as loss of revenue due to down time of the plant in some cases. Preventive maintenance involve regular activities that are performed to prevent the damage of the equipment, this include water treatment, lubrication of moving parts and evaluation of the overall operation of the boiler [6]. Predictive maintenance entails monitoring, examination and tests on the equipment assessing the problems that will lead to failure if the system is allowed to continue operating [6]. It also involve techniques to predict the life of the equipment as well as developing corrective measures for future problems [7]. Predictive maintenance requires knowledge of the operation (normal and abnormal) of the system, cause and propagation of failure (aging) mechanism. In addition, programs and models are developed to predict the behaviour of the component in the future. Preventive and predictive maintenance have a potential of significantly increasing the availability and reliability of the plant, however they are costly. These preventive and predictive maintenance strategies should be based on thorough on-line Condition Monitoring (CM) of the different plant components to early detect performance drifts and consecutive alarm triggering with associated inspection and maintenance strategies.

2.1.4 Creep and thermal fatigue as aging mechanisms

During operation of the boiler system, the components operating at high temperature and pressure are continuously aging. The understanding of the aging mechanisms is often used to assess the remaining life of the components, especially boiler tubes for the plants that were built decades ago. Without forgetting metal erosion, corrosion and oxidation, the main aging mechanisms are creep, thermal fatigue and creep-fatigue interactions.

2.1.4.1 Creep

Creep is a process where metals operating at high temperatures and applied stresses below the high temperature yield stress gradually deform over a long period of time and eventually fail [8, 9]. During this process the material undergoes a permanent plastic deformation as its microstructure is gradually damaged due to creep voids forming at the grain boundaries as a result of grain boundary sliding. Over time, these voids coalescence into cracks, and the cracks also propagate with time until the component eventually fails [9]. Creep is dependent on the applied stress and the operating temperature. An increase in the applied stress and operating temperature increases the creep rate and reduces the remaining life of the component. Creep failures or creep ruptures are characterised by inter-granular voids and cracks in the microstructure, bulging or blisters in the tube, thick-edged fractures, external or internal oxide-scale thickness, longitudinal stress cracks in either the internal or external oxide scales, [10], etc.

2.1.4.2 Thermal fatigue

Thermal fatigue is a phenomena that occurs in a material that is subjected to cyclically varying temperatures in the presence or absence of external loads, which result in a change of structure and shape of the material [11, 12]. The progressing accumulation of damage on the material after each successive cycling thermal loading eventually leads to thermal fatigue failure, since in the process micro-cracks are formed, and they propagate until reaching rupture [11]. The cycling varying temperature (temperature transients) due to continuous heating and cooling of the material results in thermal stresses, which then cause the thermal fatigue.

Thermal stresses can be defined as self-balancing stresses produced by a thermal gradient or non-uniform temperature distribution as well as differing coefficient of thermal expansion [13, 14]. These thermal stresses develop in solid material whenever any part of the solid body is constrained from attaining the size and shape it would have freely assumed due to a change in temperature [13]. There are two mechanisms that result in a thermal stress in materials. In the first mechanism the stress results from a temperature gradient within a body due to constraints. The stress is generated by the forces that result as the body expand or contract against the constraints due to the temperature gradient [15, 16]. These constraints can be external or internal. External constraints are imposed on the whole system, constraining it from expanding or contracting when experiencing a temperature change. However, internal constraints are within the material since the amounts of expansion or contraction in the material differs with location yet the material must still remain continuous [15]. For example, consider a tube with a heating outer boundary condition and keeping the initial condition at the inner boundary. A temperature gradient will be induced along the radius causing the tube to expand inwards. However, the material will expand faster near the outer boundary than the inner boundary leading to an internal thermal constraints. This will result in an axisymmetric stress in the thickness of the tube material, as shown in Figure 2-5.

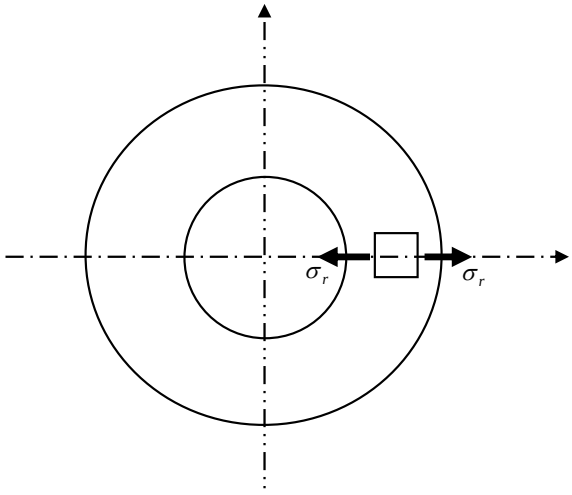

Figure 2-5. Radial stress due to radial temperature difference.

The second mechanism is related to the curvature from an axial temperature variation along the length of a tubular body [16]. The curvature of the axial temperature profile is directly proportional to the second derivative of the temperature profile. This implies that a constant or linear temperature distribution would not result in thermal stresses in the axial direction [16]. The axial/ longitudinal stress due to axial temperature variation tends to bend the tube from the axial axis, as shown in Figure 2-6. In a boiler, the heat exchanger headers are more prone to experience such thermal stresses, due to the variation of steam temperature from the different tubes along the length of the header.

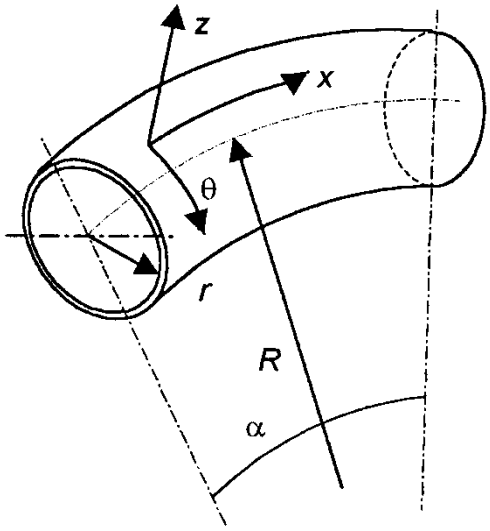

Figure 2-6. The induced shape of the body due to axial temperature variation [17].

2.1.4.3 Creep – fatigue interaction

In certain cases, both creep and thermal fatigue are present and these phenomena interact with one another in a process called creep-fatigue interaction or fatigue-creep interaction. For example, in thermal fatigue the main parameter governing its significance is the amplitude of the stress variation, regardless of the duration of the cycle [18]. However, in some instances the time-dependence appears including phenomena dependent on the environment as well as those independent on it [18]. The combination of creep and fatigue accelerate the rate to failure of the component. In cases where creep is dominant, then creep is accelerated by fatigue and fatigue is accelerated by creep in instances where fatigue is dominant.

2.1.5 Practical background summary

In summary, the practical background illustrates that there are two fluid streams in the operation of a boiler; the water-steam and the flue gas stream. These streams are separated by tube walls. Changing the parameters of one stream affect the other stream through the tube wall. However, the wall also experiences some damages with time since it is made of steel.

2.2 Theoretical background

The interaction between the flue gas stream and the water-steam stream in the boiler tubes is through conduction heat transfer within the walls of the tubes. Therefore, in order to understand the interaction, in this section conduction heat transfer is reviewed by revising the derivation of the conduction heat transfer equation as well as introducing the methods of solving this equation.

2.2.1 Conduction heat transfer

The flow of heat in a material driven by a temperature gradient in the material through molecular interaction in between neighbouring molecules is referred to as *conduction heat transfer* [19]. This result in the diffusion of heat/ energy from a region with high temperature to the lower temperature region [20]. Conduction heat transfer is a very important component of heat transfer and for this project, so the fundamental understanding of the heat conduction equation is important. Different formulations of the heat conduction equation are typically applied for the different coordinate systems such as Cartesian, Cylindrical and Spherical.

2.2.1.1 The heat conduction equation in Cartesian coordinates

Consider a heat conducting slab with heat transfer in three dimensions. If a differential control volume, shown in Figure 2-7, is extracted from the plane and described in Cartesian coordinates as shown in the figure, the heat conduction equation can be derived.

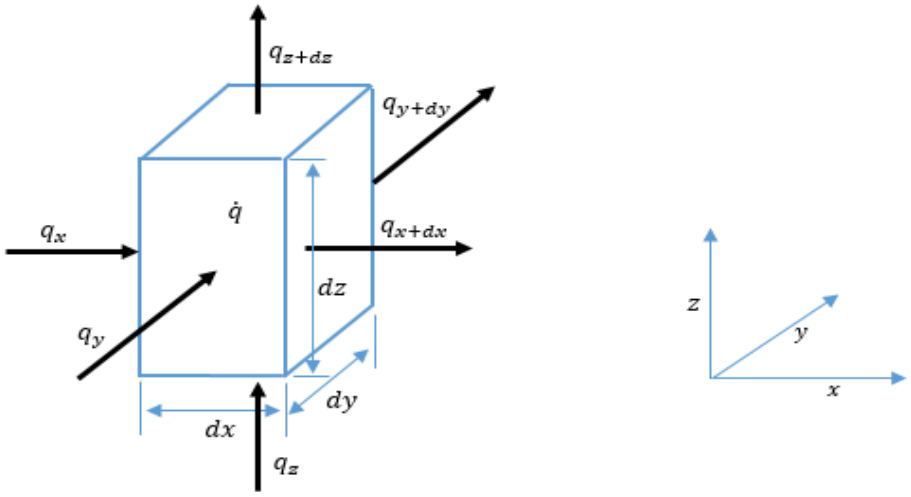

Figure 2-7. Differential Control Volume (element) in Cartesian Coordinates.

If energy balance is done across the differential control volume in Figure 2-7, the resulting equation is:

$$\dot{E}_{in} + \dot{E}_{gen} - \dot{E}_{out} = \dot{E}_{st} \tag{2.1}$$

with $\dot{E}_{in}$ and $\dot{E}_{out}$ being the rate of energy entering and leaving the control volume, respectively. While $\dot{E}_{gen}$ is the rate at which energy is generated within the control volume, for example in case of a nuclear or chemical reaction. $\dot{E}_{st}$ is the rate at which energy is stored within the control volume.

The energy balance given by equation (2.1) can be rewritten in terms of the heat conducted in and out of the element, denoted by *q*, as:

$$q_x + q_y + q_z + \dot{E}_{gen} - q_{x+dx} - q_{y+dy} - q_{z+dz} = \dot{E}_{st} \tag{2.2}$$

The rate at which energy is generated and the rate at which energy is stored are given by:

$$\dot{E}_{gen} = \dot{q}dxdydz \tag{2.3}$$

$$\dot{E}_{st} = \rho c dxdydz \frac{\partial T}{\partial t} \tag{2.4}$$

with $\dot{q}$ the energy generated per unit volume, c the specific heat of the material and ρ the density of the material.

The heat conducted out of the element can be expressed using the Taylor series. For this derivation if the first two terms of the series are considered, then:

$$q_{x+dx} = q_x + \frac{\partial q_x}{\partial x} dx, \qquad q_{y+dy} = q_y + \frac{\partial q_y}{\partial y} dy, \qquad \mathrm{q}_{z+dz} = q_z + \frac{\partial q_z}{\partial z} dz \tag{2.5}$$

Substituting equations (2.3), (2.4) and (2.5) into (2.2) results to:

$$-\frac{\partial q_x}{\partial x} dx - \frac{\partial q_y}{\partial y} dy - \frac{\partial q_z}{\partial z} dz + \dot{q}dxdydz = \rho c dxdydz \frac{\partial T}{\partial t} \tag{2.6}$$

The mathematical physicist Joseph Fourier stated that the conducted heat is related to the temperature gradient and this relationship is given by:

$$q_x = -kdydz \frac{\partial T}{\partial x}, \qquad \mathrm{q}_y = -kdxdz \frac{\partial T}{\partial y}, \qquad q_z = -kdxdy \frac{\partial T}{\partial z} \tag{2.7}$$

This is known as Fourier's law, where k is the thermal conductivity of the material.

Substituting equations (2.7) into (2.6) result in:

$$\left[\begin{array}{l} -\frac{\partial}{\partial x}\left(-kdydz\frac{\partial T}{\partial x}\right)dx-\frac{\partial}{\partial y}\left(-kdxdz\frac{\partial T}{\partial y}\right)dy \\ -\frac{\partial}{\partial z}\left(-kdxdy\frac{\partial T}{\partial z}\right)dz+\dot{q}dxdydz \end{array}\right]=\rho cdxdydz\frac{\partial T}{\partial t} \tag{2.8}$$

Dividing by the size of the differential control volume, $dxdydz$ leads to:

$$\frac{\partial}{\partial x}\left(k\frac{\partial T}{\partial x}\right)+\frac{\partial}{\partial y}\left(k\frac{\partial T}{\partial y}\right)+\frac{\partial}{\partial z}\left(k\frac{\partial T}{\partial z}\right)+\dot{q}=\rho c\frac{\partial T}{\partial t} \tag{2.9}$$

This is the heat conduction partial differential equation in Cartesian coordinates, which is expressed on a per unit volume basis. This equation characterises a three dimensional (3D) heat transfer scenario. However, if simplified heat transfer scenarios are addressed, then the equation can be adapted to suit those scenarios.

Consider a wall of infinite length such that the variation of temperature in the z-direction is negligible i.e. $dT/dz=0,$ compared to the x and y directions as shown in Figure 2-8a. For this scenario the equation can be adapted as:

$$\frac{\partial}{\partial x}\left(k\frac{\partial T}{\partial x}\right)+\frac{\partial}{\partial y}\left(k\frac{\partial T}{\partial y}\right)+\dot{q}=\rho c\frac{\partial T}{\partial t} \tag{2.10}$$

This represents the heat conduction partial differential equation for a 2D scenario. If the wall is infinitely long and also infinitely wide such that the variation of temperature in the y direction is also negligible, $dT/dy=0,$ refer to Figure 2-8b, then the equation can be adapted as:

$$\frac{\partial}{\partial x}\left(k\frac{\partial T}{\partial x}\right)+\dot{q}=\rho c\frac{\partial T}{\partial t} \tag{2.11}$$

This is a 1D heat conduction partial differential equation. If there is no internal heat generation, then the equation can be written as:

$$\frac{\partial^2 T}{\partial x^2}=\frac{1}{\kappa}\frac{\partial T}{\partial t} \tag{2.12}$$

with $\kappa=k/\rho c$, the thermal diffusivity of the material, assuming that the thermo-physical properties do not vary with x.

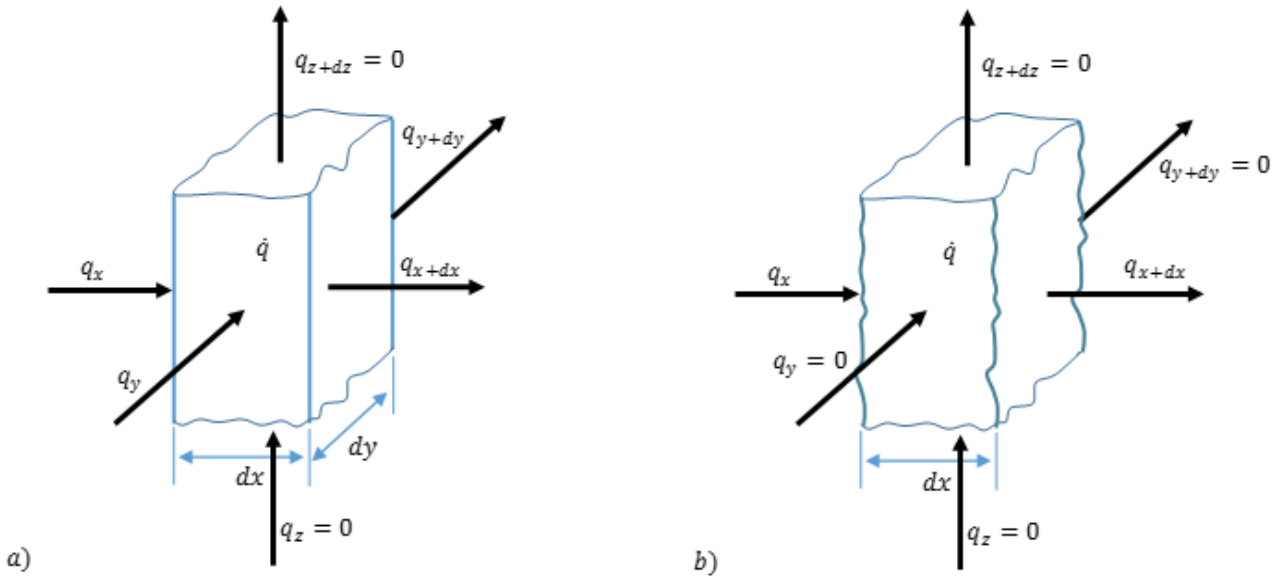

Figure 2-8. Wall Scenarios a) infinite long wall (2D) b) infinite long and wide wall (1D).

2.2.1.2 The heat conduction equation in cylindrical coordinates

Usually, for cylindrical components such as a cylindrical rod or a tube, cylindrical coordinates are preferred to describe the heat conduction in that component. This is because the cylindrical geometry is best described using cylindrical coordinates compared to Cartesian coordinates.

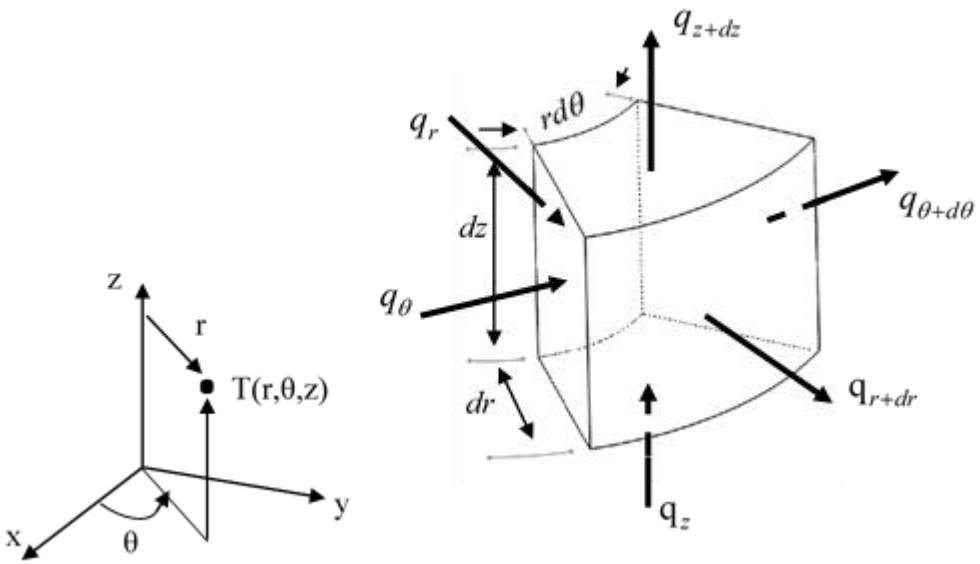

Figure 2-9. Differential Control Volume in Cylindrical Coordinates.

As with the subsection above, performing an energy balance on a differential control volume shown in Figure 2-9 results in:

$$\dot{E}_{in} + \dot{E}_{gen} - \dot{E}_{out} = \dot{E}_{st} \tag{2.13}$$

However, the energy balance given by equation (2.13) can be written in terms of the rate at which heat is conducted by the material, denoted by q, as:

$$q_r + q_\theta + q_z + \dot{E}_{gen} - q_{r+dr} - q_{\theta+d\theta} - q_{z+dz} = \dot{E}_{st} \tag{2.14}$$

The rate at which energy is generated and the rate at which energy is stored are given by:

$$\dot{E}_{gen} = \dot{q} r dr d\theta dz \tag{2.15}$$

$$\dot{E}_{st} = \rho c r dr d\theta dz \frac{\partial T}{\partial t} \tag{2.16}$$

From Taylor series, the rate at which heat is conducted out of the material can be given as:

$$q_{r+dr} = q_r + \frac{\partial q_r}{\partial r} dr, \qquad q_{\theta+d\theta} = q_\theta + \frac{\partial q_\theta}{\partial \theta} d\theta, \qquad \mathrm{q}_{z+dz} = q_z + \frac{\partial q_z}{\partial z} dz \tag{2.17}$$

Substituting equations (2.15), (2.16) and (2.17) into equation (2.14), leads to:

$$-\frac{\partial q_r}{\partial r} dr - \frac{\partial q_\theta}{\partial \theta} d\theta - \frac{\partial q_z}{\partial z} dz + \dot{q} r dr d\theta dz = \rho c r dr d\theta dz \frac{\partial T}{\partial t} \tag{2.18}$$

However, from Fourier's law the relation of q to temperature is given by:

$$q_r = -k r d\theta dz \frac{\partial T}{\partial r}, \qquad \mathrm{q}_\theta = -k dr dz \frac{1}{r} \frac{\partial T}{\partial \theta}, \qquad q_z = -k r dr d\theta \frac{\partial T}{\partial z} \tag{2.19}$$

Note that the $1/r$ in the equation for q_θ ensures that the equation is dimensionally homogeneous. Substituting equation (2.19) into equation (2.18), results in:

$$\begin{bmatrix} -\frac{\partial}{\partial r}\left(-k r d\theta dz \frac{\partial T}{\partial r}\right) dr - \frac{\partial}{\partial \theta}\left(-k dr dz \frac{1}{r} \frac{\partial T}{\partial \theta}\right) d\theta \\ -\frac{\partial}{\partial z}\left(-k r dr d\theta \frac{\partial T}{\partial z}\right) dz + \dot{q} r dr d\theta dz \end{bmatrix} = \rho c r dr d\theta dz \frac{\partial T}{\partial t} \tag{2.20}$$

Dividing by the size of the control volume, $r dr d\theta dz$ on both side results in:

$$\frac{1}{r}\frac{\partial}{\partial r}\left(rk\frac{\partial T}{\partial r}\right) + \frac{1}{r^2}\frac{\partial}{\partial \theta}\left(k\frac{\partial T}{\partial \theta}\right) + \frac{\partial}{\partial z}\left(k\frac{\partial T}{\partial z}\right) + \dot{q} = \rho c \frac{\partial T}{\partial t} \tag{2.21}$$

Equation (2.21) is the heat diffusion equation in three dimensions (3D) written in cylindrical coordinates. Therefore, the conduction heat transfer for all components with a cylindrical geometry can be characterised by equation (2.21). However, the equation is adaptable to simplified problems depending on the assumptions that are employed.

Consider a case where there is no change of temperature with respect to the tangential coordinate direction θ , then $\partial T / \partial \theta$ becomes zero. This reduces the 3D equation to a 2D equation, written as:

$$\frac{1}{r}\frac{\partial}{\partial r}\left(rk\frac{\partial T}{\partial r}\right)+\frac{\partial}{\partial z}\left(k\frac{\partial T}{\partial z}\right)+\dot{q}=\rho c\frac{\partial T}{\partial t} \tag{2.22}$$

In addition, if for the same case as above, the length of the cylindrical component is infinitely long such that the axial temperature variation is negligible compared to the radial temperature variation, then the problem reduces to 1D and is represented as:

$$\frac{1}{r}\frac{\partial}{\partial r}\left(rk\frac{\partial T}{\partial r}\right)+\dot{q}=\rho c\frac{\partial T}{\partial t} \tag{2.23}$$

In the heat exchangers used in coal fired power plant boilers, there is no internal heat generation $\left(\dot{q}=0\right),$ thus equation (2.23) further simplifies to:

$$\frac{1}{r}\frac{\partial}{\partial r}\left(rk\frac{\partial T}{\partial r}\right)=\rho c\frac{\partial T}{\partial t} \tag{2.24}$$

If it is assumed that the thermo-physical properties of the material do not vary with respect to radius and time, as with most cases, then the thermal conductivity, *k*, is seen as a constant for the differentiation. Thus from rearranging, equation (2.24) becomes:

$$\frac{\partial T}{\partial t}=\frac{k}{\rho c}\frac{1}{r}\frac{\partial}{\partial r}\left(r\frac{\partial T}{\partial r}\right) \tag{2.25}$$

Differentiating the equation result in:

$$\frac{\partial T}{\partial t}=\kappa\left(\frac{\partial^2 T}{\partial r^2}+\frac{1}{r}\frac{\partial T}{\partial r}\right) \tag{2.26}$$

with $\kappa = k/\rho c$, the thermal diffusivity of the material.

2.2.2 Exact analytical solutions to transient conduction heat transfer problems

The conduction equation presented in the subsections above can be solved analytically for simplified cases to get exact continuous solutions. These exact solutions are still important in this era of modern computers because they have the advantage of showing which parameter has a direct influence on the solution. Furthermore, they clearly show how the derived solution depends on certain dimensionless quantities, thus allowing the analysis to be generalised for any case. These exact solutions also help in understanding the basic behaviour and physical phenomenon of the problem [21].

In solving the conduction equation for a particular scenario, certain mathematical functions, theorems, series, principles and methods for solving partial differential equations are used. These include the separation of variables method and the principle of superposition amongst others [22]. Moreover, the application of such mathematical operations depends on the characteristics of the partial differential equation and its boundary conditions. The considered characteristics include knowing whether the equation and the applied boundary conditions are homogeneous or nonhomogeneous. In particular, the separation of variable method is applicable if the partial differential equation and its boundary conditions are linear and homogeneous [22]. Since the heat conduction equation derived in the subsections above is linear and homogeneous, the separation of variables method is applicable.

After the application of the separation of variables method to the conduction equation, it yields two differential equations. One being an ordinary differential equation of first order and the other being a second order differential equation. In a case where the heat conduction equation in cylindrical coordinates is being solved, the second order differential equation after the separation of variables method becomes a Bessel's differential equation. The Bessel's equation is solved using the Bessel's functions. These Bessel's functions are briefly explained in Appendix B. However, to reach a solution, the principle of superposition, Sturm-Liouville systems and the orthogonality property are used in the derivation [22, 23, 24, 25], as demonstrated in Appendix C. The principle of superposition involves summing the general solution to the heat conduction equation, resulting in a continuous solution made up of a sum of series.

However, solving the heat conduction equation analytically has limitations. It is often impossible to find exact analytical solutions to cases with complex geometries. In this project, simple cases of physical transient heat conduction are considered. These cases are: an infinite plate in Cartesian coordinates and an infinitely long cylindrical rod and an infinitely long tube in cylindrical coordinates, with different cases of initial and boundary conditions. Also, only derivations of exact analytical

solutions for a specific case for an infinite plate are presented in Appendix A and for a specific case of an infinitely long cylindrical rod are presented in Appendix C.

On the other hand, exact analytical solutions to the conduction heat transfer equation and the transient simple heat exchanger analysis are not limited to solving using trigonometric or the Bessel's functions only. Laplace transformation can also be used for this purpose.

2.2.2.1 Lumped capacity system criteria

In certain cases it is possible to simplify the analyses of the transient heat conduction problems based on the assumptions made. Consider a slab that is exposed to the sunlight for a long period such that equilibrium has been reached within the body. If this slab is moved to a cooler place, how long will it take to cool it to the temperature of the new environment?

In general, there are two distinguishable ways on how a body will heat-up or cool down depending on the conditions, as illustrated in Figure 2-10 for cooling. One way is when there is no large temperature gradient within the material. The temperature within the material can be assumed to be the same at all locations at any unit time, however this value will change continuously as time progresses [26], as demonstrated in Figure 2-10a for cooling. Such is observed in a material which is either small in size, has a high thermal conductivity or the imposed heat transfer coefficient is small. The second way is when there are large temperature gradients within the material [26], as demonstrated in Figure 2-10b for cooling. The temperature within the material is changing with both location and time. Such is observed in a material which is either big in size, has a low thermal conductivity or the imposed heat transfer coefficient is high.

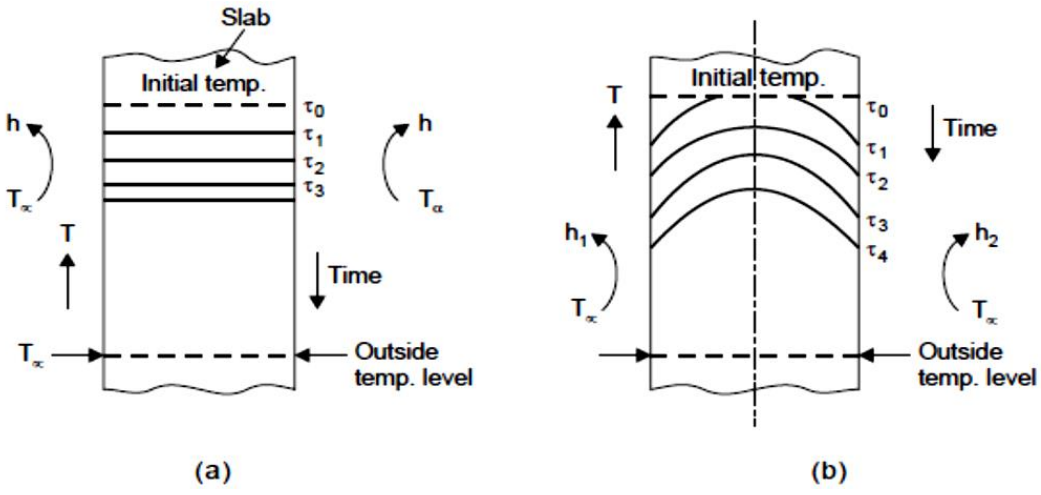

Figure 2-10. Cooling down a) without large temperature gradient in the body b) with a large temperature gradient in the body [26].

In the first case, where there is no large temperature gradient within the material, it can be assumed that there is no conduction within the material and the whole material be considered to have a certain temperature at a particular time instant. Thus modelling it as a lumped heat capacity system, as illustrated in Figure 2-11.

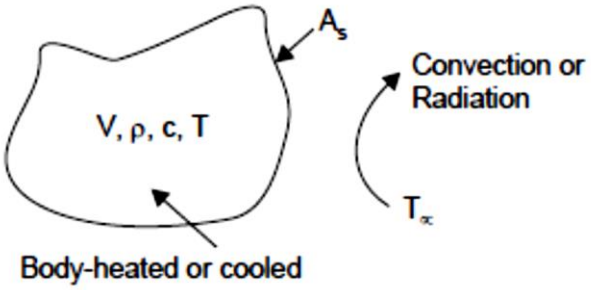

Figure 2-11. Lumped heat capacity system [26].

Performing an energy balance over the system leads to:

$$q = hA\left(T - T_{\infty}\right) = -c\rho V \frac{dT}{dt} \tag{2.27}$$

The solution to equation (2.27) is given by equation (2.28) which calculates the temperature of the body at a given time.

$$\frac{T(t) - T_{\infty}}{T_0 - T_{\infty}} = e^{-\left(\frac{hA_s}{\rho cV}\right)t} \tag{2.28}$$

with $T(t)$ the temperature of the body, T_{∞} the temperature of the fluid stream, T_0 the initial temperature, h the heat transfer coefficient, ρ the density of the body, c the specific heat capacity of the body, V the volume of the body, A_s the surface area of the body and t the time. The details of the derivation of equation (2.28) are given by Kothandaraman [26].

The lumped capacity system given by Figure 2-11 can be modelled in a form of a thermal network on an electrical system setup as shown on Figure 2-12. On Figure 2-12, initially the thermal capacity of the system is "charged" to a potential of T_0 through closing the switch S. When the switch is opened, the thermal energy stored in the thermal capacitor is dissipated by the thermal resistor in the network [20]. The representation of the thermal system in an electrical circuit setup is possible since an electric system that behaves like the thermal system can be constructed if the ratio

$$\frac{hA_s}{\rho cV} = \frac{1}{R_{th}C_{th}}, \quad R_{th} = \frac{1}{hA_s} \quad \text{and} \quad C_{th} = \rho cV$$

equals to $\frac{1}{R_e C_e}$ where R_e and C_e are the electrical resistance and capacitance of the system respectively [20]. The thermal system stores energy and the electrical systems stores charge. In addition, the flow of energy in the thermal system is called heat and the flow of charge on the electrical system is called electrical current [20].

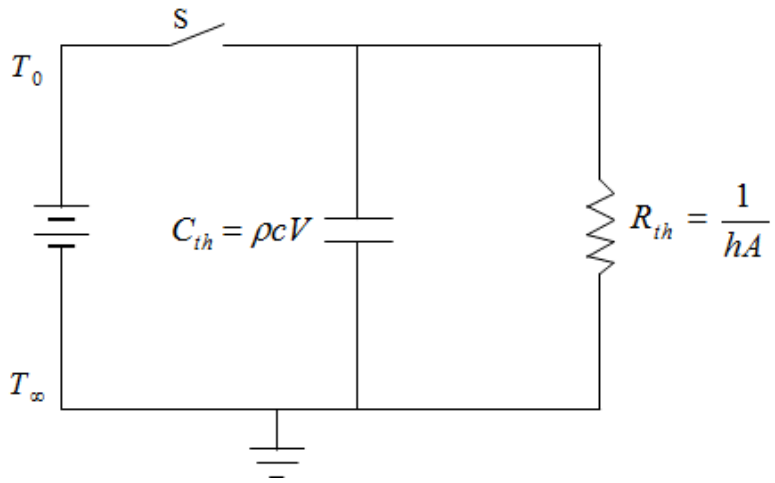

Figure 2-12. A thermal network of the lumped capacity system on Figure 2-11 represented in an electrical setup [20].

For the thermal system, equation (2.28) demonstrates that the temperature decays or rises exponentially and the rate depends on the parameter $\left(\frac{hA_s}{\rho cV}\right)$, as illustrated in Figure 2-13.

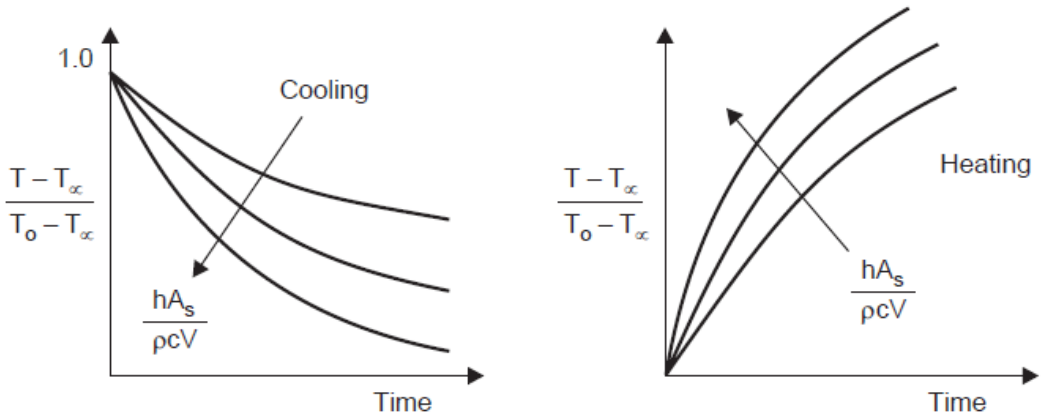

Figure 2-13. Transient temperature decay for cooling and rise for heating [26].

This exponential behaviour of the temperature as a function of time can be used to analyse the transient response time of the system. The transient response time is the time it takes to propagate heat from one side of the metal to the other side until an equilibrium state is reached. The transient response characteristic of a body with respect to cooling or heating is characterised by the time required for the

temperature to drop to $1/e$ of the original value in cooling or to rise to $1-1/e$ of the final value for heating [26]. This characteristic is called the thermal time constant and is given by:

$$\tau_c = \frac{\rho c V}{h A_s} \tag{2.29}$$

The thermal time constant can be defined as a measure of how quickly the body can respond to a change. A small thermal time constant implies a fast response for the system. This is for a first order linear time invariant (LTI) system. An example of a response of a first order LTI system to a step change is illustrated on Figure 2-14.

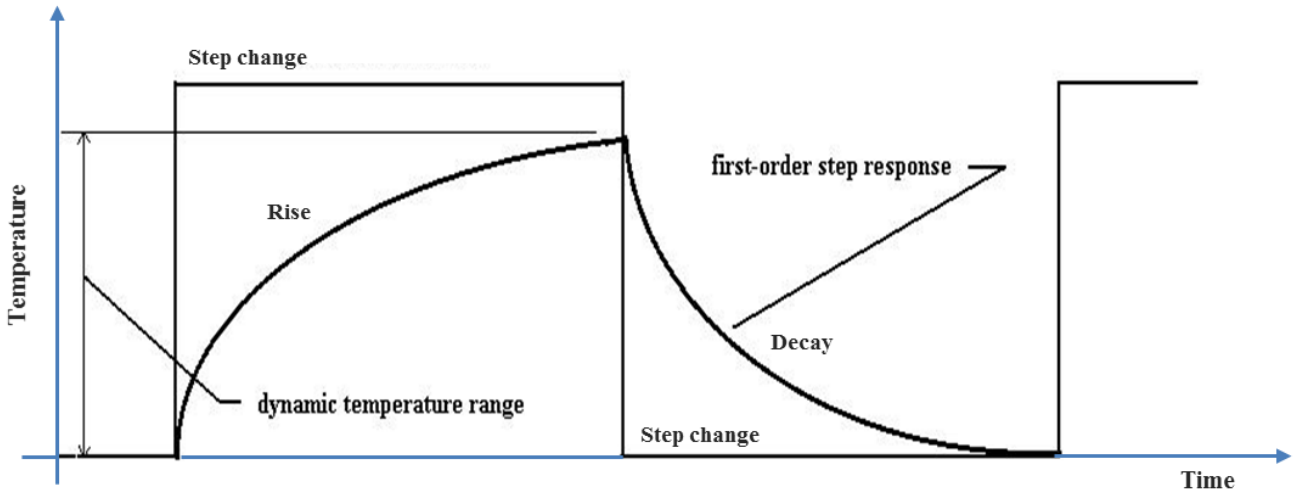

Figure 2-14. Response of a first order linear time invariant on heating (rise) or cooling (decay).

The graphical illustration of the time constant from a step change is shown on Figure 2-15. In simple terms, the time constant can be defined as the time the system temperature will take to rise to 63.2% of the final temperature difference in heating, as shown on Figure 2-15a or drop to 36.8% of the difference in cooling as illustrated in Figure 2-15b.

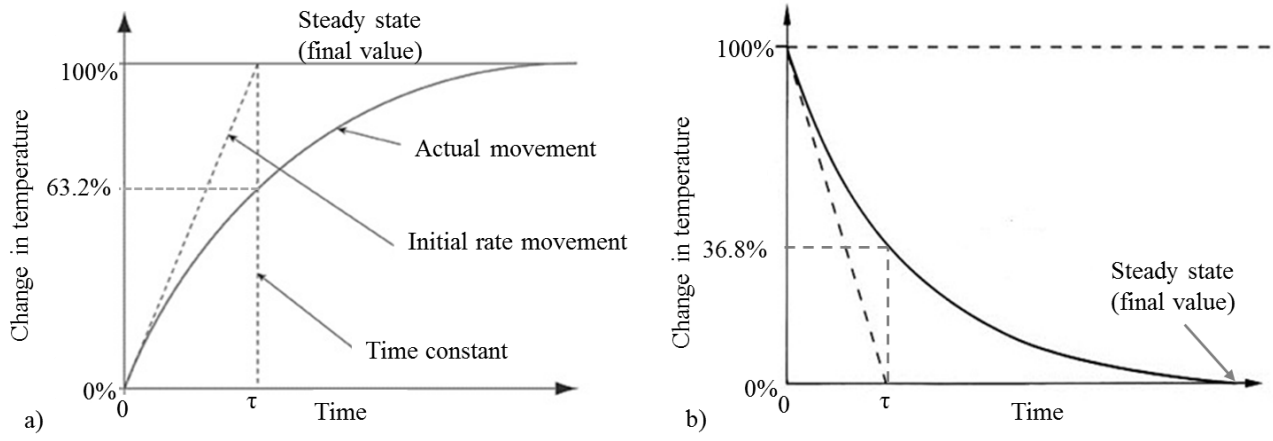

Figure 2-15. Time constant after a step change illustration a) temperature rise b) temperature drop.

The exponent of the solution to the lumped capacity system given by equation (2.28) can be written in terms of two dimensionless groups: the Fourier and Biot number.

$$\frac{hA_s t}{\rho V c} = \frac{hL}{k}\left(\frac{kt}{\rho c L^2}\right) = \frac{hL}{k}\left(\frac{\kappa t}{L^2}\right) = Bi.Fo$$

with the Fourier number, $Fo = \frac{\kappa t}{L^2}$ and the Biot number, $Bi = \frac{hL}{k}$.

The Fourier number signifies the depth of heat penetration in the solid body in time with respect to the dimension of the body, thus relating it to the time response of the system [26]. A large Fourier number signifies a quick cooling or heating. On the other hand, the Biot number characterises the relation between the flow of heat inside and outside the solid material. It is the ratio of the conductive resistance against the conductive-convective-radiative resistance at the boundary of the material. It provides a criteria to measure the temperature variation within the solid compared to the temperature difference between the solid surface and the fluid [27]. If the Biot number is small, then the conduction within the solid is high compared to the conduction-convection-radiation outside, thus the temperature variation within the solid will be small. Therefore, the Biot number can be used as a characterisation criteria for the temperature distribution within the solid, as illustrated in Figure 2-16. For the application of the lumped capacity system analyses, the system's Biot number should be $Bi < 0.1$, which implies that the temperatures within the solid compared to the surroundings will be within five percent from each other [28]. In cases where the lumped capacity system generates too much of inaccuracy, the exact analytical solutions or other methods are used to get the temperature distribution within the solid accurately enough.

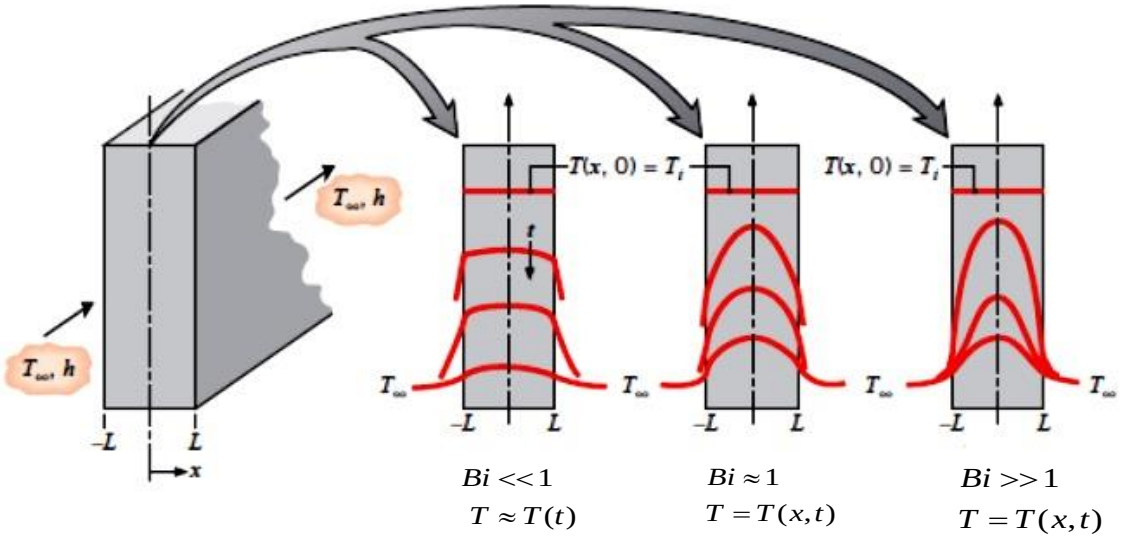

Figure 2-16. Transient temperature distribution in a plane wall for different Biot numbers which at time t = 0 was symmetrically cooled by convection [27].

2.2.3 Numerical solutions to heat transfer problems

Since exact analytical solutions are limited to simplified scenarios, they are hardly extended to industrial scenarios which often involve complex geometries and arrangements. However, industrial scenarios can be modelled as an approximation of the exact solution using numerical methods to approximate the solution to the governing equations. These approximate numerical solutions are derived in terms of the dependent variables of the governing equation at specified points over the whole computational domain with the assumption that since the governing equation is valid over the whole domain, then it should be valid for sub domains on the main computational domain [29]. This leads to a system of algebraic equations which are solved to get the values of the variables at the different points.

These numerical methods include the finite difference method (FDM), finite volume method (FVM) and the finite element method (FEM) amongst others. These are different techniques to setup the systems of algebraic equations. The FDM directly discretises the governing equation in terms of the variables of the equation at nodal points defined over the computational domain, using the expansion of the Taylor series to simplify the derivatives [29]. The FVM discretises the computational domain into control volumes, each control volume associated with a point node. Then the governing equation is integrated over the discretised control volume with the solution written in terms of the variables at the nodes [29]. In the FEM, the solution is approximated and written in terms of interpolation functions related to the point nodes. The integrals are then evaluated over discretised elements [29]. In this project, the FVM is used to solve the transient conduction heat transfer equation, as demonstrated in Appendix D.

In solving the heat conduction equation for time dependent problems, the equation is discretised in space and also in time (Time-wise discretisation), as demonstrated in Figure 2-17. Discretising the equation in space involve solving for the temperature at discrete points or nodes in physical space. Solving for the temperature at these space nodes is valid for a certain point in time. However, for transient problems the temperature is changing in space as well as with time. Thus, in addition to the discretisation in space, the equation is also discretised in time. Discretising in time involves selecting a suitable time step, Δt and solving for the unknown nodal temperatures repeatedly for each Δt until the temperatures at the desired time is found [28].

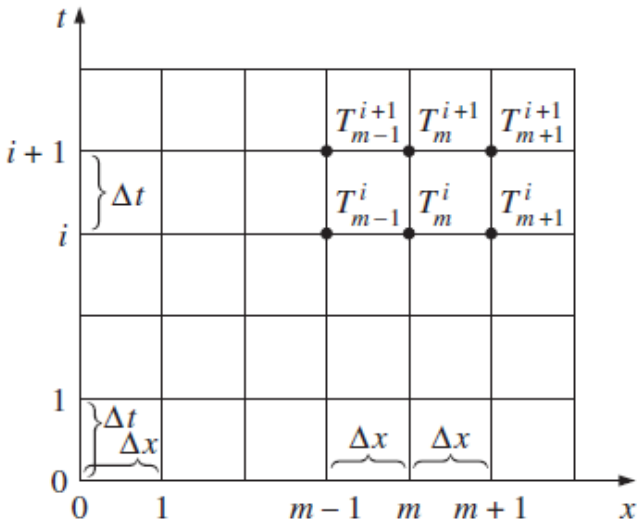

Figure 2-17. Numerical formulation for time dependent problems which involve discretisation in physical space and in time [28].

Since the nodal temperature in transient problems is changing after each time step, it is possible for the solution to use the temperatures at the previous time step or the temperatures at the new time step or a combination of the temperatures at both the previous and the new time step. A constant α which is an integration weighting factor between the old and the new time step is used as a criteria to differentiate the scheme used, as illustrated in Figure 2-18. If $\alpha = 0,$ the solution scheme is *explicit* since it only uses the known temperatures. If $\alpha = 1,$ the solution scheme is *fully implicit*, since it only uses the unknown temperatures. For $0 < \alpha < 1,$ the solution scheme is *semi-implicit*, since it uses both known and unknown temperatures. A special case of a semi-implicit scheme is for $\alpha = 1/2$ and it is called the *Crank-Nicolson Scheme*. It should be mentioned that there is no scheme that is necessarily better than the other, all schemes have their advantages and disadvantages.

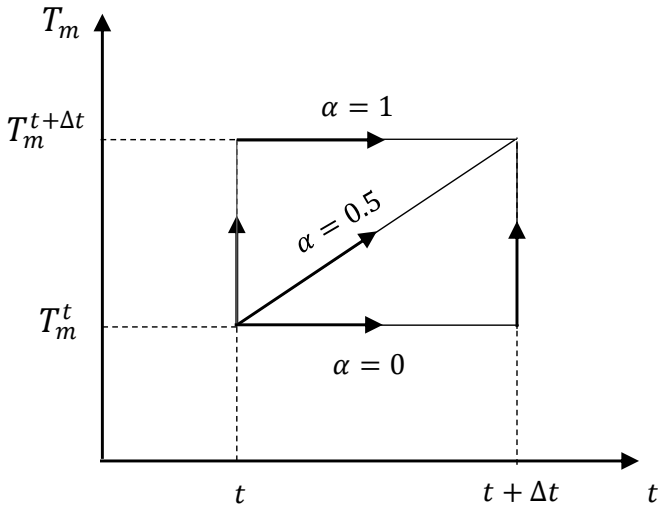

Figure 2-18. Variation of temperature within a time step for a certain node in space, m.

2.2.3.1 Stability and convergence

The success and precision of a numerical algorithm can be measured by its stability and convergence. Precision is related to the step size; if the step size is smaller, the solution becomes more precise but compilation time and effort increases [30, 31].

For a numerical method to be convergent, its solution should approach the exact solution as time and space step sizes approaches zero. If the error does not approach zero in the limit, then it is divergent. If the errors associated with solution, truncation and round off errors, increases without bound as the solution method proceeds, the solution is said to be unstable [30]. Yet if the errors do not increase, then the solution is stable. Therefore, stability is necessary for convergence to occur [30].

The explicit scheme of transient numerical solution is easy to compute but it is not unconditionally stable. The stability criterion can be derived from the Von Neumann analysis and it is found to be related to the Fourier number, Fo of the grid. Thus, after simplifications the stability criterion of the explicit scheme is given by:

$$Fo = \frac{\kappa \Delta t}{\left(\Delta x\right)^2} < \frac{1}{2} \tag{2.30}$$

The Crank-Nicolson scheme is often referred to as unconditionally stable, but it solution has a physical meaning when the grid's Fourier number is less than one [32]. Moreover, the fully implicit scheme is unconditionally stable and its results are physically meaningful for any grid's Fourier number [28, 32, 33]. However, for the implicit scheme the set of equations has to be solved simultaneously for each time step [28].

2.2.4 Thermal-fluid software Flownex application to heat transfer problems

The above analytical and numerical solutions are applied to transient heat conduction in solids. On the other hand, the heat transfer occurring at the solid boundaries is mainly driven by convection and radiation of the fluids flowing on these boundaries, which depend on the flow features of these fluids. In the present work, the fluid boundary conditions are calculated using a thermo-hydraulic software package. At a later stage the consistency of the boundary heat transfer calculations using such a software will be verified by benchmarking the results with other numerical codes as well as with real plant measurements on other research projects in the Eskom Energy Efficiency Specialisation centre.

Software simulation simplifies the modelling of thermo-hydraulic systems by coding, verifying and validating the numerical methods governing the solution into a program that is user friendly. Most of these software model the system for steady state. There are a few software packages which can capture

the dynamic behaviour of the thermo-hydraulic systems. Commercially available software packages for dynamic modelling include Sinda/Fluint and Flownex. In this project, Flownex is used to investigate the dynamic behaviour of a boiler heat exchanger, as it is part of the software packages chosen by Eskom for their engineering toolbox policy.

Flownex is a thermal-fluid network simulation code which has a capability to perform detailed analyses of complex thermal-fluid systems such as power plants [34, 35]. Nodes and elements are used to build a thermal-fluid network on Flownex, as shown on Figure 2-19. The elements include pipes, pumps, fans, compressors and turbines with the nodes at both ends of the element. By convention, in a network diagram, elements are represented by circles and nodes represented by squares.

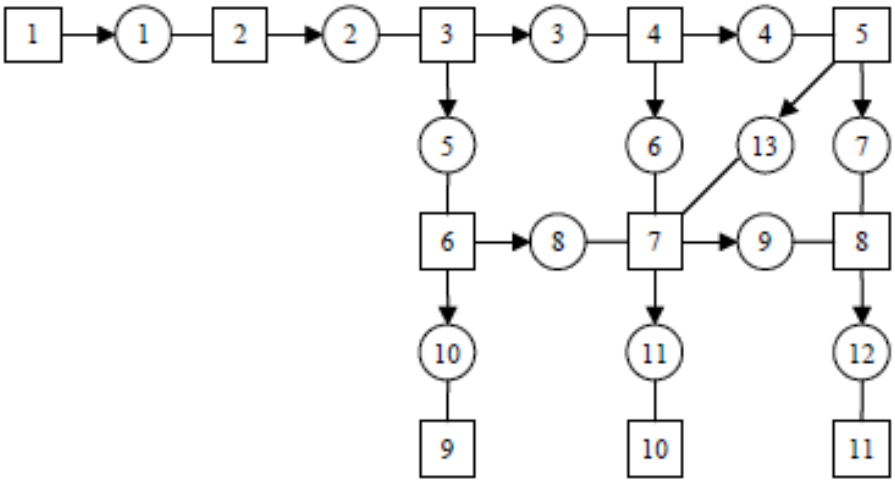

Figure 2-19. An example of a Flownex network representation [35].

Flownex solver is based on the Implicit Pressure Correction Method (IPCM) which solves the one dimensional (1D) conservation of mass (continuity) and conservation of energy equations at each node of the network and conservation of momentum equation on each element [34, 35]. This gives Flownex an ability to predict complex phenomena such a temperature and pressure waves in a pipe [34].

The conservation of mass equation in kg/s is given by equation (2.31), which implies that there is no change of mass contained in a system, thus the mass in the system does not change with time.

$$V\frac{\partial \rho}{\partial t} + \dot{m}_e - \dot{m}_i = 0 \tag{2.31}$$

with $V, \rho, \dot{m}$ and t the volume, the density, the mass flow rate and time, respectively. The subscripts e and i denotes the exits and inlets of the control volume [36]. This equation is sometimes called the continuity equation.

Cengel and Cimbala [37] states that if there is no net force acting on a system or a control volume, then the momentum of that system or control volume is constant. This is known as the conservation of momentum principle. Thus, the conservation of linear momentum equation for incompressible fluids in Pa is given by:

$$\rho L \frac{\partial V}{\partial t} + (p_{0,e} - p_{0,i}) + \rho g (z_e - z_i) + \Delta p_{0,L} = 0 \tag{2.32}$$

For compressible fluids the equation is:

$$\rho L \frac{\partial V}{\partial t} + \frac{p}{p_0}(p_{0,e} - p_{0,i}) + \frac{1}{2}\rho v^2 \frac{1}{T_0}(T_{0,e} - T_{0,i}) + \rho g (z_e - z_i) + \Delta p_{0,L} = 0 \tag{2.33}$$

with L, v and subscript 0 representing the length of the control volume, the fluid velocity and total pressure or temperature, respectively [36].

According to the conservation of energy principle, the net energy transferred to or from a system during a process must be equal to the change in energy content of the system [37]. In a system, energy can be transfer by heat and/or work, and for a control volume, energy can be transferred by mass as well [37]. The conservation of energy equation in W for a control volume is given by:

$$\dot{Q} - \dot{W} = V \frac{\partial}{\partial t}(\rho h_0 - p) + \dot{m}_e h_{0,e} - \dot{m}_i h_{0,i} + \dot{m}_e g z_e - \dot{m}_i g z_i \tag{2.34}$$

with $\dot{Q}, \dot{W}, h_0, g$ and z the heat input to the fluid, the work done by the fluid on the surrounding environment, the total enthalpy, the acceleration due to gravity and the elevation from the ground, respectively [36].

A generic flow element that can be modelled in Flownex is shown in Figure 2-20.

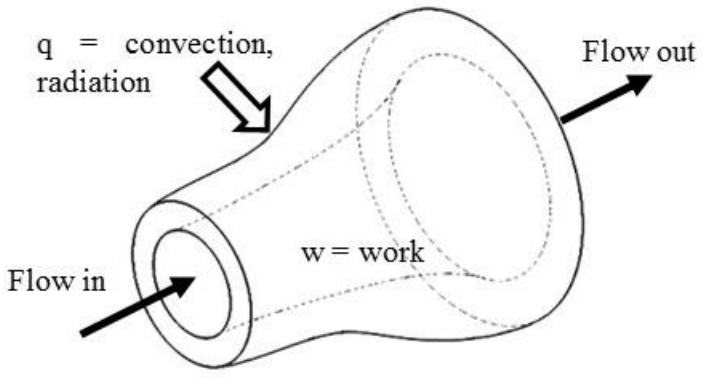

Figure 2-20. A generic flow element.

Flownex is capable of simulating a thermal-fluid system for both steady state and dynamic flows. In addition, it can predict fast and slow transients quickly and accurately [34]. Also, it is capable of solving multiple gas and liquid networks which are connected together by a heat exchanger or a heat transfer (HT) element [35]. Flownex has the ability to handle conductive, convective and radiative heat transfer. In the HT element, the temperature distribution in a solid per increment is linear [38]. In addition, the HT element has two area discretisation schemes, one is based on average areas and the other is based on linear area change discretisation. This allows Flownex to be able to solve heat conduction through any shape, with the assumption that increasing the number of nodes on the thickness discretisation will increase the accuracy of the solution. The HT element also allows for discretisation of the thickness of a component as illustrated in Figure 2-21. In order to ensure that there is a node at each boundary, the elements at the boundaries are half control volumes.

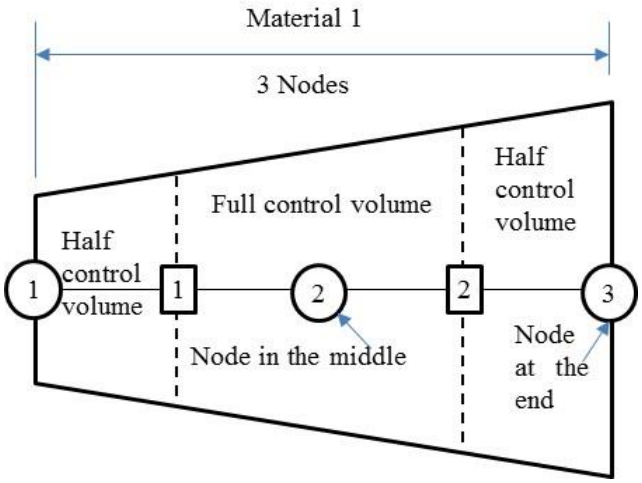

Figure 2-21. Representation of the discretisation of the thickness of the component on the heat transfer (HT) element.

In the HT element, the convective heat transfer is constant throughout an element or an increment if the element is discretised axially [38].

On Flownex, the user can easily build a complex network using built-in standard components such as heat exchangers and turbines [34]. The Flownex code has been validated against other thermal-fluid simulation codes and experimental data [35]. Flownex has a capability of directly linking it with other external computational codes which gets input from Flownex to solve and send results back to Flownex and vice versa or both. These codes include Microsoft excel, Engineering Equation Solver (EES) and MathCad, which have a component on Flownex.

2.2.5 Theoretical background summary

In this section, the theory of conduction heat transfer was revised, deriving both the Cartesian and cylindrical forms of the heat conduction equation. A brief discussion of the mathematical functions and techniques that are used in solving the heat conduction equation analytically were presented. The lumped capacity criteria was also presented, which in turn introduced the Fourier and Biot dimensionless numbers which are useful in transient conduction. The Fourier number together with the time constant are useful in the analyses of the transient response of a system.

Numerical methods to solving the heat conduction equation were presented, briefly explaining the space and time-wise discretisation. Lastly, Flownex and its use to thermal-fluid systems was introduced.

Chapter 3

3 Literature survey

This chapter presents a survey of previous work that was done by researchers in modelling the dynamic behaviour of heat exchangers. The main focus of the survey was based on the approaches used to model the heat exchangers and the errors associated with the modelling.

3.1 Approaches of modelling heat exchangers in transient regime

Ever since Profos published the first dynamic model of a simple heat exchanger in 1943 and Takahashi showed the first transfer functions for ordinary heat exchangers in 1951, a number of researches have been undertaken in the study of heat exchanger dynamic modelling [39]. In these studies, different approaches of modelling a heat exchanger under dynamic/ transient conditions were used. These approaches included the use of exact analytical solutions, numerical methods, a combination of analytical and numerical methods, modelling codes and other techniques.

Gvozdenac [40] investigated the dynamic response of a single pass cross flow heat exchanger analytically. The solutions to the temperature distributions for both fluids and the wall were found using Laplace transforms and the modified Bessel series. Gvozdenac [39] provided an analytical solution by which the dynamic performance of parallel, counter and cross flow heat exchangers can be analysed and compared. The mathematical model consists of three linear partial differential equations which were solved using Laplace transforms. Despite the similarity in the governing partial differential equations, the analyses of the parallel, counter and cross flow heat exchangers were done separately. Yin and Jensen [41] developed an analytical model to approximate the dynamic behaviour of a single-phase fluid and a wall heat exchanger subjected to step changes in fluid temperature or mass flow rate. An integral method was used to characterise the temperature distribution in the single phase fluid and the wall. Abdelghani-Idrissi et al. [42] approximated the dynamic temperature behaviour along a counter flow heat exchanger by the first order response with time constant for a sudden change in mass flow rate. They used explicit analytical solutions which compared well with experimental data.

Chang et al. [43] used the finite difference numerical technique to investigate the dynamic response of a shell/tube heat exchanger with a step change on the inlet temperature. The finite difference method was used to discretise the governing equations and the SIMPLER solution algorithm was used for the calculation procedure. Bracco et al. [44] employed numerical discretisation in the simulation of a parallel and a counter flow double-pipe heat exchanger for both steady and dynamic conditions. The

discretisation of equations was based on the energy balance method. The thermodynamic model was implemented on the Mathlab /Simulink environment.

Analytical and numerical methods have some limitations. The analytical solutions are sometimes complicated and difficult to implement. On the other hand, the numerical solution sometimes have problems with instability and divergence of results. Thus, other researchers suggested a method that combines both the analytical and numerical methods. Roetzel and Xuan [45] developed a method of predicting the transient response of a shell/tube heat exchanger through solving the governing equations by a numerical inverse Laplace transform. Ansari and Mortazavi [46] used a numerical method based on the analytical solution of energy balance to model the transient response of a countercurrent heat exchanger. The time constant, extended from the lumped capacity system, was used to analyse the transient time response.

3.2 Applications of thermal-fluids software to model heat exchangers in transient regime

Thermal-fluid software packages are also used to model the dynamic response of a heat exchanger. However, there are a few available software packages to model the transient behaviour of heat exchangers. The commercially available software packages include Sinda/Fluint and Flownex, as mentioned in the previous chapter. Olivier [34] investigated the applicability of the one-dimensional thermal-fluid network approach to modelling the performance of a heat exchanger under transient regime. In the study, two different solution algorithms were compared to one another. These algorithms were the Implicit Pressure Correction Method (IPCM) which Flownex is based on and the Runge Kutta method with Trapezoidal Damping (RKTD) which the generalised thermal-fluid solver Xnet is based on. The IPCM and RKTD employ a staggered grid discretisation scheme on the one dimensional governing equations. Xnet and Flownex were used to predict the transient response of a shell/tube heat exchanger, and their results compared well, thus verifying Flownex.

3.3 Classification and investigation of potential modelling errors

Approaches for modelling the dynamic behaviour of the heat exchangers involve analytical methods, numerical methods, etc. In most cases the numerical methods are preferred due to their versatility, simplicity and availability. However, the results of the numerical methods always have a factor of uncertainty [47]. Thus, in order to reduce the uncertainty, an understanding of the origin of the error and how it propagates is important.

In the application of the numerical discretisation, Water and Wright [48] stated that in principle there are infinite ways of formulating finite difference numerical approximation to the one dimensional heat conduction equation. No single scheme or a family of numerical schemes is known to be superior to the others. They all involve representing a continuous material with a network of nodes and thermal capacities. The number of nodes must be large enough to provide sufficient accuracy provided they are distributed correctly, but on the other hand small enough to avoid excessive computation effort. Waters & Wright [48] and Hensen & Nakhi [47] presented the possible errors and suggested criteria to analyse and minimise these errors. Hensen and Nakhi [47] explained that the total error between the exact solution of the heat conduction equation and the numerical approximation is a combination of the truncation errors, rounding errors and "history errors". Truncation errors originate when the differential equation is replaced by the finite differences and can be minimised by using a scheme with higher truncation error order. The rounding errors result from performing computational analyses with numerical values that have limited significant figures and can be minimised by using double precision arithmetic. The history errors result from the accumulation of errors from previous steps and is related to the growth factor. They also presented that the accuracy of the finite difference scheme can be controlled by appropriate choices of the Fourier number and the factor relating the explicit and/or fully implicit method.

Tuomaala et al. [49] examined errors in the heat flux at the external boundary of a homogeneous slab when even and uneven gridding approaches are employed. The potential of uneven gridding to obtaining a rational compromise between accuracy and computational effort was presented. The surface Biot number and the space increment ratio were the two main parameters for the rational uneven gridding approach. Rational uneven gridding presented more accurate results for small thermal nodes compared to even gridding. Holopainen et al. [50] mentioned that the total number of nodes can be reduced by placing the densest gridding in sections where the curvature of the temperature gradient is steepest when using an uneven gridding method.

3.4 Summary of the literature survey

This literature survey summarised some work of other researchers in terms of the approaches followed in modelling a heat exchanger under transient regime. It further illustrated the potential errors that may arise in the analyses and methods to minimise those errors.

In this project, some of the errors that arise during the modelling are illustrated. However, this project does not present a scientific study on the error analyses and how to minimise them.

Chapter 4

4 Boiler heat exchanger modelling approaches

This chapter presents modelling approaches of a boiler heat exchanger. It entails a systematic presentation of the approaches for modelling heat exchangers. It starts by presenting the use of exact analytical solutions, then the application of numerical methods follows. It finishes with the application of Flownex in modelling boiler heat exchangers. In each approach, issues that needs to be addressed in modelling a boiler heat exchanger with that approach are illuminated.

Carbon steel with properties given in Table 4-1, is used in the analysis.

Table 4-1. Carbon Steel (C ≈ 0.5%) properties [20].

Property	**Symbol**	**Units**	**Value**
Thermal Conductivity	k	W/m.°C	54
Specific Heat Capacity	C	J/kg.°C	465
Density	ρ	Kg/m^3	7833
Diffusivity	κ	m^2/s	1.483×10^{-5}
Thermal expansion Coefficient	α	$°C^{-1}$	13×10^{-6}
Young's Modulus	E	Pa	200×10^6
Poison ratio	υ	-	0.3

4.1 Definitions and terminology

Transients: for a certain body, if there is a change of the boundary values, then a certain time must elapse in order for the body to reach equilibrium temperature conditions. This equilibrium temperature condition is referred to as the steady state condition [20]. However, the phenomenon the body undergoes as it changes its temperature with space and time due to the induced disturbance is referred to as the transients. In the analysis of the transient, the change in internal energy of the body with time is taken into account [20].

The terminology that is used in the transient conduction heat transfer analyses is as follows;
Original state: The state in the body before time equals zero, as demonstrated in Figure 4-1a.
Initial condition/state: the state at time equals to zero, when a change is applied to the boundary conditions, as demonstrated in Figure 4-1b.

Boundaries: the physical limits of the solid, as demonstrated in Figure 4-1c.

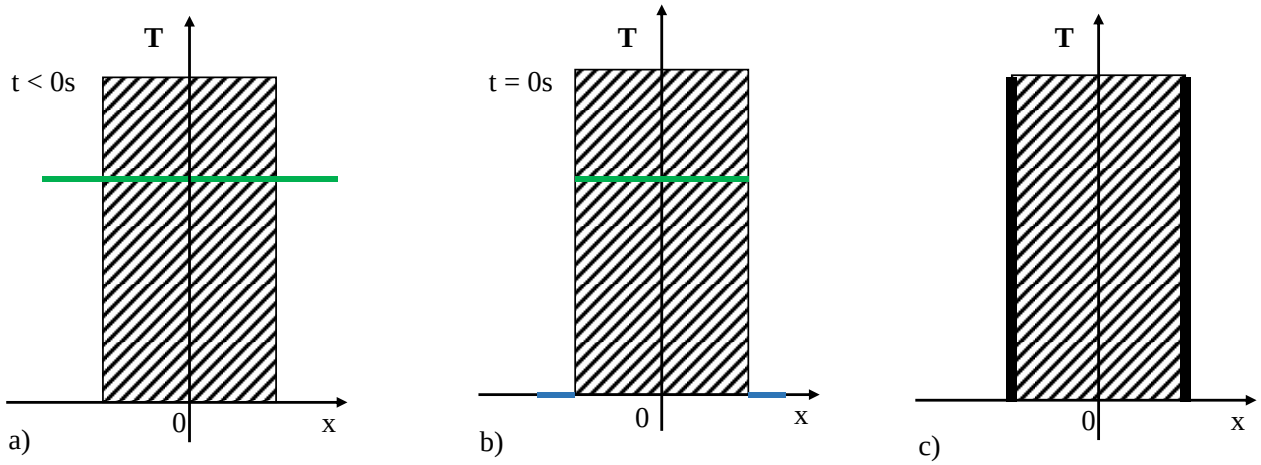

Figure 4-1. Terminology a) Original state, b) Initial condition/ state c) Boundary.

4.2 Application of the exact analytical solution method

In this section, known exact analytical solutions to transient heat conduction 1D scenarios are addressed. Solving the heat conduction equation analytically has limitations. It is often impossible to find exact solutions to cases with complex geometries. Here, simple cases of physical transient heat conduction are considered. These cases are: an infinite plate in Cartesian coordinates and an infinitely long rod and an infinitely long tube in cylindrical coordinates, with different cases of initial and boundary condition.

4.2.1 Infinite plate with constant temperatures at boundaries

A tube wall can be approximated as a plate, especially when it has a large inner radius. Thus, an infinite plate is analysed as a first simple case towards a boiler tube analysis. Consider the infinite plate with thickness *2L* as shown in Figure 4-2. In the figure, the axis are positioned such that the thickness of the plate which is characterised by the *x* axis begins from *–L* to *L* with the vertical axis characterising the temperature. The temperature distribution in the plate and the surroundings for time, $t < 0$ is given by a constant T_{or} as shown in Figure 4-2a. However, at time $t = 0$ a temperature T_L is instantaneously imposed at both boundaries of the plate, as shown in Figure 4-2b with $T_L = 0$. Due to similar boundary conditions, this case has a symmetry at $x = 0$.

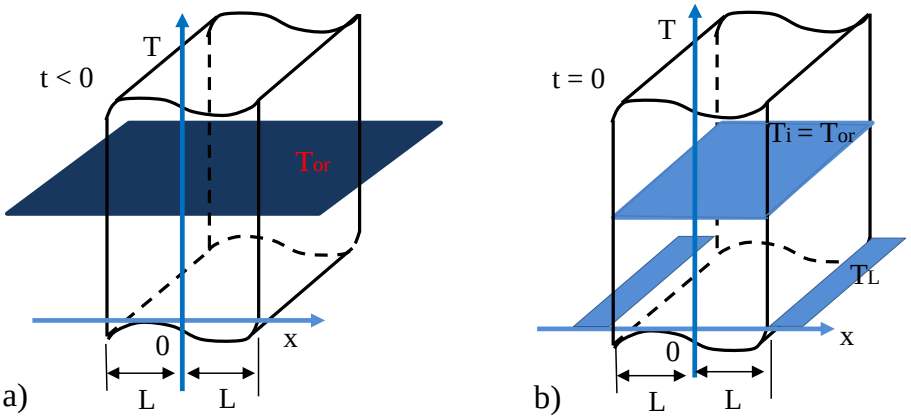

Figure 4-2. The temperature distribution for the infinite plate with constant temperature imposed at the boundaries to initiate a transient a) original state and b) initial condition.

Thus, the initial and boundary conditions can be summarised as:

$$T(x,0) = T_i, \quad t = 0 \qquad \text{initial condition} \tag{4.1}$$

$$T(\pm \mathrm{L}, \mathrm{t}) = 0, \qquad t > 0 \qquad \text{boundary condition} \tag{4.2}$$

Due to the symmetry of this case, it is deduced that:

$$\left(\frac{dT}{dx}\right)_{x\,=\,0} = 0 \tag{4.3}$$

According to Holman [20] and Luikov [51] the solution for the temperature distribution within the material after the initiation of the transient for this case is given by:

$$T(x,t) = T_i \sum_{n=1}^{\infty} \frac{2}{\lambda_n L} \sin(\lambda_n L)\cos(\lambda_n x) e^{-\kappa \lambda_n^2 t} \tag{4.4}$$

with $\lambda_n, n = 1, 2, 3, \ldots$ the roots of:

$$\cos(\lambda_n L) = 0$$

The derivation of equation (4.4) from equation (2.12), as shown by Holman [20] and Luikov [51] is summarised in Appendix A. The temperature distribution from equation (4.4) is graphically shown in Figure 4-3.

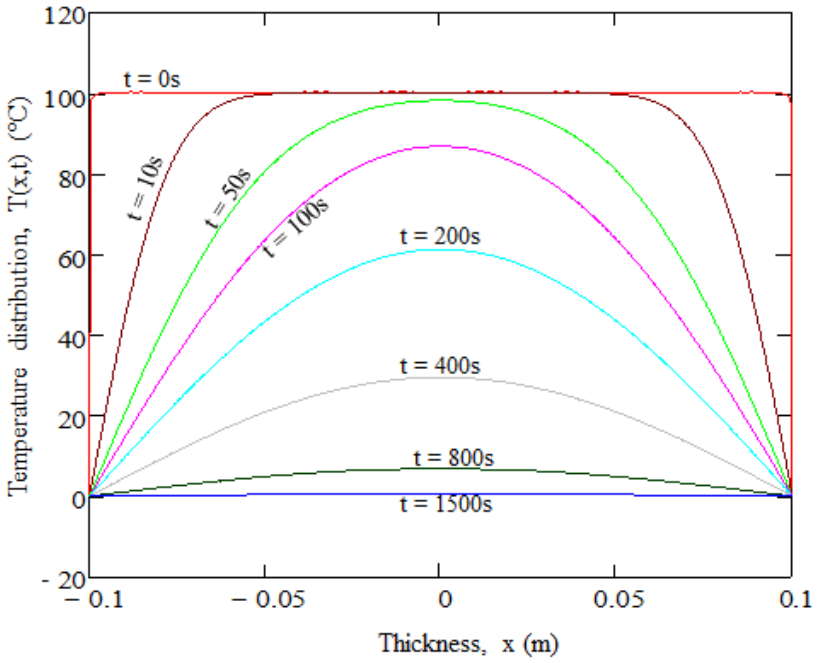

Figure 4-3. Temperature distribution within the infinite steel plate with respect to thickness, x (m) and time, t (seconds) for a case where, initial temperature T_i = 100 °C and temperatures at both boundaries are T_L = 0 °C.

The abrupt change of the boundary conditions results in temperature gradients within the material, as demonstrated in Figure 4-3. These temperature gradients generate forces within the material due to material continuity constraints and thus resulting in thermal stresses, as illustrated in Figure 4-4.

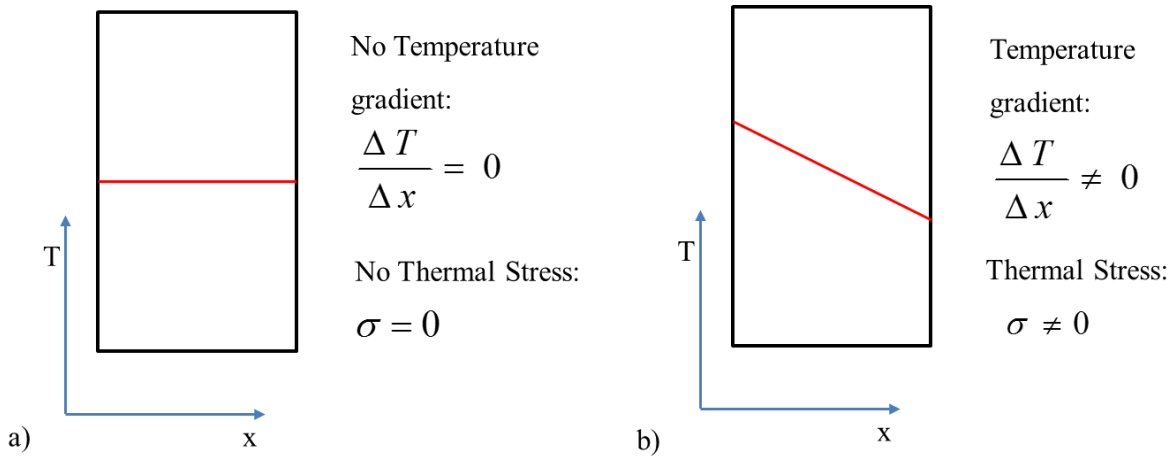

Figure 4-4. Relation between temperature gradients and thermal stresses.

The relationship between the temperature gradients and the thermal stresses within the material is given by equation (4.5) assuming there is no deformation, and the strain $\varepsilon = 0$.

$$\sigma(x,t) = -\alpha E \frac{dT}{dx} \tag{4.5}$$

Thus, the equation for thermal stresses in an infinite plate with the same constant temperatures imposed at the boundaries at time $t=0$ is obtained by differentiating equation (4.4) and substituting it on equation (4.5) to give:

$$\sigma(x,t)=\alpha E\left(T_i\sum_{n=1}^{\infty}\frac{2}{L}\sin(\lambda_n L)\sin(\lambda_n x)e^{-\kappa\lambda_n^2 t}\right) \tag{4.6}$$

This results in the thermal stress distribution given by Figure 4-5. Figure 4-5 shows that the thermal stress is dependent on the temperature gradient. The thermal stress is higher at the highest temperature gradient. Immediately after imposing the boundary condition, the stress is the highest and it decreases as the system adjust itself towards thermodynamic equilibrium, i.e. constant temperature within the body. In this particular case, the stress approaches infinity immediately after the boundary conditions are changed. However, in real life such is not possible, since there is always a temperature gradient at the boundary.

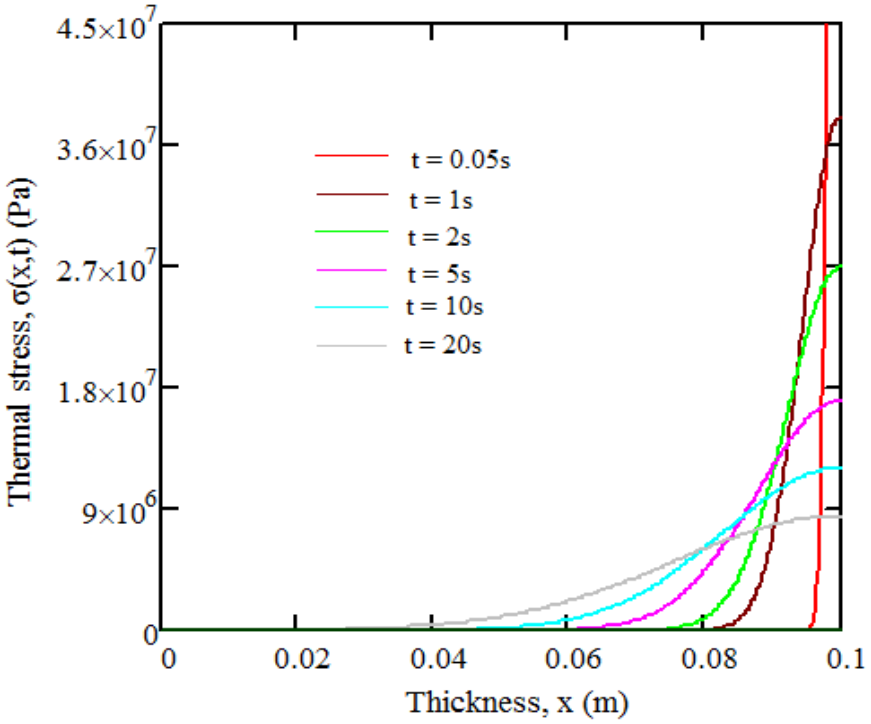

Figure 4-5. Thermal stress distribution within the infinite plate with respect to thickness, x (m) and time, t (seconds) for a case where, initial temperature T_i = 100 °C and temperatures at the boundaries T_L = 0 °C.

4.2.2 Infinite plate with convection at the boundaries

Hereafter, the exact analytical solution for analysing transient heat conduction problems is extended to a case of an infinite plate with imposed temperature gradients through a constant (convection) heat transfer coefficients at the boundaries at time *t = 0*. As mentioned in subsection 4.2.1 above, this case simulates real problems better since there is always a finite temperature gradient at the boundaries even when the heat transfer conditions are suddenly changed at the initial state.

The imposed heat transfer coefficient is such that the problem is symmetrical and the Biot number is greater than one. Originally, the plate and its surroundings had a constant temperature of T_{or} for time $t < 0$, as demonstrated in Figure 4-6a. At time $t = 0$, a fluid with a temperature $T_L = 0$ and convection heat transfer coefficient, h is imposed on the boundaries, as illustrated in Figure 4-6b.

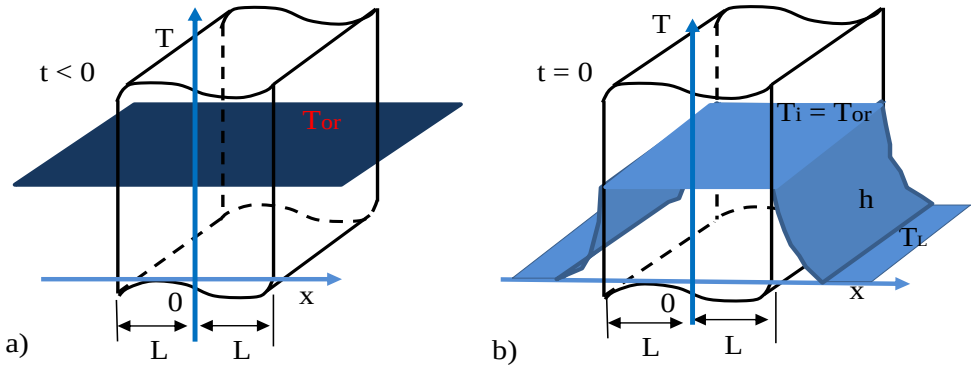

Figure 4-6. The temperature distribution for the infinite plate with a temperature gradient imposed at the boundaries to initiate a transient a) original state and b) initial condition.

According to Luikov [51], the solution for the temperature distribution within the material after inducing the transient for this case is given by equation (4.7), as:

$$\mathrm{T}(x,t) = T_i \sum_{n=1}^{\infty} \left\{ A_n \cos\left(\mu_n \frac{x}{L} \right) \exp\left[-\mu_n^2 Fo \right] \right\} \tag{4.7}$$

with $A_n = \dfrac{2\sin\mu_n}{\mu_n + \sin\mu_n \cos\mu_n} = (-1)^{n+1} \dfrac{2Bi\left(Bi^2 + \mu_n^2\right)^{1/2}}{\mu_n\left(Bi^2 + Bi + \mu_n^2\right)}$

and $\mu_n, n = 1, 2, 3, \ldots$ solutions of:

$$\cot\mu = \frac{\mu}{Bi}$$

An in-depth derivation of this equation is detailed in Luikov [51]. The temperature distribution from equation (4.7) is graphically shown in Figure 4-7.

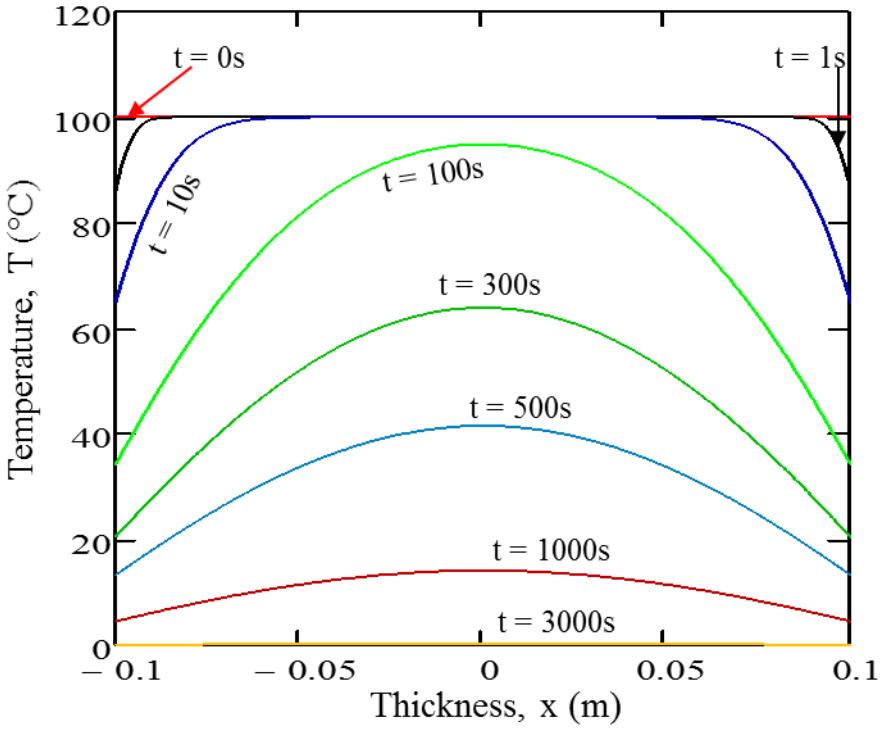

Figure 4-7. Temperature distribution within the infinite steel plate with respect to thickness, x (m) and time, t (seconds) for a case where, initial temperature Ti = 100 °C, fluid temperature, T_L = 0 °C and a Bi = 3.7.

Cengel [28] states that for Fourier number greater than 0.2, $(Fo > 0.2)$ keeping the first term in equation (4.7) and neglecting the remaining terms in the series results in an error of under 2%.

As mentioned in subsection 4.2.1 above, the change of the conditions in the boundaries induces temperature gradients in the material and these gradients result in thermal stresses. From equations (4.5) and (4.7), the thermal stresses for this case are quantified by:

$$\sigma(x,t) = -\alpha E\left(T_i \sum_{n}^{\infty} A_n \frac{\mu_n}{L} \sin\left(\mu_n \frac{x}{L}\right) \exp\left(-\mu_n^2 Fo\right)\right) \tag{4.8}$$

This results in a thermal stress distribution as given by Figure 4-8. Figure 4-8 also shows that the thermal stress is dependent on the temperature gradient. The thermal stress is higher at the highest temperature gradient. Immediately after imposing the boundary conditions, the stress is the highest and it reduces as the system adjust itself towards equilibrium. In this particular case, the stress does not tend to infinity immediately after the boundary conditions are changed compared to the case in Figure 4-5. This is due to the temperature gradients at the boundaries generated by imposing a fluid with convection heat transfer at the boundaries, compared to imposing a constant temperature.

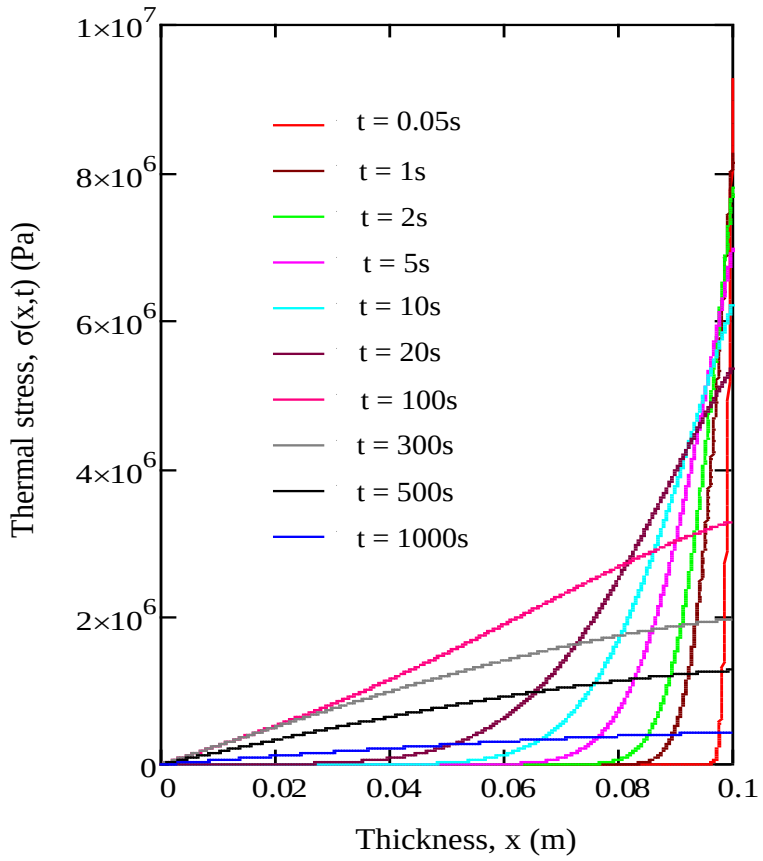

Figure 4-8. Thermal stress distribution within the infinite plate with respect to thickness, x (m) and time, t (seconds) for a case where, initial temperature T_i = 100 °C, fluid temperature, T_L = 0 °C and Bi = 3.7.

It has been demonstrated that the thermal stresses are a function of the temperature gradients, thus the focus onwards will be on temperature calculations.

4.2.3 Infinite cylindrical rod with constant temperature at the boundary

Since the boiler is made of tubes which have relatively small diameters and are cylindrical in shape, then its analysis is more accurate if done using cylindrical coordinates. Thus, this subsection introduces the analysis of transient heat transfer problems which are characterised using cylindrical coordinates. This is done through the analysis of an infinitely long cylindrical rod.

Consider an infinitely long cylindrical rod in which the axial variation of temperature is negligible compared to the radial variation of temperature, as shown in Figure 4-9. The temperature distribution in the rod and its surroundings for time, $t < 0$ is given by a constant T_{or} as shown in Figure 4-9a. At time $t = 0$ a temperature T_a is instantaneously imposed at the boundary of the rod, as shown in Figure 4-9b with $T_a = 0$. Due to similar boundary conditions at $r = -a$ and $r = a$, this case has a symmetry at $r = 0$.

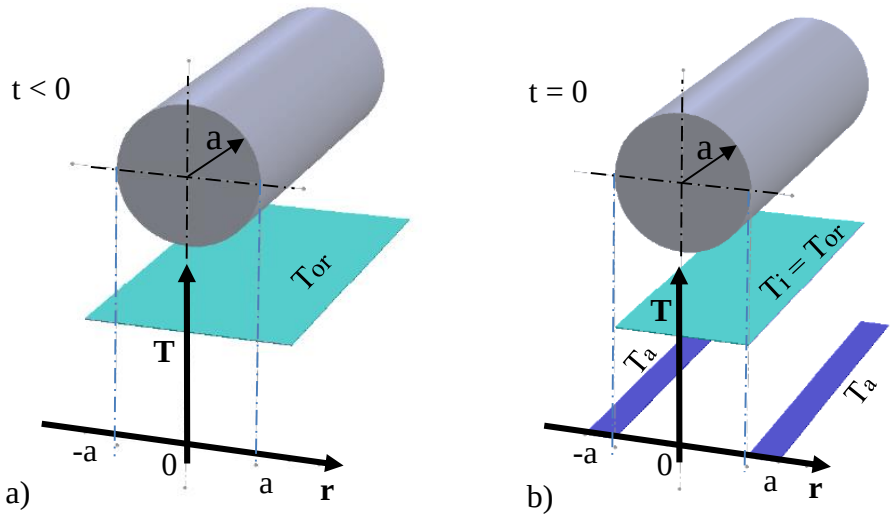

Figure 4-9. Temperature distribution for an infinitely long cylindrical rod with constant temperature imposed at the boundary to initiate a transient a) original state b) initial condition.

According to Carslaw and Jaeger [24], the temperature within the cylinder at a certain time instant and a certain radius can be calculated as:

$$T(r,t) = \frac{2T_i}{a}\sum_{n=1}^{\infty}\frac{J_0(\lambda_n r)}{\lambda_n J_1(a\lambda_n)}e^{-\lambda_n^2 \kappa t} \tag{4.9}$$

with $\lambda_n, n = 1,2,3,\ldots$ roots of:

$$J_0(a\lambda_n) = 0$$

However, choosing to work with dimensionless temperature by using dimensionless variables then:

$$T(r,\tau) = \frac{T(r,t)}{T_i} = 2\sum_{n=1}^{\infty}\frac{J_0\left(\frac{r}{a}\beta_n\right)}{\beta_n J_1(\beta_n)}e^{-\beta_n^2 \tau} \tag{4.10}$$

with

$$\beta_n = a\lambda_n, \quad \tau = \frac{\kappa t}{a^2} \quad \text{and } \kappa = \frac{k}{\rho c}$$

and $\beta_n, n = 1,2,3,\ldots$ roots to:

$$J_0(\beta_n) = 0$$

This solution consists of the Bessel's series which are revised in Appendix B. The derivation of the solution for the temperature distribution as established by Carslaw and Jaeger [24] is summarised in Appendix C. The temperature distribution from equation (4.10) is graphically shown in Figure 4-10.

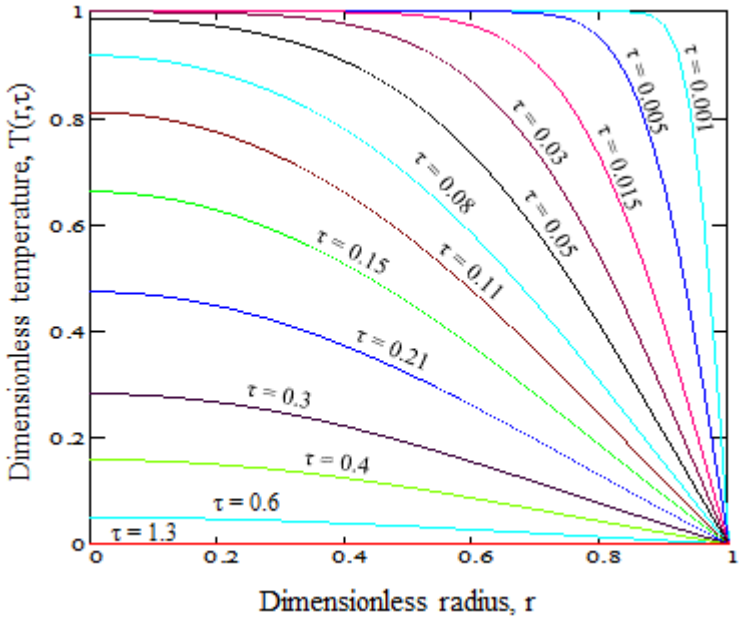

Figure 4-10. Dimensionless temperature distribution within the infinitely long cylindrical steel rod with respect to dimensionless radius r and dimensionless time, τ for a case with, initial temperature T_i and boundary temperature, $T_a = 0$.

4.2.4 Infinite cylindrical rod with convection on the boundary

Now consider a case where the infinitely long cylindrical rod has a temperature gradient imposed at the boundary at time $t = 0$, as shown in Figure 4-11. The infinitely long cylindrical rod had its temperature and the surrounding temperatures originally set at a constant temperature, T_{or}, as illustrated in Figure 4-11a. However, at time $t = 0$ a fluid with temperature $T_a = 0$ and heat transfer coefficient h is imposed at the boundary, as demonstrated in Figure 4-11b.

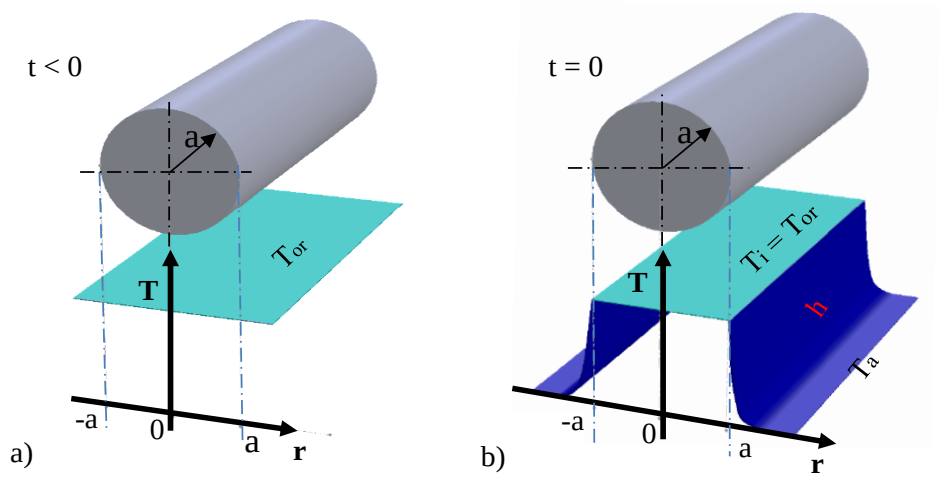

Figure 4-11. Temperature distribution for an infinitely long cylindrical rod with a temperature gradient imposed at the boundary to initiate a transient a) original state b) initial condition.

According to Carslaw and Jaeger [24], the temperature distribution within the rod with respect to time and radius after inducing the transient is given by:

$$T(r,t) = \frac{2T_i h}{a} \sum_{n=1}^{\infty} \frac{J_0(\lambda_n r)}{(h^2 + \lambda_n^2) J_0(a\lambda_n)} e^{-\lambda_n^2 \kappa t} \tag{4.11}$$

where $\lambda_n, n = 1, 2, 3, \ldots$ are roots of:

$$\lambda J_1(\lambda a) = h J_0(\lambda a)$$

Simplifying equation (4.11) to work with dimensionless variables, let:

$$\beta_n = a\lambda_n, \quad \tau = \frac{\kappa t}{a^2} \quad \text{and} \quad A = ah$$

Thus, the dimensionless temperature distribution is given by:

$$T(r,\tau) = \frac{T(r,t)}{T_i} = \sum_{n=1}^{\infty} \frac{2AJ_0\left(\frac{r}{a}\beta_n\right)}{(\beta_n^2 + A^2) J_0(\beta_n)} e^{-\beta_n^2 \tau} \tag{4.12}$$

where $\beta_n, n = 1, 2, 3, \ldots$ are the roots of:

$$\beta J_1(\beta) = A J_0(\beta)$$

This solution also consists of the Bessel's series which are revised in Appendix B. An in-depth derivation of the solution for the temperature distribution is detailed in Carslaw and Jaeger [24].

The temperature distribution from equation (4.12) is graphically shown in Figure 4-12. At shorter time instances, the temperature at the boundary of the rod is higher than that of the fluid, however as time progresses the temperature moves towards the temperature of the fluid until it attains it, first at the boundary then varies radially until it reaches the whole body at steady or equilibrium state.

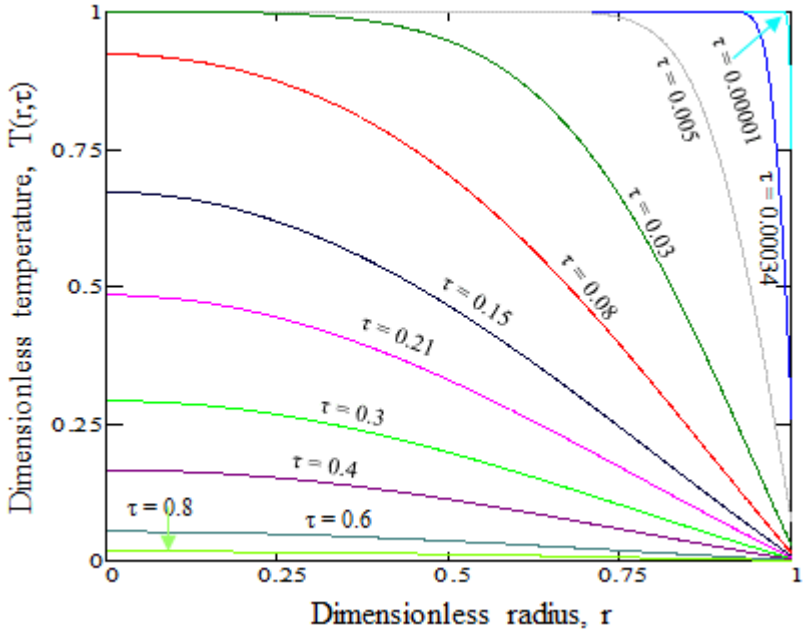

Figure 4-12. Dimensionless temperature distribution within the infinitely long cylindrical steel rod with respect to dimensionless radius r and dimensionless time, τ for a case with, initial temperature, T_i and a fluid with a temperature, $T_a = 0$ and heat transfer coefficient h = 3000.

4.2.5 Infinitely long tube

A rod cannot represent a tube, but it was merely introduced as a base case to the analyses of a tube. Thus, in this section exact analytical solutions of an infinitely long tube are used in the analyses. For this case, axial and circumferential temperature variations are neglected, only radial temperature variation is considered.

Consider an infinitely long tube with inner radius, *a* and outer radius, *b*, as shown in Figure 4-13.

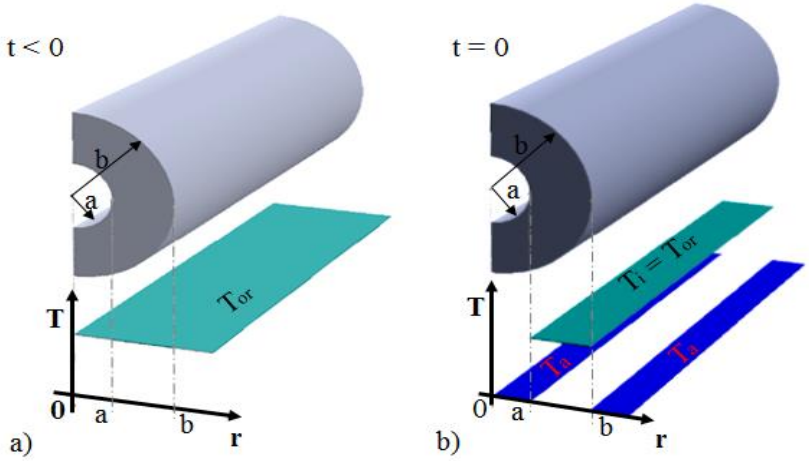

Figure 4-13. Temperature distribution for an infinitely long tube with same constant temperatures imposed at the boundaries to initiate a transient a) original state b) initial condition.

As with the previous cases, consider the infinitely long tube in which its temperature and the surrounding temperatures originally $(t < 0)$ are at a constant temperature, T_{or}, as illustrated in Figure 4-13a. However, at time $t = 0$ the temperatures at both the inner and outer boundary are changed to zero, $T_a = 0$ and $T_b = 0$, as demonstrated in Figure 4-13b.

According to Luikov [51], for such induced transient, the temperature distribution within the infinitely long tube with respect to time and radius starting immediately after the initiation of the transient is given by:

$$T(r,t) = T_i \pi \sum_{n=1}^{\infty} \frac{J_0(\lambda_n b) V_0(\lambda_n r)}{[J_0(\lambda_n a) + J_0(\lambda_n b)]} e^{-\lambda_n^2 \kappa t} \tag{4.13}$$

where $\lambda_n, n = 1, 2, 3, \ldots$ are roots of the characteristic equation given by:

$$J_0(\lambda b) Y_0(\lambda a) - J_0(\lambda a) Y_0(\lambda b) = 0$$

However, before writing the solution in terms of dimensionless variables, let:

$$\beta_n = \lambda_n a, \quad \tau = \frac{\kappa t}{a^2} \quad \text{and} \quad m = \frac{b}{a}$$

Thus, the dimensionless temperature distribution is given by:

$$T(r,\tau) = \pi \sum_{n=1}^{\infty} \frac{J_0(\beta_n) V_0\left(\frac{r}{a}\beta_n\right)}{[J_0(\beta_n) + J_0(m\beta_n)]} e^{-\beta_n^2 \tau} \tag{4.14}$$

where $\beta_n, n = 1, 2, 3, \ldots$ are roots of:

$$J_0(m\beta) Y_0(\beta) - J_0(\beta) Y_0(m\beta) = 0$$

The full derivation of the solution for the temperature distribution is detailed by Luikov [51]. The dimensionless temperature distribution from equation (4.14) is graphically shown in Figure 4-14. At dimensionless time, $\tau = 0$ the graph has some oscillations which intensify near the boundaries. These oscillations are due to insufficient summed series in the solution, in order for the continuous graphs to be able to define the step change in temperature or a discontinuity at the boundaries, as described in Ingersoll et al [52]. However, increasing the number of summed terms requires a more numerically accurate computer software and it will take time to solve.

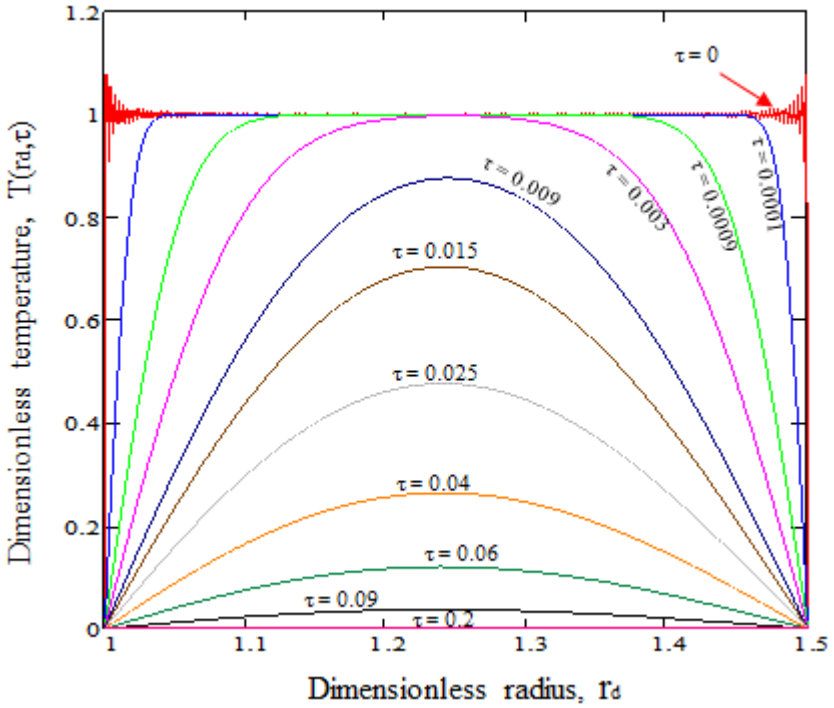

Figure 4-14. Dimensionless temperature distribution within the infinitely long tube with respect to dimensionless radius, r_d and dimensionless time, τ for a case with, initial temperature, T_i and inner and outer boundary temperature, $T_a = 0$ and $T_b = 0$, respectively.

For a tube, different transients can be initiated at the boundaries. Consider a case where the transient introduced at the inner boundary is different to that of the outer boundary of an infinitely long tube, illustrated in Figure 4-15.

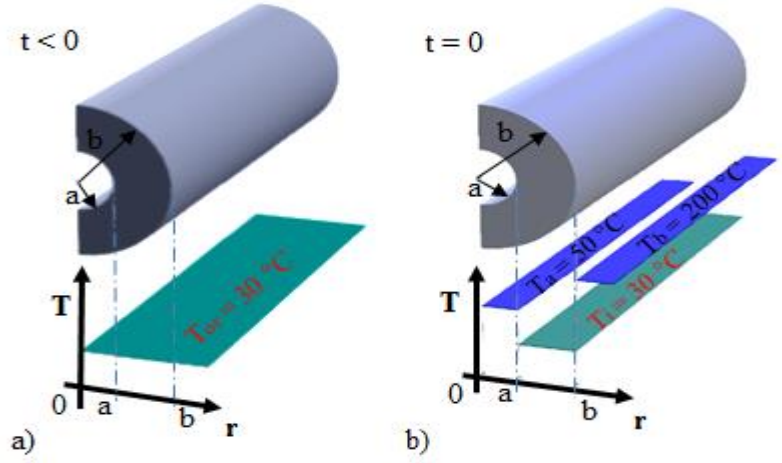

Figure 4-15. Temperature distribution for an infinitely long tube with different temperatures imposed at the different boundaries to initiate a transient a) original state b) initial condition.

Originally $(t < 0s)$ the infinitely long tube had its whole body temperature and the surrounding temperatures set at a constant temperature, $T_{or} = 30\ °C$ as illustrated in Figure 4-15a. At time $t = 0s$

the temperature at the inner boundary is changed to 50 °C, $T_a = 50\ °C,$ and the temperature at the outer boundary is changed to 200°C, $T_b = 200\ °C,$ as demonstrated in Figure 4-15b.

According to Luikov [51], the temperature distribution within the infinitely long tube with respect to time and radius after inducing the transient is given by:

$$T(r,t) = \frac{T_a \ln\left(\frac{b}{r}\right) + T_b \ln\left(\frac{r}{a}\right)}{\ln\left(\frac{b}{a}\right)} + \pi \sum_{n=1}^{\infty} \frac{J_0(\lambda_n b) V_0(\lambda_n r) e^{-\lambda_n^2 \kappa t}}{J_0(\lambda_n a) + J_0(\lambda_n b)} \left(T_i - \frac{T_b J_0(\lambda_n a) - T_a J_0(\lambda_n b)}{J_0(\lambda_n a) - J_0(\lambda_n b)} \right) \quad (4.15)$$

where $\lambda_n, n = 1, 2, 3, \ldots$ are roots of:

$$J_0(\lambda b) Y_0(\lambda a) - J_0(\lambda a) Y_0(\lambda b) = 0$$

The full derivation of the solution for the temperature distribution is detailed by Luikov [51]. The temperature distribution from equation (4.15) is graphically shown in Figure 4-16.

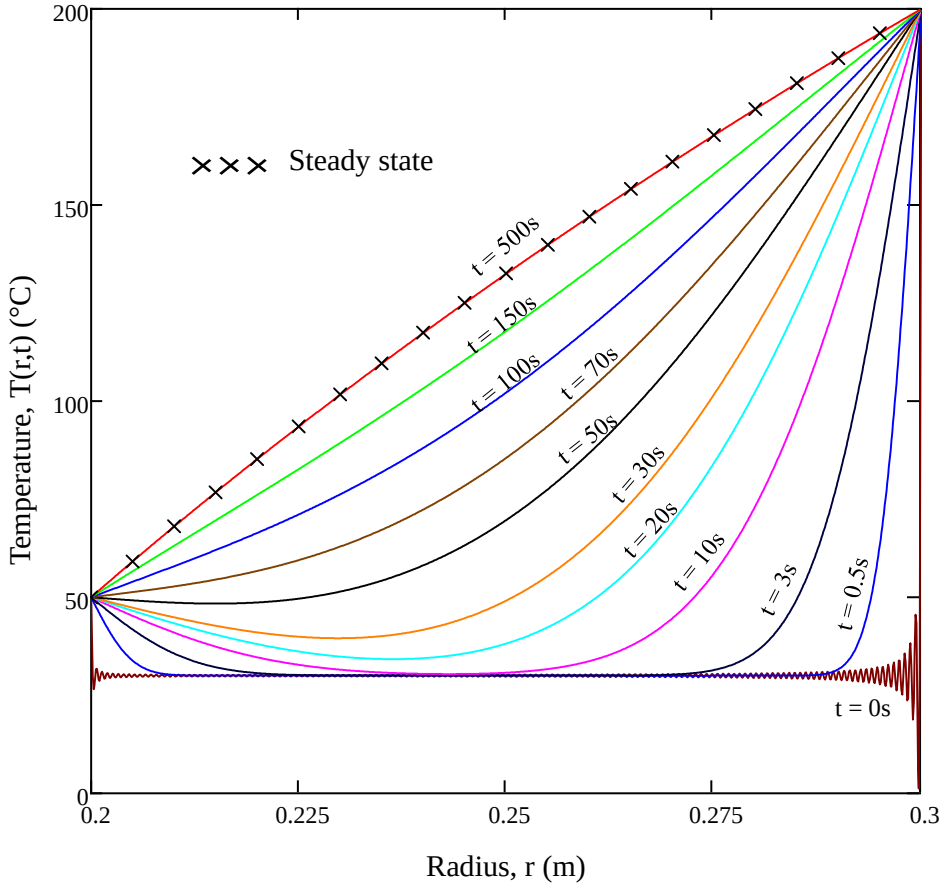

Figure 4-16. Temperature distribution within the radius of an infinitely long tube of 0.2 m inner radius and 0.3 m outer radius, subjected to a step change of temperature to 50 °C on the inner boundary and 200 °C on the outer boundary, originally at 30 °C.

Considering another different transient on the infinitely long tube. Originally $(t < 0s)$ the infinitely long tube had its whole body temperature and the surrounding temperatures at a constant temperature, $T_{or} = 120\ °C,$ as illustrated in Figure 4-17a. At time $t = 0s$ the temperature at the inner boundary is changed to 50 °C, $T_a = 50\ °C,$ and the temperature at the outer boundary is changed to 200 °C, $T_b = 200\ °C,$ as demonstrated in Figure 4-17b.

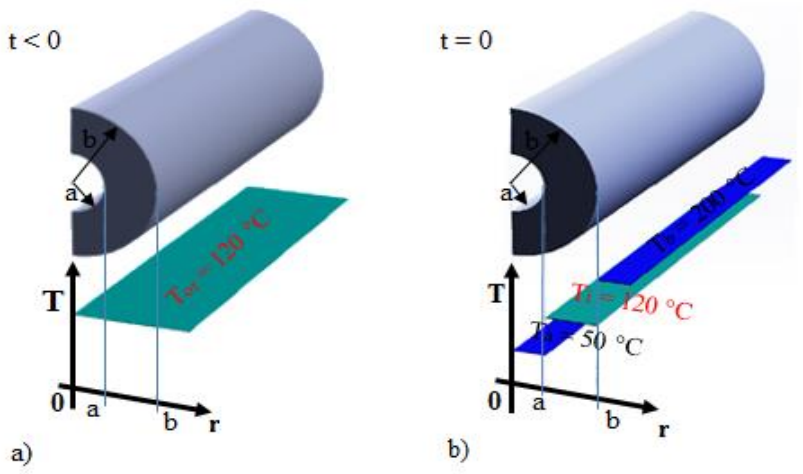

Figure 4-17. Temperature distribution for an infinitely long tube a) original state b) initial condition

This transient is also mathematically described by equation (4.15) and the transient radial temperature distribution is graphically shown in Figure 4-18.

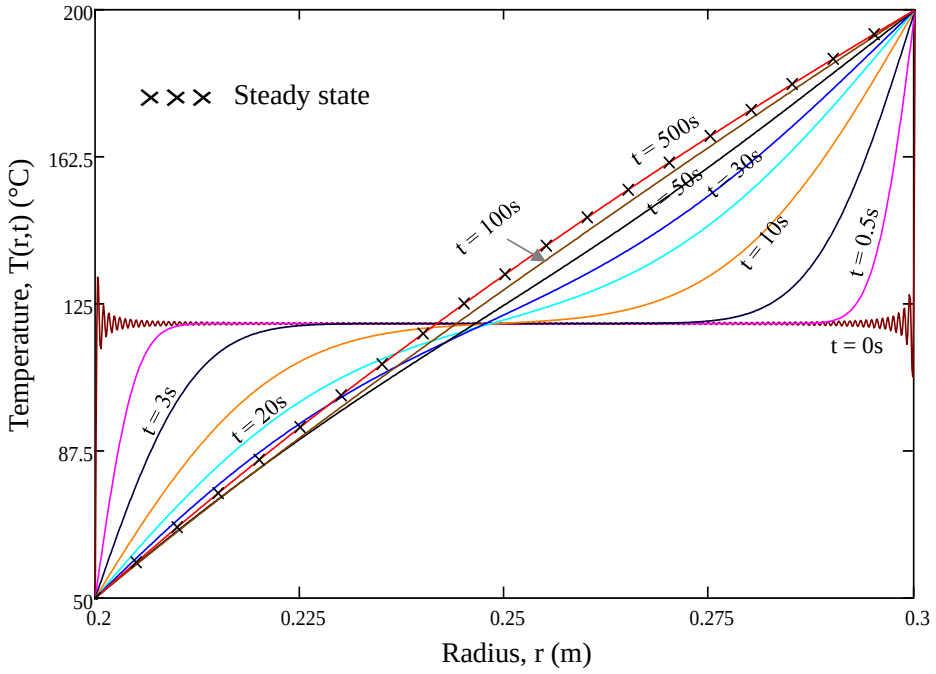

Figure 4-18. Temperature distribution within the radius of an infinitely long tube of 0.2 m inner radius and 0.3 m outer radius, subjected to a step change of temperature to 50 °C on the inner boundary and 200 °C on the outer boundary, originally at 120 °C.

4.2.6 Summary

This section illustrated the application of the exact analytical solutions to transient heat transfer problems. Although the problems that were analysed are relatively simple, it established the understanding of transient conduction heat transfer. In addition, it demonstrated the temperature and thermal stresses distribution within the material from just after the initiation of the transient until equilibrium is reached.

However, these exact solutions are limited to only simplified problems. Attempting to extend them to analysing real problems with geometry complications and boundary conditions changing with time is impossible. Thus, another method of analyses is required to analyse the boiler heat exchangers which has tubes with complex geometries and time-dependant boundary conditions.

4.3 Application of finite volume numerical method

Due to the limitations of the exact analytical solutions in analysing heat transfer problems with complex geometries, complicated boundaries amongst others, numerical methods are used for such problems. As introduced in chapter 2, numerical methods are approximations of the exact solution of the heat conduction equation found through discretising the computational domain, discretising the governing equations and solving the resulting algebraic equations. Here, the finite volume method (FVM) is used to analyse an infinitely long tube. The derivations of the FVM are presented in Appendix D. The derived equations were solved via matrix multiplication with a code written on MathCad.

4.3.1 Finite volume method on an infinitely long tube

Characterising the transient radial temperature distribution within the material on an infinitely long tube with FVM entails deriving the solution. The FVM requires that the problem should be discretised in physical space as well as with time, as illustrated in Appendix D.

4.3.1.1 Discretisation in space

Discretisation in space involves discretising the thickness of the tube into small control volumes which is a mesh of nodes on the radius since there is no variation in the axial and circumferential directions, as illustrated in Figure 4-19. Half control volumes are employed on the boundaries, to ensure that the temperature nodes are positioned exactly on the tube surfaces. This enables direct calculation or specification of the surface temperatures.

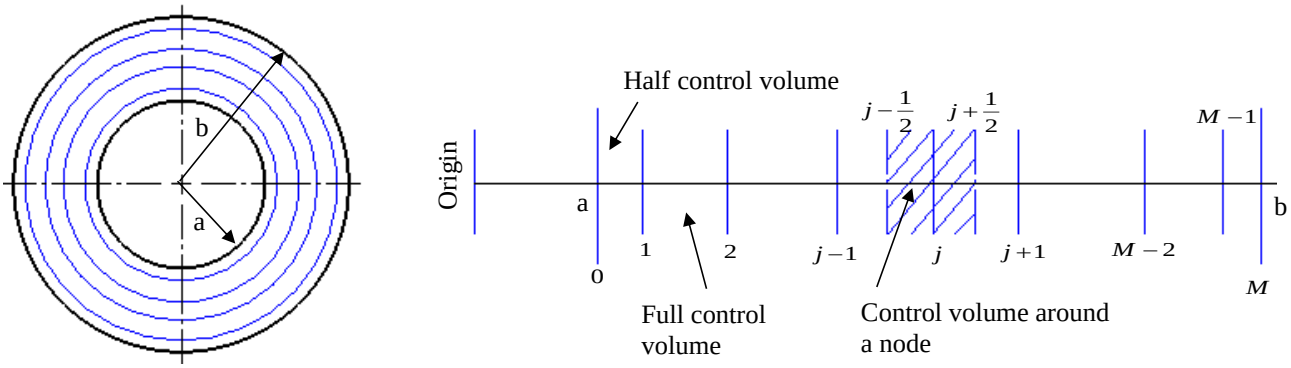

Figure 4-19.Radial discretisation of the thickness of the tube.

Applying the FVM entails integrating the governing one dimensional heat conduction equation over the control volume that is defined around each grid point. The heat fluxes crossing the boundaries of the control volumes are approximated by writing them in terms of the discrete values of the temperatures at the grid points. For the internal nodes the heat fluxes at the boundaries are conduction heat fluxes. Thus, the temperature differentials on the boundaries are approximated via the discrete temperature gradients based on the values of the temperatures at the neighbouring nodes. After simplifications, the equation for interior nodes is given by:

$$\frac{\partial T_j}{\partial t} \approx a_{j+1}T_{j+1} + a_{j-1}T_{j-1} - a_j T_j \tag{4.16}$$

with

$$a_{j-1} = \frac{2\kappa r_{j-\frac{1}{2}}}{\left(r_{j+\frac{1}{2}}^2 - r_{j-\frac{1}{2}}^2\right)\left(r_j - r_{j-1}\right)}$$

$$a_{j+1} = \frac{2\kappa r_{j+\frac{1}{2}}}{\left(r_{j+\frac{1}{2}}^2 - r_{j-\frac{1}{2}}^2\right)\left(r_{j+1} - r_j\right)}$$

$$a_j = a_{j-1} + a_{j+1}$$

However, at the boundaries the equations for a_{j-1}, a_j and a_{j+1} differ depending on the boundary conditions that are applied, but equation (4.16) still applies.

4.3.1.2 Time-wise discretisation

For transient problems, time-wise discretisation is also needed. If the time dependent source on right hand side of equation (4.16) is defined by:

$$S_p(t) = a_{j+1}T_{j+1} + a_{j-1}T_{j-1} - a_j T_j \tag{4.17}$$

Equating the defined source term to the terms on the left hand side of equation (4.16) and integrating over a discrete time step with size Δt results in equation (4.18) for a specific node j in space. Since the source term is an unknown function of time, then it can be approximated as a weighted average between the old time step and the new time step.

$$T_j^{i+1} \approx T_j^i + \left(\alpha S_j^{i+1} + (1-\alpha) S_j^i\right)\Delta t \tag{4.18}$$

The superscripts i and $i+1$ represent the old and the new time steps, respectively. α is an integration weighting factor that determines which time-wise integration scheme to be used. If $\alpha = 0$ the solution scheme is *explicit* since it is solved from known temperatures and if $\alpha = 1$ the solution scheme is *fully implicit*, since it only uses the unknown temperatures. For $0 < \alpha < 1$ the solution scheme is *semi-implicit*, since it uses both known and unknown temperatures. A special case of a semi – implicit scheme is for $\alpha = 0.5$ and it is called the *Crank-Nicolson Scheme*.

4.3.2 Infinitely long tube with constant temperatures at boundaries

Consider a case of an infinitely long tube where the transients introduced at the inner boundary is different to that of the outer boundary, as illustrated in Figure 4-20.

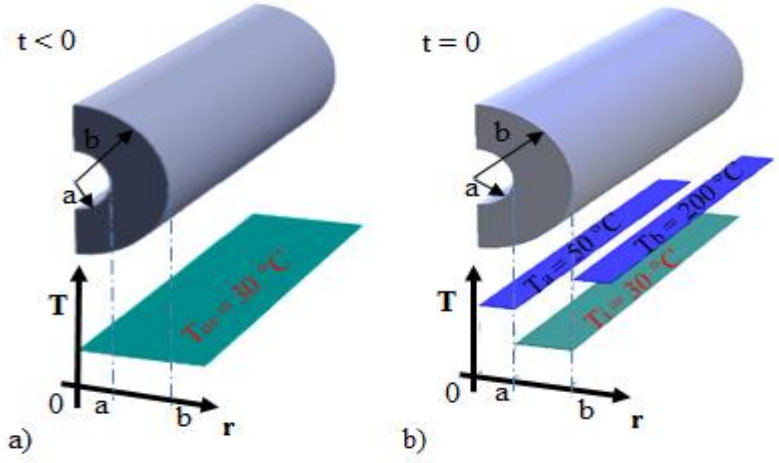

Figure 4-20. Temperature distribution for an infinitely long tube with different constant temperatures imposed at the different boundaries to initiate a transient a) original state b) initial condition.

Originally $(t < 0s)$ the infinitely long tube's whole body and the surrounding are at a constant temperature, $T_{or} = 30\ °C,$ as illustrated in Figure 4-20a. At time $t = 0s$ the temperature at the inner boundary is changed to 50 °C, $T_a = 50\ °C,$ and the temperature at the outer boundary is changed to 200 °C, $T_b = 200\ °C,$ as demonstrated in Figure 4-20b.

In characterising the transient radial temperature distribution for such a case, the internal nodes are defined by the combination of equations (4.16) and (4.18). The internal nodes for the first time step $i=0$ are defined as $T_j = T_{or}$. For this case the inner and outer boundary temperatures are specified as $T_0 = T_a$ and $T_M = T_{b,}$ respectively, for all time steps. The temperature distribution within the material at specific radius and time was calculated by performing matrix multiplications in MathCad and illustrated graphically on Figure 4-21 for 995 nodes on the radius and a time step of size $\Delta t = 0.01\text{s}$.

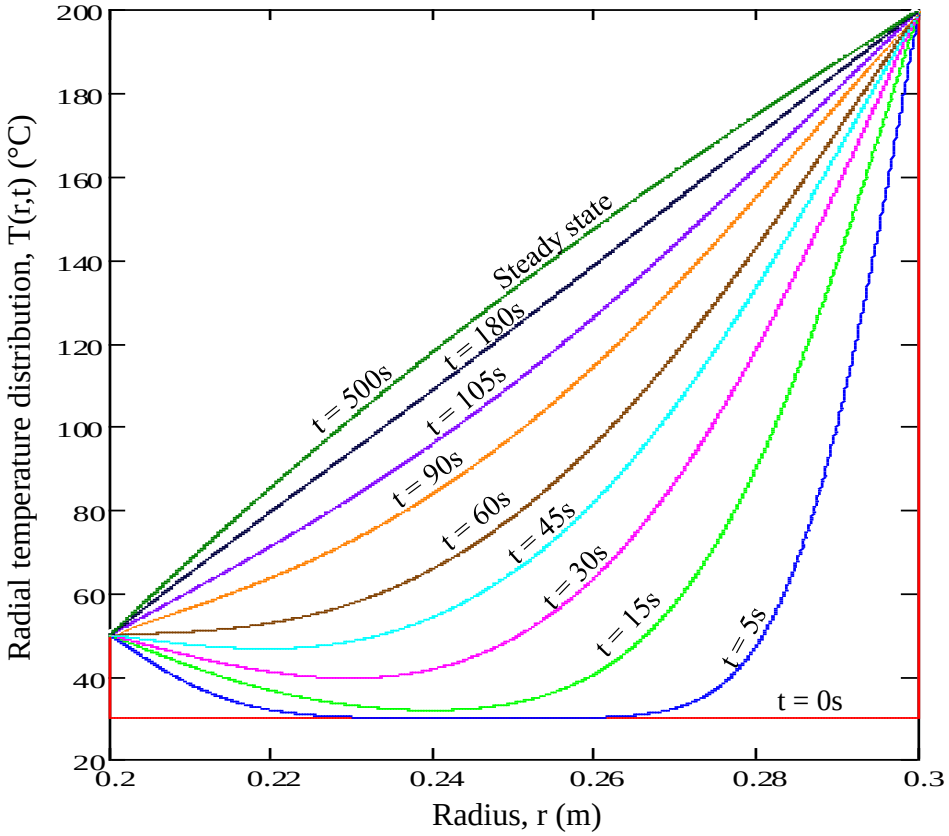

Figure 4-21. Temperature distribution within the thickness of an infinitely long tube of 0.2 m inner radius and 0.3 m outer radius, subjected to a step change of temperature to 50 °C on the inner boundary and 200 °C on the outer boundary, originally at 30 °C.

For a good numerical solution, the generated temperature distribution curves has to be the same as those from exact analytical solution for the same scenario. This accuracy depends on the space and time-wise discretisation.

4.3.2.1 Dependence on the discretisation in physical space

Hereafter, the dependence of the discretisation in physical space on the results of the numerical solution for the particular case of an infinitely long tube with constant temperatures imposed at the boundary at initial state is checked. This checking is done through a comparison of the numerical solution to the

exact analytical solution. A fine time step of size $\Delta t = 0.01s$ is used with two different number of nodes on the radius (radius grid), as illustrated in Figure 4-22 and Figure 4-23. This also serves as a verification of the numerical solution derivation and implementation.

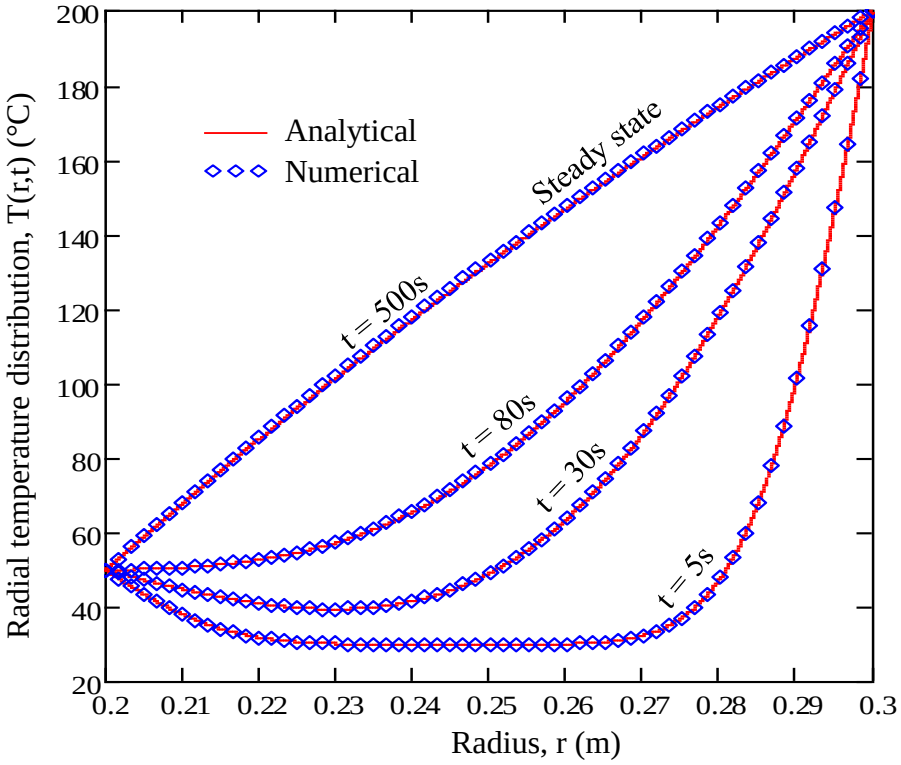

Figure 4-22. Comparison of numerical solution (blue shapes) vs exact analytical solution (continuous red line) for a fine radial grid of 61 nodes and a fine time grid of Δt = 0.01s.

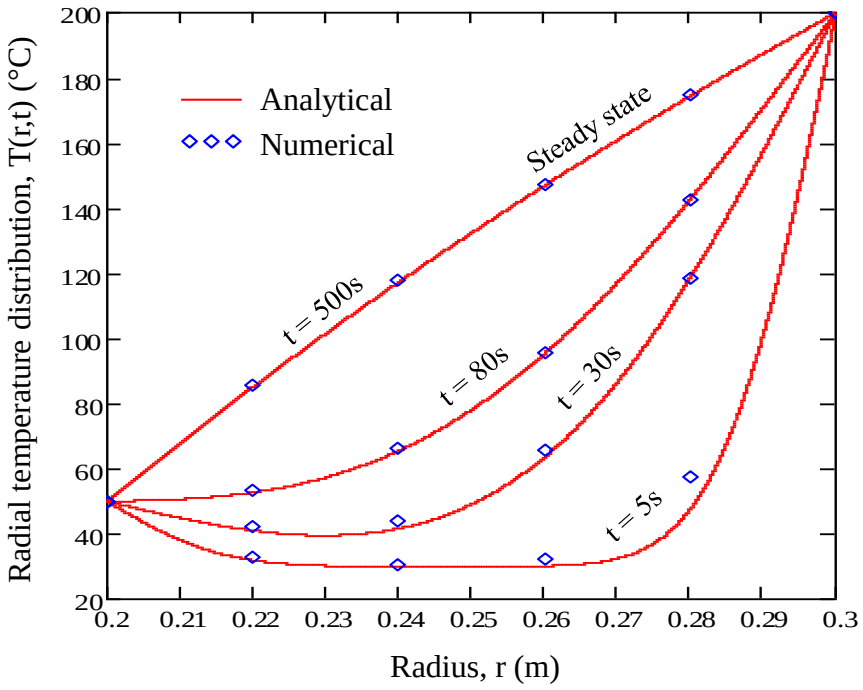

Figure 4-23. Comparison of numerical solutions (blue shapes) vs analytical solutions (continuous red lines) for a radial grid of 6 nodes and the same fine time grid as on Figure 4-22 of Δt = 0.01s.

Figure 4-22 and Figure 4-23 illustrate that the accuracy of the temperature distribution from the numerical method at a certain radius decreases with the number of nodes, thus resulting in errors on the calculated temperature values.

If the error is defined as the difference in temperature at a particular radius for the numerical solution compared to the exact analytical solution at a particular time, then this error can be characterised with the Two Norm. The Two Norm is the square root of the sum of the square of the absolute error of all the entries and it is given by:

$$\|e\|_2 = \sqrt{\sum_{i=0}^{n} |e_i|^2} \tag{4.19}$$

With $e_i = T_{exact} - T_{numerical}$. An increase in the Two Norm implies an increase in the overall error on the whole temperature profile. Figure 4-24 illustrates the Two Norm for the particular case analysed here and it shows that for this case the error associated with the numerical solution decreases when the radius grid nodes increases.

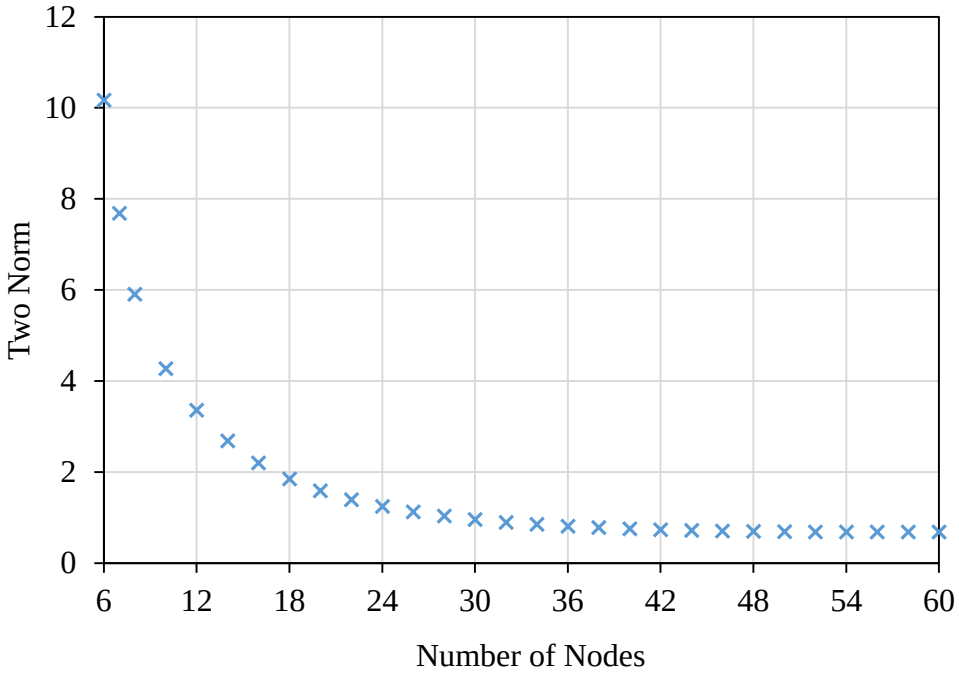

Figure 4-24. Two Norm graph with change in number of nodes at time t = 5s for time step size of Δt = 0.01s.

A close inspection of the error in the whole temperature profile as per the FVM numerical analyses is given in Figure 4-25 and Figure 4-26. It illustrates that the numerical solution gives the temperature at the centre of each discrete grid spacing, which then represent the temperature of that particular grid spacing as demonstrated by the step graphs. As the grid becomes smaller the approximation of the temperature in the grid spacing becomes better.

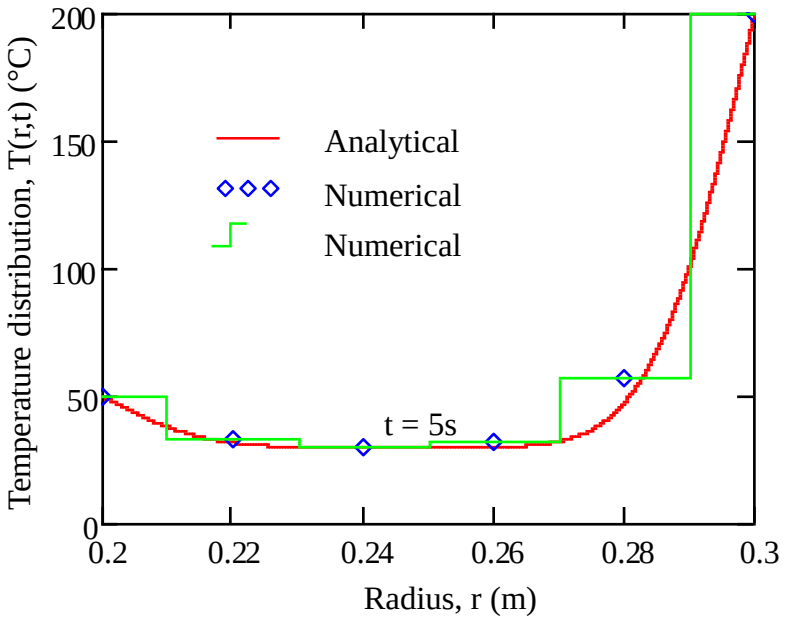

Figure 4-25. Comparison of numerical solutions (blue shapes) vs analytical solutions (continuous red line) for 6 nodes and the same fine time grid of Δt = 0.01s at time t = 5s.

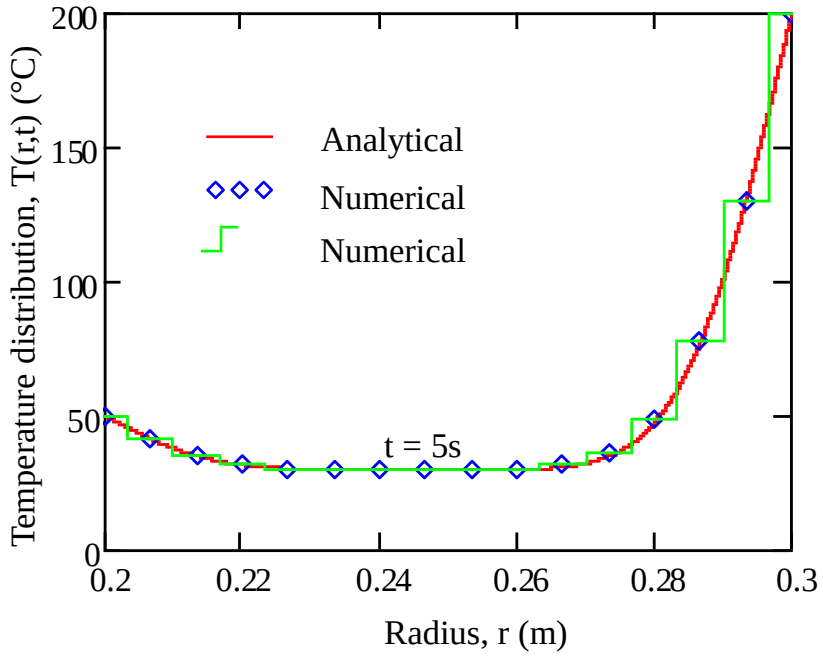

Figure 4-26. Comparison of numerical solutions (blue shapes) vs analytical solutions (continuous red line) for 16 nodes and the same fine time grid as in Figure 4-25 of Δt = 0.01s at time t = 5s.

4.3.2.2 Dependence on time-wise discretisation

The time step size between solving time steps at a particular radius is investigated hereafter for the same example case as for the thickness grid spacing seen in the previous subsection. For this investigation, the thickness number of nodes is kept at 61 nodes, as illustrated in Figure 4-22 and Figure 4-24 for the thickness grid to generate minimal errors. Two cases of different time step sizes Δt are

investigated. Figure 4-27 and Figure 4-28 demonstrate that the inaccuracy of the numerical solution increases with an increase in time step size between solving steps.

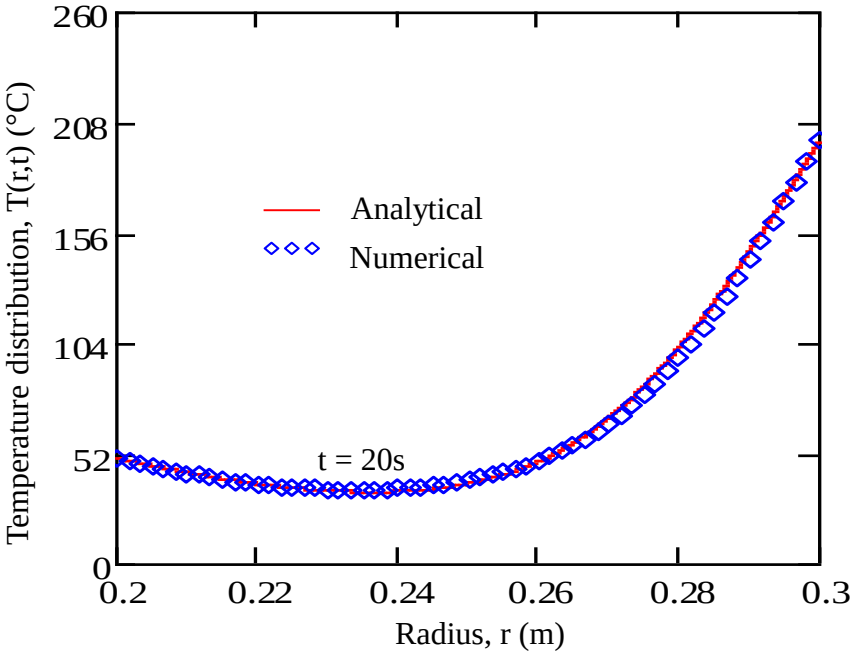

Figure 4-27. Comparison of numerical solutions vs analytical solutions for thickness grid of 61 nodes and time step size of Δt = 5s at time t = 20s.

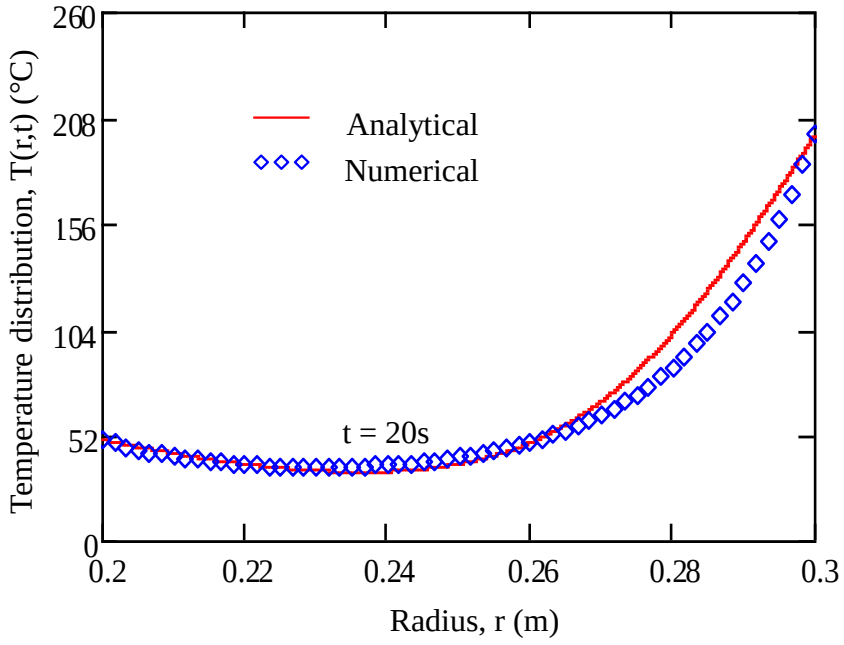

Figure 4-28. Comparison of numerical solutions vs analytical solutions for thickness grid of 61 nodes and time step size of Δt = 20s at time t = 20s.

The error due to time-wise discretisation can be characterised using the Two Norm, as illustrated in Figure 4-29, for the case of an infinitely long tube analysed here. Figure 4-29 illustrates that the error reduces as the time step size decreases.

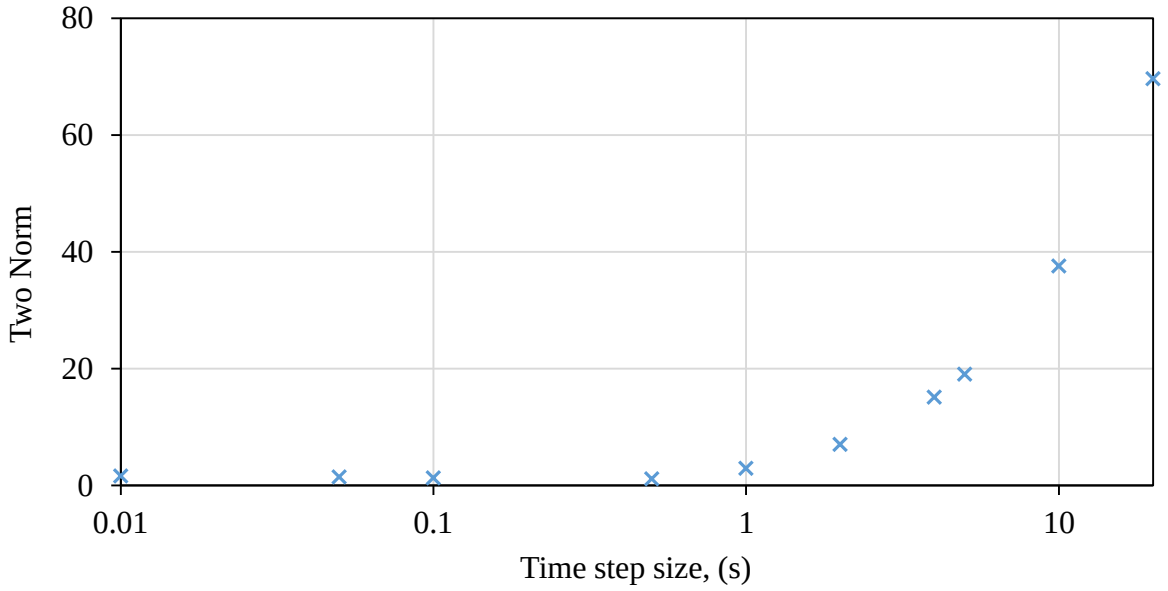

Figure 4-29. Two Norm graph with change in time step size at time t = 20s for 61 nodes.

4.3.3 Infinitely long tube with convection at the boundaries

This subsection presents the last example of numerical solution that will be used to be compared with Flownex results in the next chapter. This numerical solution is applied to an infinitely long tube in which temperature gradients are imposed at the initial state at both boundaries through heat transfer coefficients.

The original state and initial condition of the case analysed here are shown in Figure 4-30.

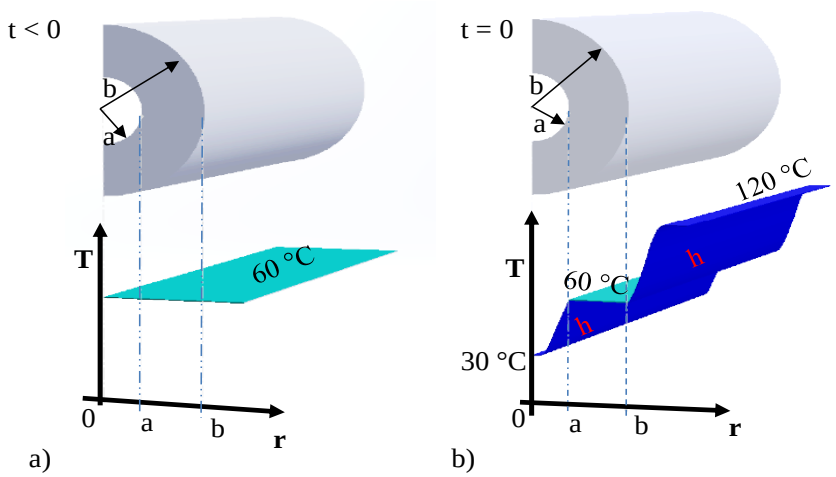

Figure 4-30. Temperature distribution for an infinitely long tube with convection imposed at the boundaries to initiate a transient a) original state b) initial condition.

This case is such that the infinitely long tube originally had its temperature and the surrounding temperatures set at a constant temperature, $T_{or} = 60\ °C$, as illustrated in Figure 4-30a. At time $t = 0s$ a

fluid with temperature $T_{fa} = 30\ °C$ and heat transfer coefficient $h = 2000\ W/m^2 °C$ is imposed at the inner boundary and another fluid with temperature $T_{fb} = 120\ °C$ and heat transfer coefficient $h = 2000\ W/m^2 °C$ is imposed on the outer boundary, as demonstrated in Figure 4-30b.

In characterising the transient radial temperature distribution for such a case, the interior nodes are defined by the combination of equations (4.16) and (4.18). The interior nodes for the first time step $i = 0$ are defined as $T_j = T_{or}$. At the boundaries the equations are derived with the half control volume. For the inner boundary, the derived equation is:

$$\frac{\partial T_0}{\partial t} \approx a_W T_{fa} - a_0 T_0 + a_1 T_1 \tag{4.20}$$

with

$$a_W = \frac{2\kappa Bi_0}{\left(r_{1/2}^2 - r_0^2\right)}$$

$$a_1 = \frac{2\kappa r_{1/2}}{\left(r_{1/2}^2 - r_0^2\right)\left(r_1 - r_0\right)}$$

$$a_0 = a_1 + a_W$$

and for the outer boundary the derived equation becomes:

$$\frac{\partial T_M}{\partial t} \approx a_{M-1} T_{M-1} - a_M T_M + a_W T_{fb} \tag{4.21}$$

with

$$a_{M-1} = \frac{2\kappa r_{M-1/2}}{\left(\left(r_M\right)^2 - \left(r_{M-1/2}\right)^2\right)\left(r_M - r_{M-1}\right)}$$

$$a_E = \frac{2\kappa Bi_M}{\left(\left(r_M\right)^2 - \left(r_{M-1/2}\right)^2\right)}$$

$$a_M = a_{M-1} + a_E$$

where $Bi = \frac{hr}{k}$ is the local Biot number. Performing matrix multiplications in MathCad, a temperature distribution within the material at specific radius and time was calculated. This temperature distribution

is graphically illustrated on Figure 4-31 for a fine grid with 3000 nodes on the radius and a small time step of size $\Delta t = 0.01\text{s}$. The radius spacing and time step size were chosen, based on trial and error to be as fine as possible to allow for radius and time grid independency in the solution.

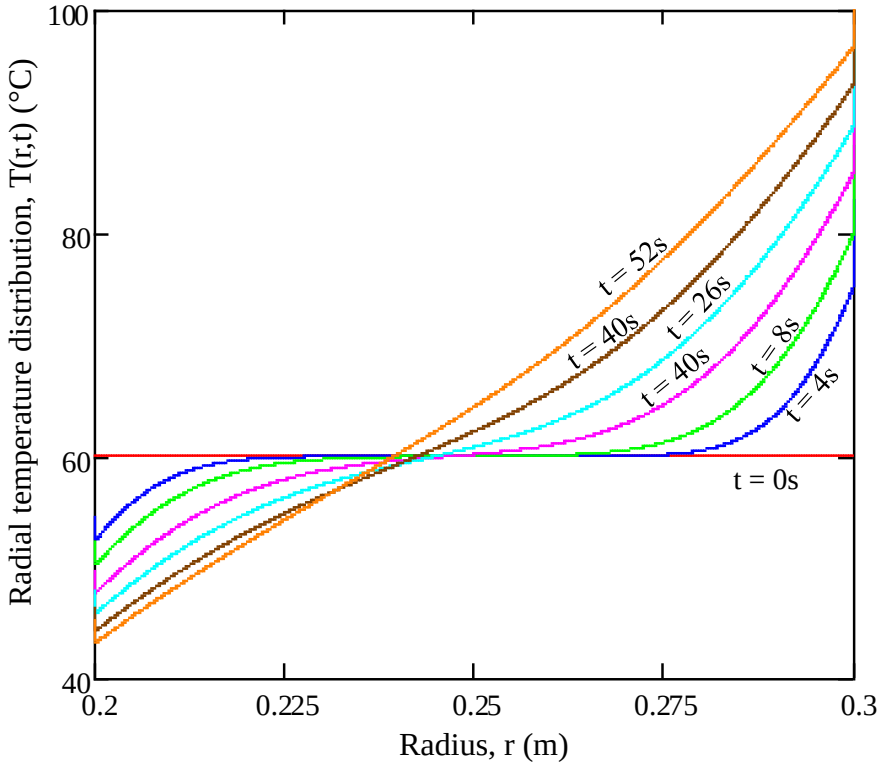

Figure 4-31. Temperature distribution for an infinitely long tube with respect to radius and time for a case in which the transient was initiated by imposing a temperature gradient.

4.3.4 Summary

This section presented the derived finite volume numerical method and then applied the solution to the analyses of the temperature distribution for an infinitely long tube with different boundary conditions.

The numerical solution was verified against the exact analytical solution for the same scenario. It was demonstrated that the numerical solution depends on discretisation in space and time for the chosen specific case, raising an awareness that this should be checked when modelling a heat exchanger. As expected, it was demonstrated for the chosen scenario that the numerical solution becomes more accurate with increasing the number of nodes in the discretisation in space as well as when the time step size is reduced. However, these results are case specific not generic.

On the other hand, writing a numerical program every time there is a need to model and analyse a heat exchanger in industry is practically not viable, especially because the industrial heat exchangers have complex geometries and time-dependent boundary conditions. Thus, a faster and simpler way of modelling a heat exchanger is desired and presented hereafter.

4.4 Application of the Flownex software

The Flownex software which is a one dimensional (1D) thermal-fluid solver as introduced in chapter 2, provides a built-in easy way of modelling a heat exchanger. Flownex is capable of modelling the transient conduction heat transfer for cases with time-dependent flow features as boundary conditions as well as cases with complex geometries and layouts.

Modelling heat transfer problems in Flownex requires a few components, mainly a pipe, heat transfer element, boundary conditions and a node; these components are shown on Figure 4-32.

Figure 4-32. Flownex Components a) Pipe b) Heat Transfer Element c) Boundary Condition d) Node.

The pipe element in Flownex can be used to model fluid flow in pipes and ducting systems with a constant or variable cross section area. It is also capable of handling gas, liquid and two-phase flow under both steady and transient state. The heat transfer (HT) element is capable of modelling heat transfer through a solid into and/or from a fluid media. This implies that it can be used to model conduction, convection and radiation heat transfer at the boundary between the fluid and the solid, and conduction within the solid. It can model a composite material with a number of material layers, with each layer discretised into a number of increments, as mentioned in chapter 2 and demonstrated in Figure 2-21. Both thermal resistance and thermal inertia can be taken into account, with the heat transfer element either connected to a flow element or a node with either single or two-phase flow. The HT element assumes a constant convective heat transfer coefficient throughout an element or increment. It further assumes a linear temperature distribution between increments in a solid. In addition, the conduction resistances in the heat transfer element are calculated using the relation of a plane wall [38]. The HT element has two area discretisation schemes namely based on average areas and based on linear area change approximation. In this project only the average area option is used.

The boundary condition component is used to specify the boundary condition of a node it is connected to in a network. The condition can be pressure, temperature, enthalpy, mass flow rate and quality for two phase flow. The node can be an end point of an element or represent a reservoir or tank [38].

4.4.1 Infinitely long tube with convection at the boundaries

As with the case in the application of the numerical solution given in subsection 4.3.3, consider a case where the infinitely long tube has temperature gradients imposed at both boundaries at time $t = 0s$, as shown in Figure 4-33.

This case is such that the infinitely long tube originally had its temperature and the surrounding temperatures set at a constant temperature, $T_{or} = 60\ °C$, as illustrated in Figure 4-33a. At time $t = 0s$ a fluid with temperature $T_{fa} = 30\ °C$ and heat transfer coefficient $h = 2000\ W/m^2°C$ is imposed at the inner boundary and another fluid with temperature $T_{fb} = 120\ °C$ and heat transfer coefficient $h = 2000\ W/m^2°C$ is imposed on the outer boundary, as demonstrated in Figure 4-33b.

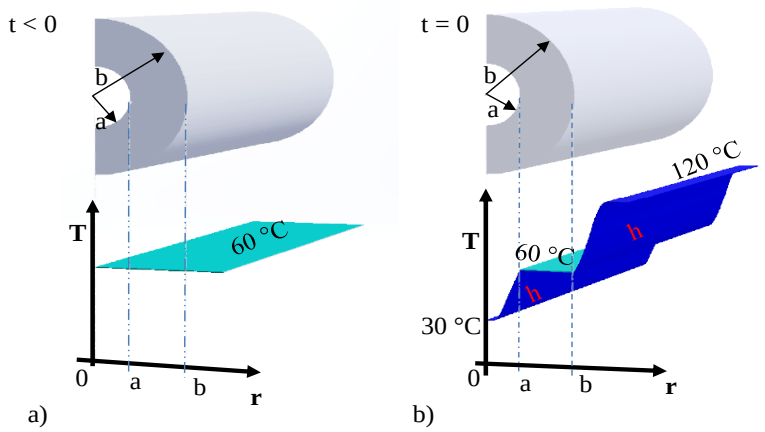

Figure 4-33. Temperature distribution for an infinitely long tube with convection imposed on the boundaries to initiate a transient a) original state b) initial condition.

In Flownex, to model the heat conduction in an infinitely long tube, a heat transfer element, three nodes and two boundary condition elements are used as demonstrated in Figure 4-34.

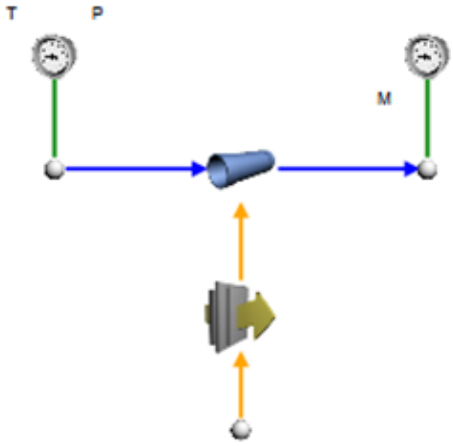

Figure 4-34. Flownex model for the case of an infinitely long tube with convection on the boundaries.

In Figure 4-34, heat is transferred from a fluid flowing outside a steel pipe at a temperature of 120 °C with a specific convective heat transfer coefficient of 2000 W/m^2.°C to water flowing within the pipe at temperature of 30 °C and convective heat transfer coefficient of 2000 W/m^2.°C. The geometry of the tube is such that the inner diameter, thickness and length are 0.4 m, 0.1 m and 0.4 m respectively. The length of the tube is chosen to be short such that there is no significant pressure drop and also no significant temperature difference between the inlet and the outlet. This case can also be modelled just by connecting the HT element between two nodes and the two methods give the same results.

A transient simulation in Flownex was modelled, with the initial temperature of both fluids being 60 °C. After 10s the inner fluid temperature immediately dropped to 30 °C and the temperature of the outer fluid suddenly increased to 120 °C, as demonstrated in Figure 4-35. The temperature of the tube near the inner wall dropped over time in response to a drop in temperature and that near the outer wall increased in response to the increase in temperature.

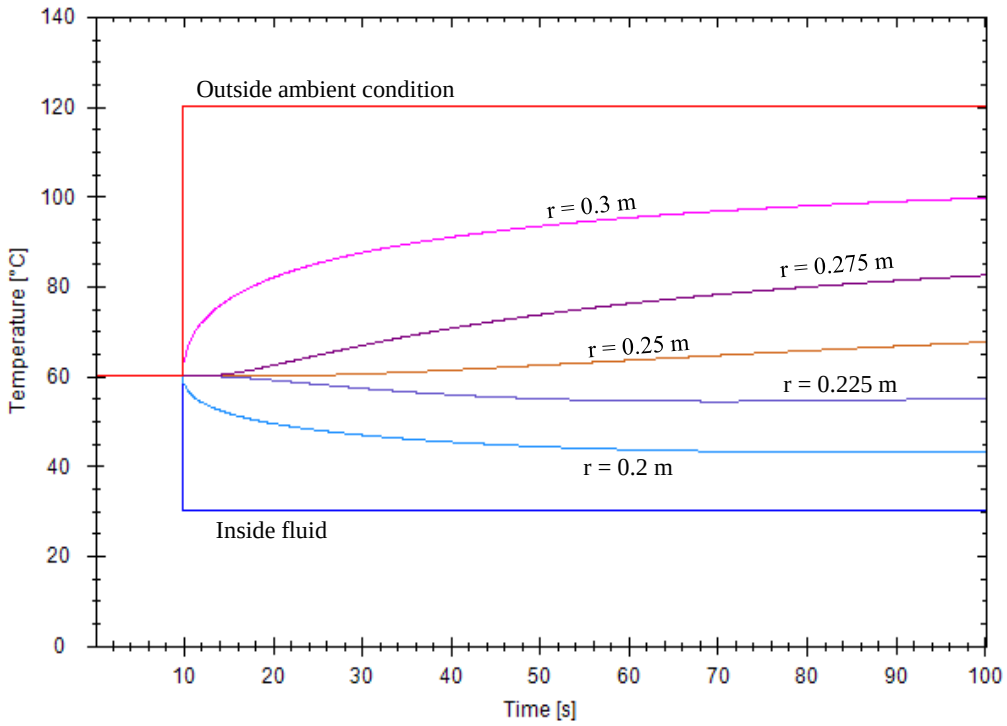

Figure 4-35. Temperature variation as function of time calculated by Flownex for certain radius in a transient simulation with r = 0.2 m the internal tube radius, r = 0.3 m the outer radius and Δt = 0.1s the time step size.

The temperature distribution with respect to radius and time for this case with the thickness of the pipe discretised 100 times and time step size $\Delta t = 0.1s$ is presented in Figure 4-36. In Flownex the original state of the case starts at time *t = 0s* until just before *t = 10s*, and the initial condition for the transient is at time *t =10s*. Thus in plotting the transient results, the start of the transient is corrected to zero seconds. This means that the temperature distribution vs radius at time *t = 10s* in Flownex is plotted as a temperature distribution at *t = 0s* in Figure 4-36.

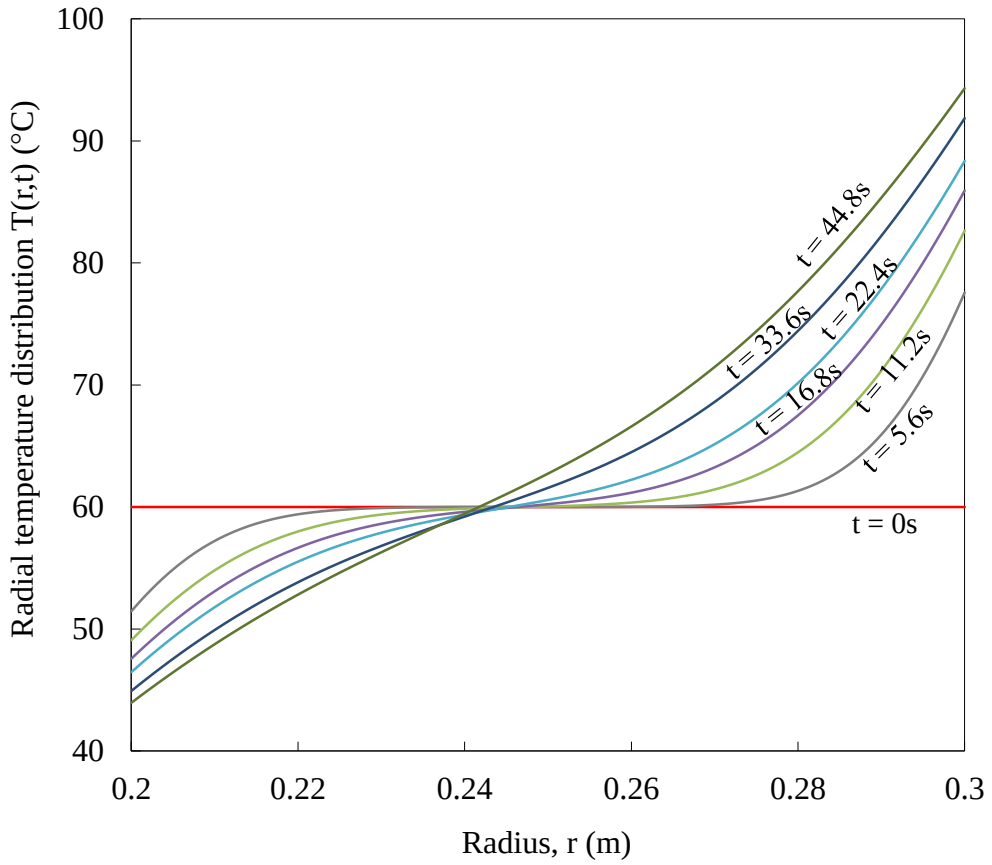

Figure 4-36. Transient temperature distribution calculated by Flownex for an infinitely long tube with respect to radius and time with the thickness discretised into 100 nodes and a time step size of 0.1s.

4.4.1.1 Dependence on the discretisation in physical space

Hereafter the dependence of the Flownex solution on radial discretisation for the case presented in this subsection is checked through comparison with the numerical solution presented in subsection 4.3.3. The results are presented in Figure 4-37.

Figure 4-37 shows results of a Flownex model with the thickness discretised into 100 nodes with only 21 nodes plotted and time step size of $\Delta t = 0.1s$ compared to a numerical solution with a relatively fine grid for both time and radius. The Flownex results are on top of the numerical results, which verifies Flownex's capability of modelling conduction heat transfer within the tube.

The thickness was then discretised into four nodes only and the time step size was kept at 0.1s. The results are shown in Figure 4-38. This figure demonstrates that the Flownex solution is dependent on the thickness discretisation. This is because of the inherent truncation errors on the adopted FVM discretisation scheme. Another reason is that the selected area discretisation scheme, standard (average areas), uses average areas to calculate the heat conducted, thus for cylindrical components the solution becomes more accurate with an increase in the number of nodes.

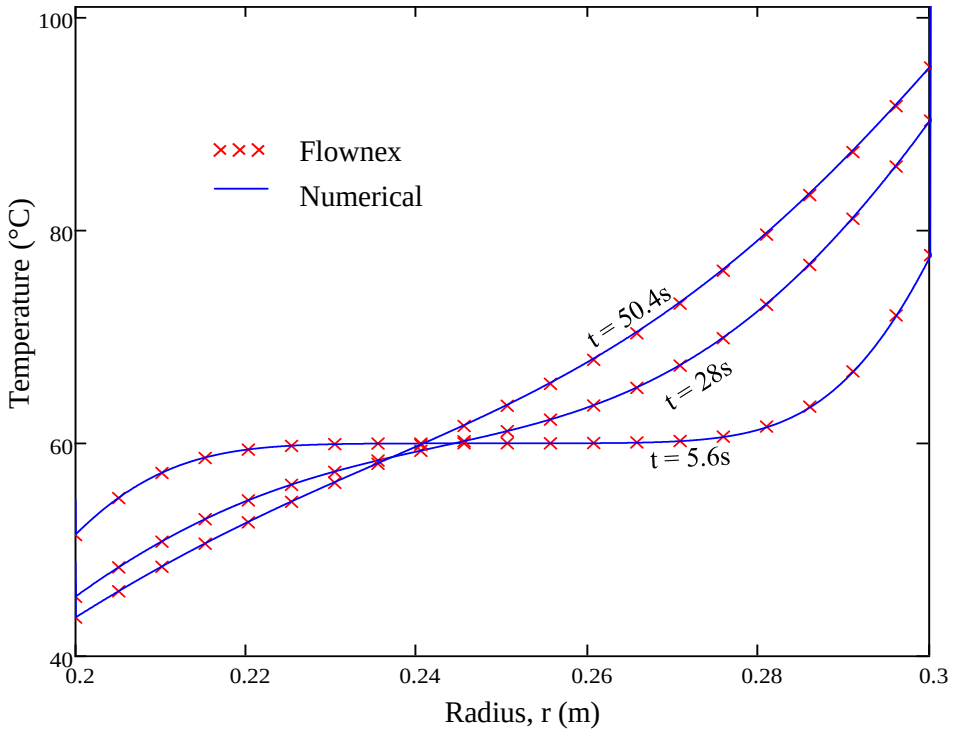

Figure 4-37. Comparison between Flownex and numerical results for an infinitely long tube subjected to convection at the boundaries to induce transients where 100 nodes and time step of 0.1s were used in Flownex with only 21 nodes plotted.

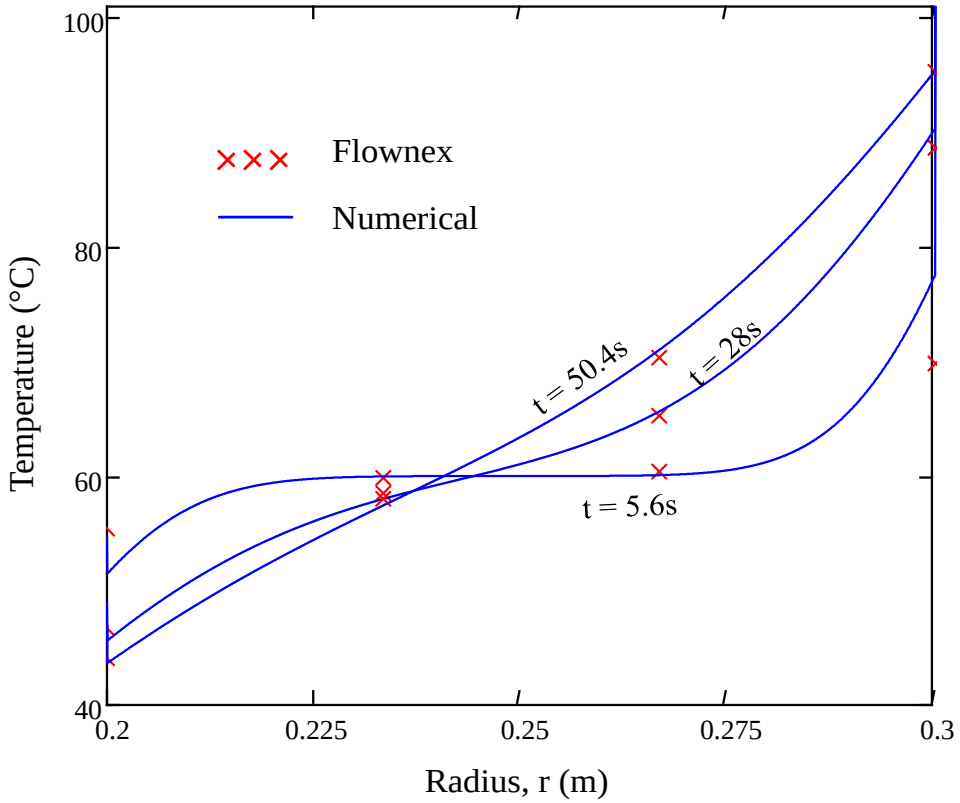

Figure 4-38. Comparison between Flownex and numerical results for an infinitely long tube subjected to convection at the boundaries to induce transients where 4 nodes and time step of 0.1s were used in Flownex.

The error associated with the discretisation of the thickness of the tube in Flownex was characterised using the Two Norm, as represented in Figure 4-39. The Two Norm was calculated from the comparison of the Flownex solution to the numerical solution defined by a fine thickness grid and time step size. As expected, Figure 4-39 shows that the accuracy of the Flownex solution increases with increase in the number of nodes on the thickness.

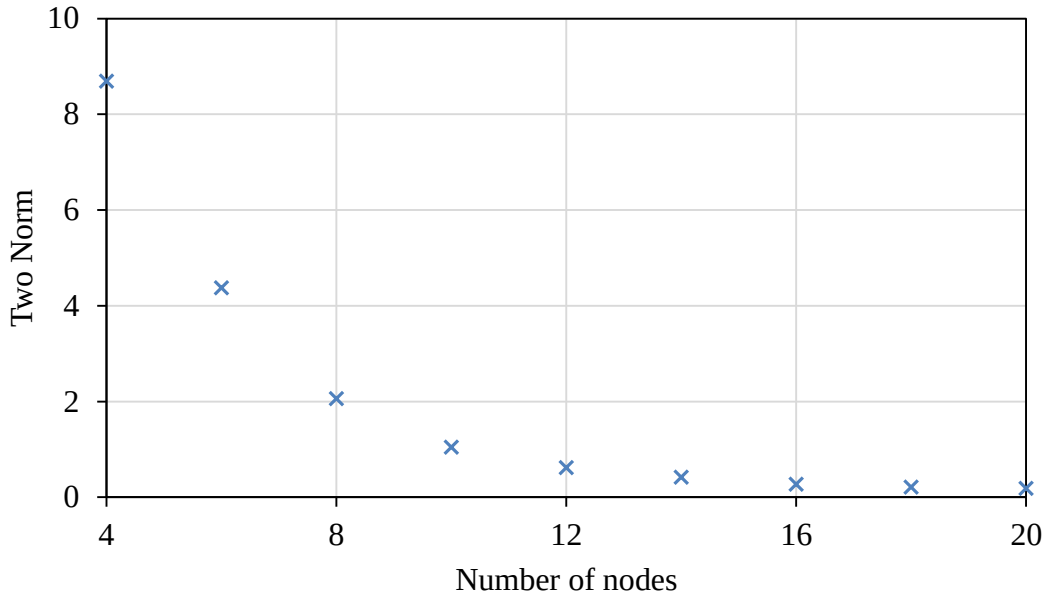

Figure 4-39. Two Norm graph with change in number of nodes on the tube thickness at time t = 5.6s for time step size of $\Delta t = 0.1\text{s}$.

4.4.2 Finite tube with one pass and convection on boundaries

A real heat exchanger is made up of tubes with finite lengths. So consider a finite tube with steam flowing inside the tube and air cross flowing on the outside of the tube as illustrated in Figure 4-40 with flow parameters given by Table 4-2. These conditions are typical of what prevails in a superheater tube of a real PF plant, however in a real PF plant the air would be the flue gas flowing outside the tube. In this analyses the heat transfer coefficients are fixed for both fluids.

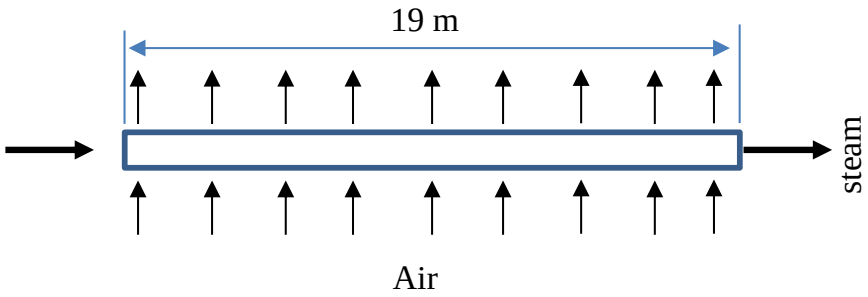

Figure 4-40. Cross flow finite tube model schematic.

Table 4-2. Flow parameters.

Parameter	Units	Steam	Air
Flow rate	kg/s	0.96	30
Inlet temperature	°C	480	1061
Inlet pressure	MPa	17.5	0.1
Heat transfer coefficients	$W/m^2°C$	4955	46.7

In addition to discretisation in radius, modelling a finite tube also require discretisation along the length of the tube.

4.4.2.1 Discretisation in the radial direction

Starting with investigating the effect of radially discretising a tube thickness in Flownex, two cases are analysed. Case 1 represents a typical boiler tube which is relatively thin wall compared to Case 2 as illustrated in Table 4-3. The air free flow area for both cases is shown on Figure 4-41.

Table 4-3. Summary of the cases analysed.

Parameter	Units	Case 1	Case 2
Inner diameter	mm	31.9	31.9
Tube thickness	mm	6.3	100
Tube length	m	19	19

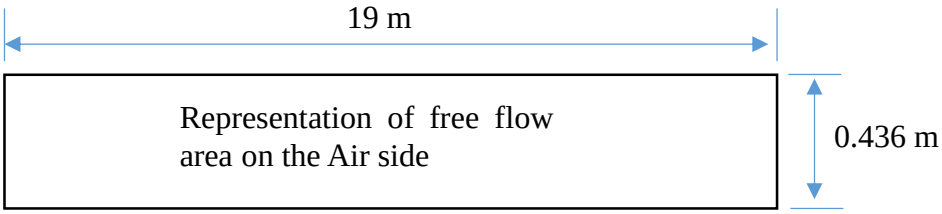

Figure 4-41. Representation of the free flow area on the air side for both Case 1 and Case 2.

In Flownex each case was modelled using the Flownex model schematic shown in Figure 4-42, with the ability to change the number of nodes in the tube thickness on the heat transfer element. The conditions, flow parameters and geometry parameters were added on the relevant Flownex components to fully model the different cases. This includes specifying the inlet temperature and pressure for both streams, specifying the mass flow rates for both streams, specifying the fluids, specifying the relevant diameters and areas for the pipes as well as customising the heat transfer element with heat transfer coefficients and the areas of the tube for both streams.

In Flownex the fluid cross flowing over the tube was modelled in the pipe with the pipe customised to the flow's inlet area and circumference such that the outside hydraulic diameter of the tube was conserved. This was done through manipulating the inlet circumference/perimeter on the Flownex inputs using the following equation:

$$P_{outer} = \frac{4A_{freeflow}}{OD_{tube}} \tag{4.22}$$

with P, A and OD the inlet perimeter, inlet area and outer diameter, respectively. The inlet area is shown on Figure 4-41. This is important for the calculation of heat transfer coefficients. However, in this analyses the heat transfer coefficients are fixed.

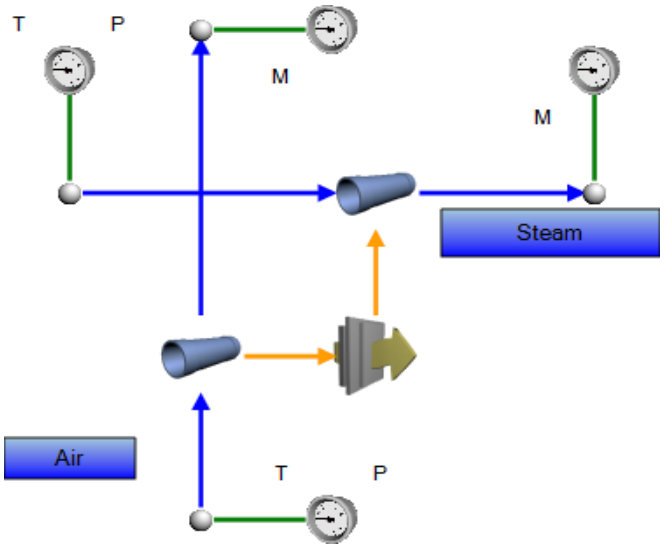

Figure 4-42. Flownex model for a finite tube with convection on the boundaries.

For steady state, the number of nodes for both models were changed and the outlet steam temperature was being monitored. The results are graphically presented in Figure 4-43. The outlet steam temperature for Case 2 is higher than that of Case 1 because Case 2 has a larger outer heat transfer surface area due to a larger outer diameter compared to Case 1.

Figure 4-43 illustrates that for Case 2 which is a thick tube, there is a change in outlet steam temperature with change in nodes. This is due to the inherent truncation errors of the adopted FVM discretisation scheme. It is also due to the selected standard (average areas) area discretisation scheme. So as the number of nodes increases it approximates the solution of the cylindrical form of the heat conduction equation better. Case 1 demonstrates that for relatively thin tube the linear approximation in Flownex has a negligible effect on the results, since the thickness can be approximated as a thin rectangular slice with a relatively small error.

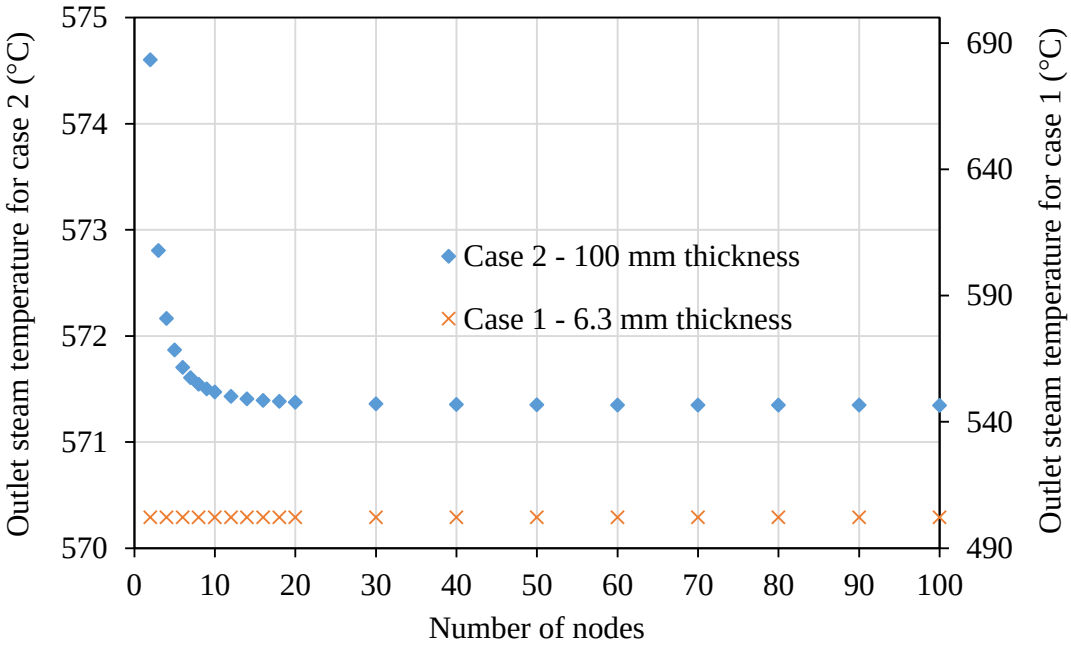

Figure 4-43. Steady state comparison of the outlet steam temperature for case 1 and case 2.

For Case 1, which is a tube with thickness of 6.3 mm, a further investigation of the effect of radial discretisation under transient conditions was performed. The transients were introduced by a step change of the inlet air temperature from 1061 °C to 1200 °C at time t = 10s, keeping all other conditions the same. The outlet steam temperature was monitored and the results are graphically presented in Figure 4-44 for one case with 2 nodes (not discretised).

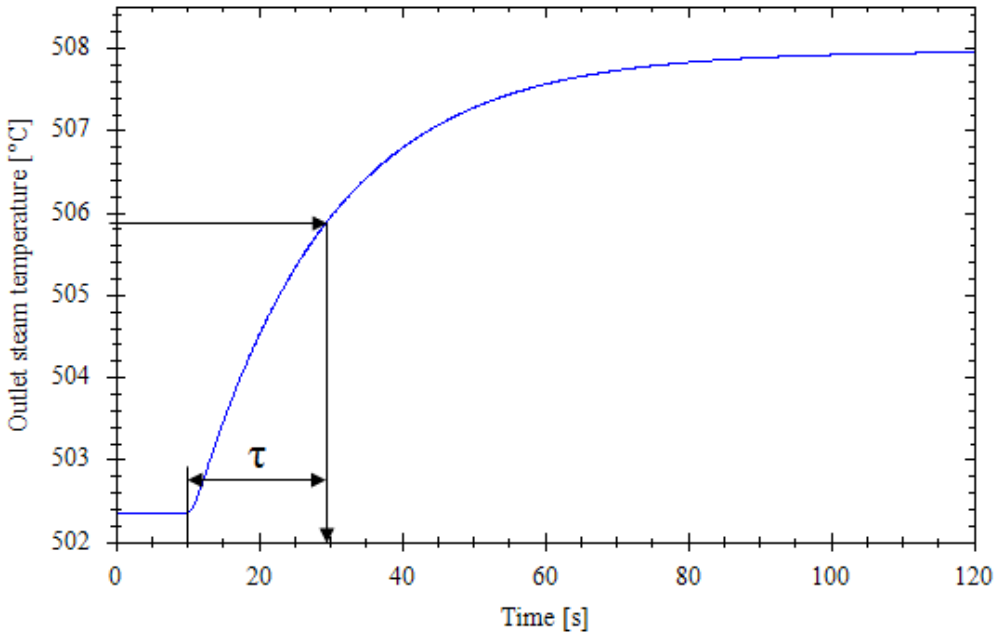

Figure 4-44. Outlet steam temperature change with time after a step change in the air inlet temperature with thickness not discretised and time step of 0.1s and time constant calculation representation.

The transient was run numerous times, each time changing the discretisation size in the thickness by changing the number of nodes in the thickness on Flownex's heat transfer element. For each discretisation size temperature vs time results, the time constant, τ was calculated as presented in the lumped capacity system discussed in chapter 2. In simple terms, the time constant is the time corresponding to 63.2 % of the difference between the temperature at the end and the start of the transient, as illustrated in Figure 4-44. In this investigation it was discovered that the time constant for all the discretisation sizes is the same, $\tau = 19.6s,$ as illustrated in Figure 4-45. Thus it can be deduced that for case 1, discretisation of the tube thickness on Flownex has a negligible effect on the transient behaviour of the system.

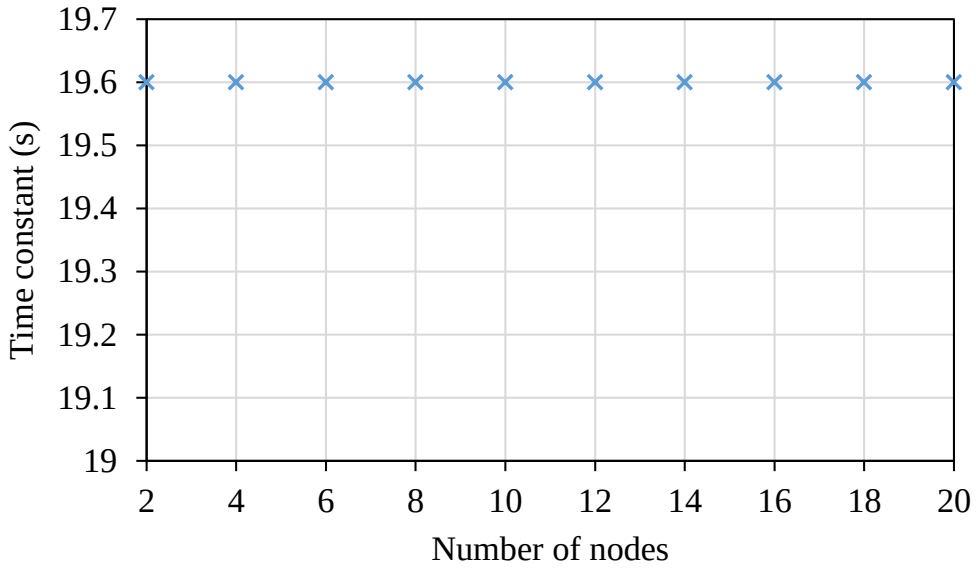

Figure 4-45. Time constant vs number of nodes on the thickness of the tube for the outlet steam temperature for Case 1.

Additionally, the outlet steam temperature at the time constant of 19.6s was monitored. At the time constant the outlet steam temperature is still undergoing transient changes. The results of the monitored outlet steam temperature are graphically presented in Figure 4-46. As with the time constant, the effects of discretising the thickness on the outlet steam temperature for Case 1 is negligible.

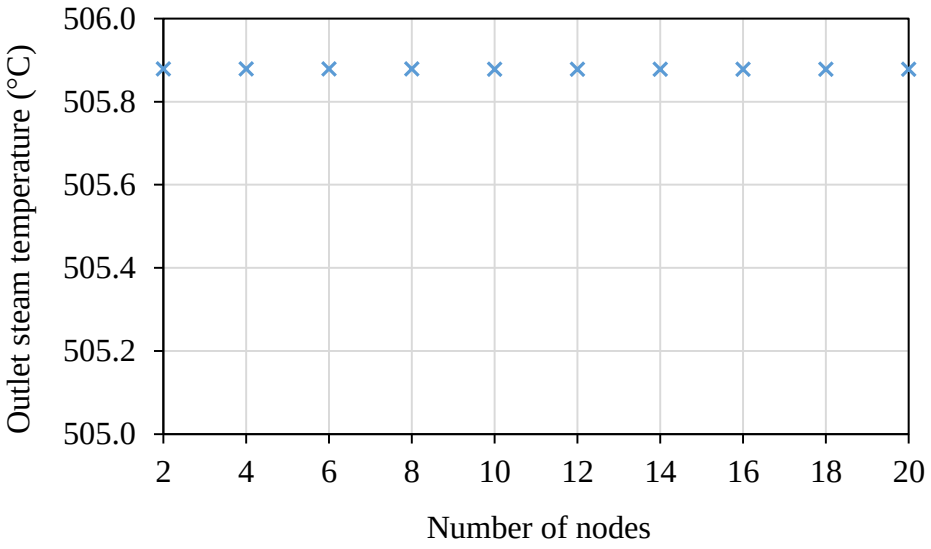

Figure 4-46. Outlet steam temperature vs number of nodes on the thickness at the time constant of 19.6 s for Case 1.

4.4.2.2 Discretisation in the length direction

A finite tube subjected to cross flow can also be discretised along the length in order to capture the correct steam temperature as it varies along the length. Discretisation along the length involves modelling small cross flow sections of the tube as illustrated in Figure 4-47 for a tube that is axially discretised 3 times. In this section, Case 1 (6.3 mm thickness tube without radial discretisation as presented above) is analysed.

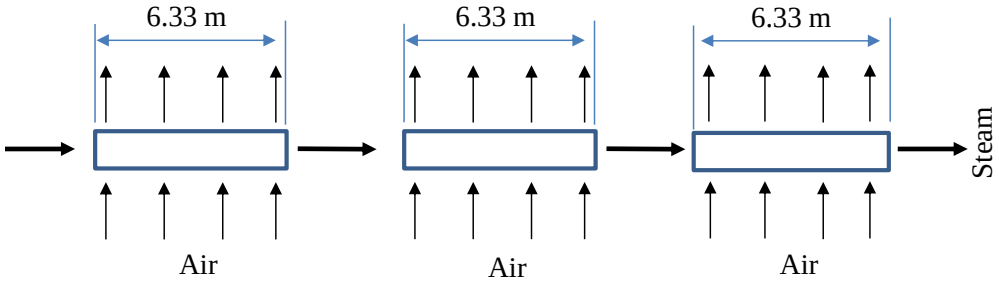

Figure 4-47.A representation of a 19 m long tube axially discretised 3 times.

In Flownex, length-wise discretising a tube that is subjected to cross- flow involves physically building the train of small heat exchangers, called “building blocks”, connecting them to one another until the desired discretisation is achieved, as demonstrated in Figure 4-48 for a tube axially discretised 3 times. The geometry and air stream flow rates of the building blocks are customised such that they suit the employed discretisation.

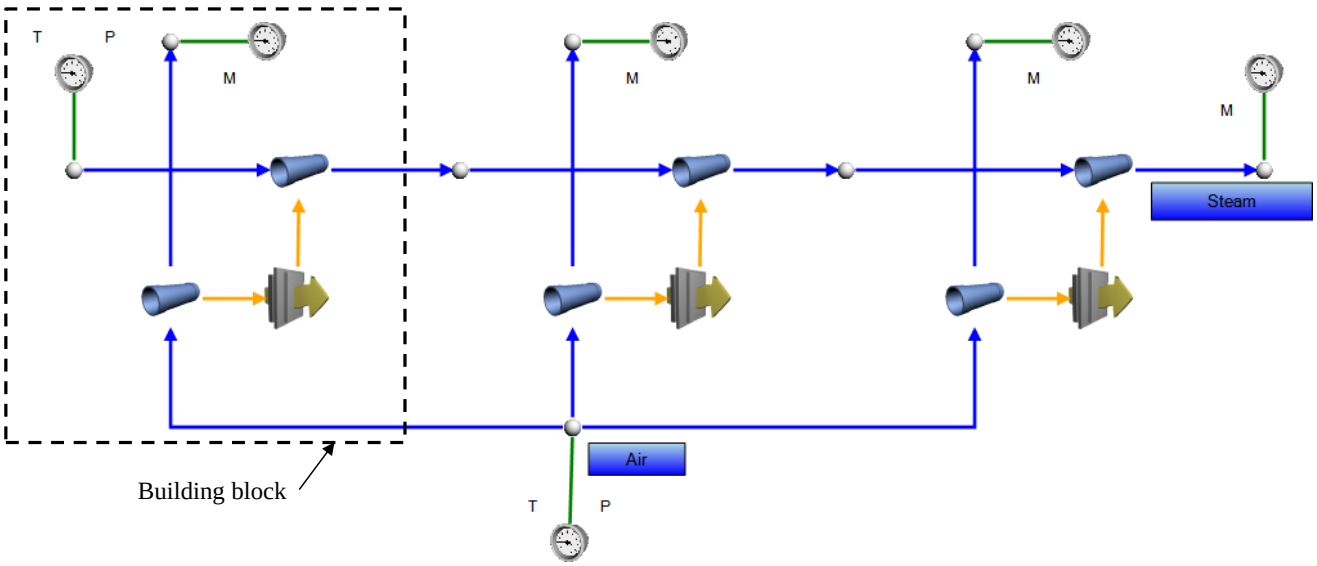

Figure 4-48. Flownex model of a tube that is axially discretised 3 times.

In the investigation of the effect of axial discretisation for case 1, the tube was discretised a number of times, each time the outlet steam temperature reached at steady state was monitored. Results from the investigation are graphically presented in Figure 4-49. It can be seen that the steam outlet temperature is affected by axially discretisation, with a bigger effect when a few building blocks are used. Even if the steam temperature seems sensitive to the number of axial discretisation, this effect should be considered relatively to the complete increase in temperature in a real heat exchanger. In fact the convective-radiative heat transfer applied to the boundaries will directly affect these temperatures, so further investigations of the relative effect of fineness of axial discretisation to the total heat transfer in a real tube bundle will be carried out in next steps of this work but are beyond the scope of this thesis.

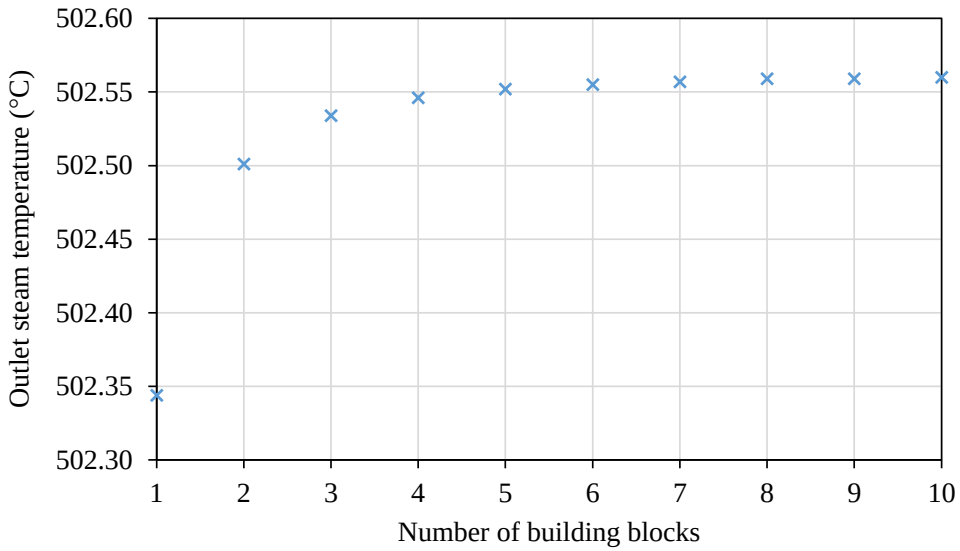

Figure 4-49. Sensitivity analyses on the effect of the number of building blocks on the outlet steam temperature under steady state.

Hereafter the effect of axial discretisation on the transient response of Case 1, i.e. a tube with thickness of 6.3 mm is calculated. The transients were introduced by a step change of the inlet air temperature from 1061 °C to 1200 °C at time t = 10s, leaving all other conditions the same for all the models.

The transients were run on different models with different axial discretisation of the tube. For each model the transient outlet steam temperature was monitored and plotted against time as it was previously shown in Figure 4-44. From this analysis the time constants were extracted and are plotted against the number of building blocks in Figure 4-50. It can be seen from Figure 4-50 that the time constant reduces with an increase in number of building blocks for this case, which shows that axial discretisation has an effect on transient outlet steam temperature.

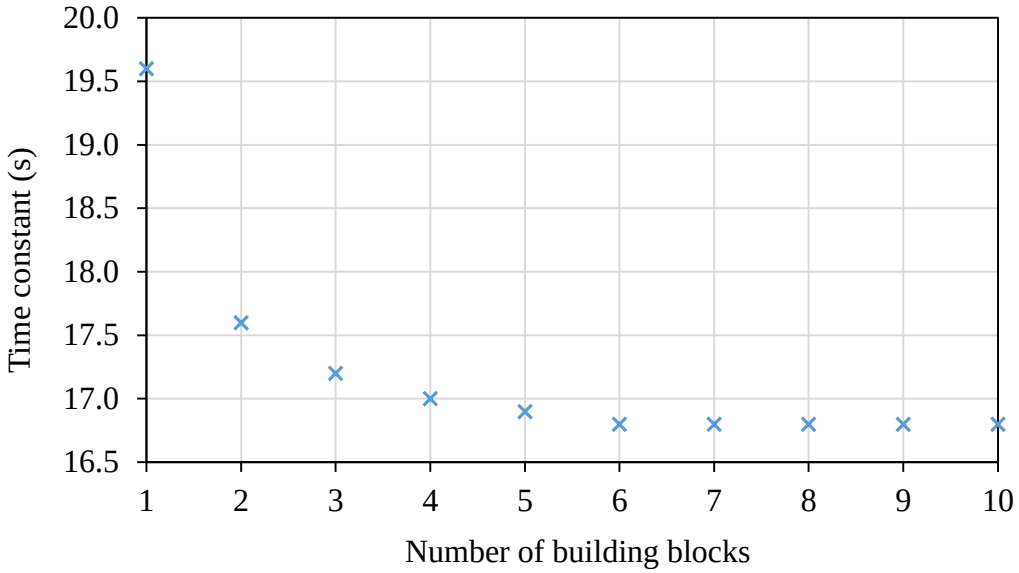

Figure 4-50. Time constant vs the number of building blocks for a transient simulation.

As previously concluded for the effect of axial discretisation on the steady state outlet steam temperature, the relative change in the time constant with the fineness of axial discretisation will also need further investigation taking into account the relative effect of this axial discretisation to other phenomena affecting the transient response time. This is beyond the scope of this thesis.

4.4.3 Finite tube with two passes

Usually, a boiler heat exchanger is made up of tubes which make two or more passes in the boiler as illustrated in chapter 2. In this subsection, a preliminary investigation of the approach of modelling a finite tube with two passes as shown in Figure 4-51 is presented. The issues that are investigated include the effect of layout simplifications and time-wise discretisation on the outlet steam temperature. Radial discretisation is not investigated in this section, thus the modelled tube does not have discretisation on

the thickness. The case modelled here is described in Figure 4-51, Figure 4-52, Table 4-4 and Table 4-5.

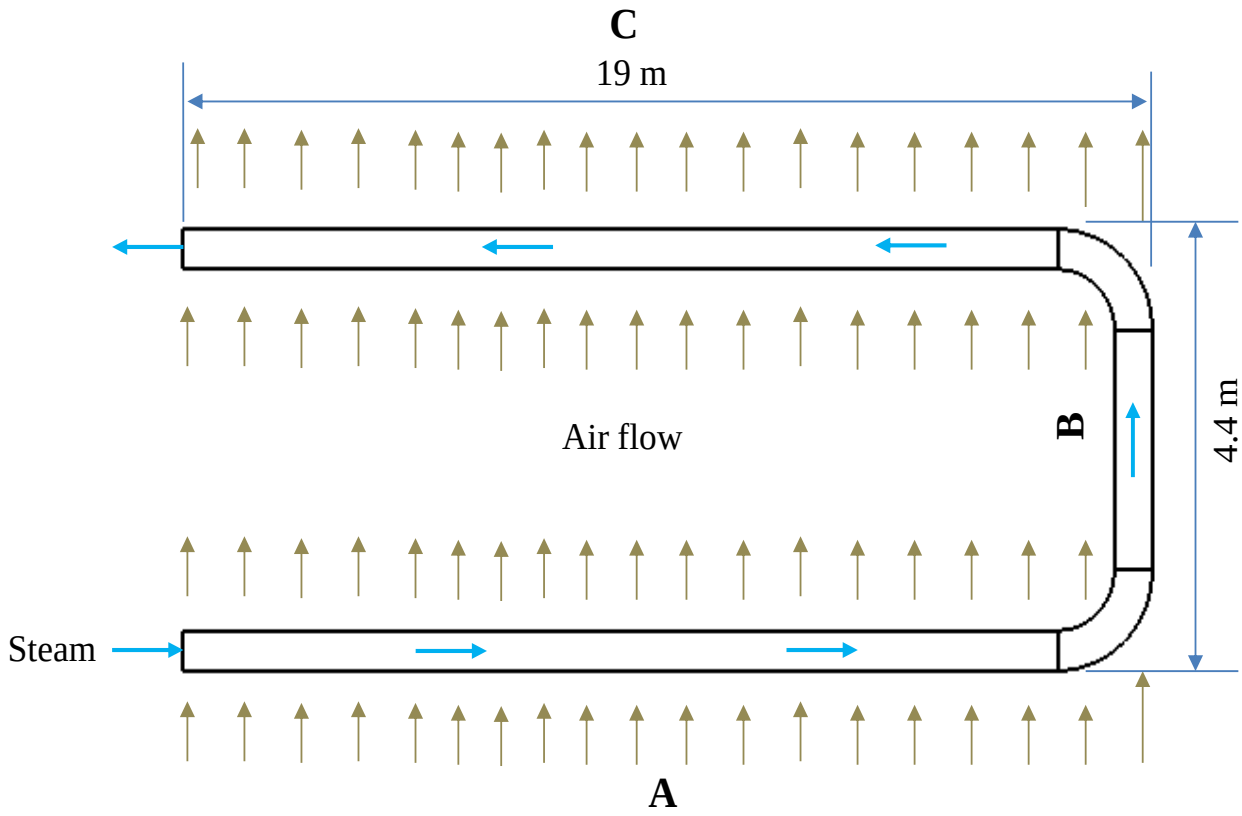

Figure 4-51. One tube with two passes experiencing cross flow over its major length.

Table 4-4. Flow parameters for the case of a finite tube with two passes.

Parameter	Units	Steam	Air
Flow rate	kg/s	0.96	30
Inlet temperature	°C	480	1061
Inlet pressure	MPa	17.5	0.1
Heat transfer coefficients	$W/m^2°C$	4955	46.7

Table 4-5. Summary of the geometry.

Parameter	Units	Value
Inner diameter	mm	31.9
Tube thickness	mm	6.3

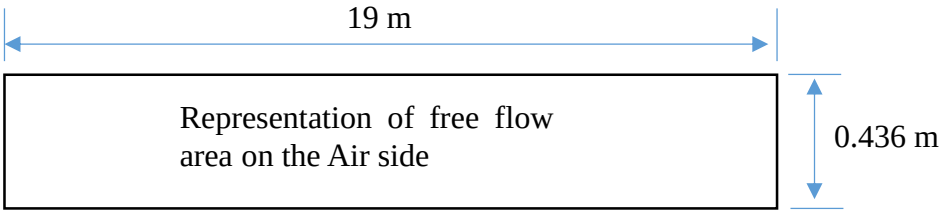

Figure 4-52. Representation of the free flow area on the air side.

4.4.3.1 Simplification of the overall layout

The modelling of the layout of a finite tube with cross flow as shown in Figure 4-51 can be simplified on Flownex depending on the accuracy required for the outlet steam temperature. The tube with two passes can be approximated by a tube with a single pass and without axial discretisation in the Flownex modelling as illustrated in Figure 4-53. This tube can also be modelled with two passes as illustrated in Figure 4-54. In this case, the vertical part of the tube is divided into two, with one part included in the bottom length and the other in the top length as illustrated by the letters A, B and C on the schematics. Also, with the two pass model, the length of the tube can be axially discretised as shown in Figure 4-55. The length of the tube in both passes can be axially discretised further until the desired outlet steam temperature accuracy is achieved.

In the modelling, the first case which is illustrated by Figure 4-53 was named SIMPLIFICATION 1. The second case which is shown on Figure 4-54 was named SIMPLIFICATION 2, and the model on Figure 4-55 was named SIMPLIFICATION 3. Further layout simplification models were done by axially discretising the length of the tube on both passes as the case from Figure 4-54 to Figure 4-55. These models were successively named SIMPLIFICATION 2+i (with i being the number of axial building blocks added per pass).

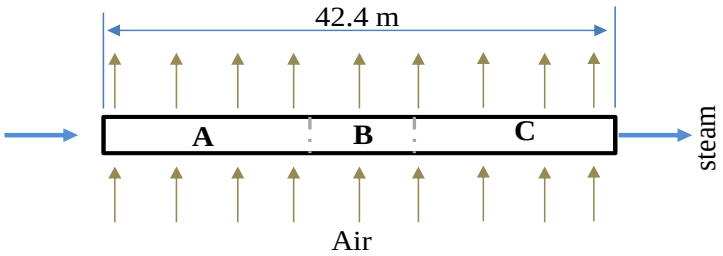

Figure 4-53. Two passes modelled as one pass, SIMPLIFICATION 1.

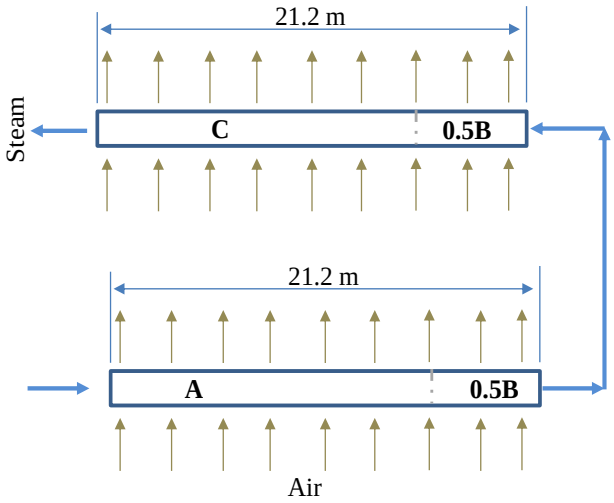

Figure 4-54. Two passes modelled as two passes without axial discretization, SIMPLIFICATION 2.

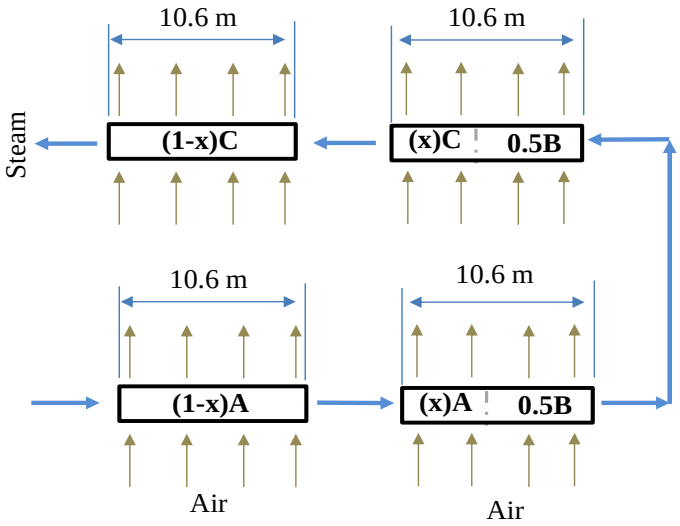

Figure 4-55. Two passes modelled as two passes with axial discretization, SIMPLIFICATION 3.

On Flownex, the first model, SIMPLIFICATION 1, is represented as shown in Figure 4-42, in subsection 4.4.2, since the air stream is assumed to be that of a one pass tube. For SIMPLIFICATION 2 the air stream is defined for both passes as shown in Figure 4-56. For each pass the temperature used is an average between the inlet and the outlet air temperatures. The outlet temperature of the first pass becomes the inlet temperature of the second pass. For SIMPLIFICATION 3 as well, the air stream is defined for both passes as shown in Figure 4-57. Due to axial discretisation on SIMPLIFICATION 3, the Flownex representation does not allow mixing of the air after the first pass. All the successive models SIMPLIFICATION 3+i do not allow mixing of the air after the first pass. Since in a real PF plant heat exchanger there is mixing after the first pass, this simplification has to be investigated further in other projects to follow and it is not part of this thesis.

On Flownex, each model was built using the building blocks discussed in subsection 4.4.2.

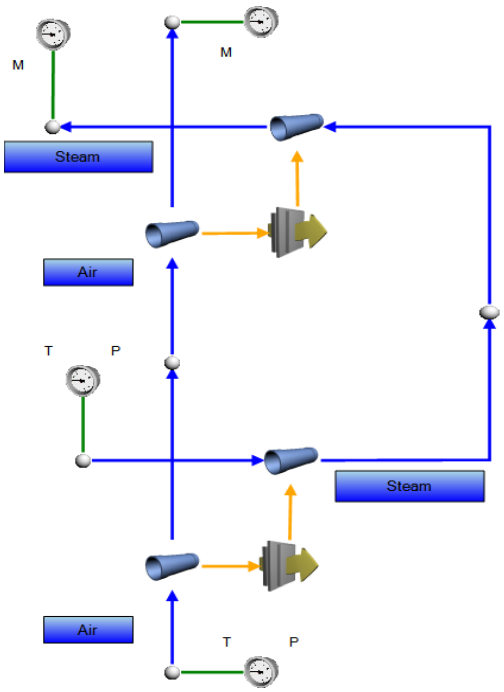

Figure 4-56. Flownex model representing SIMPLIFICATION 2 shown in Figure 4-54.

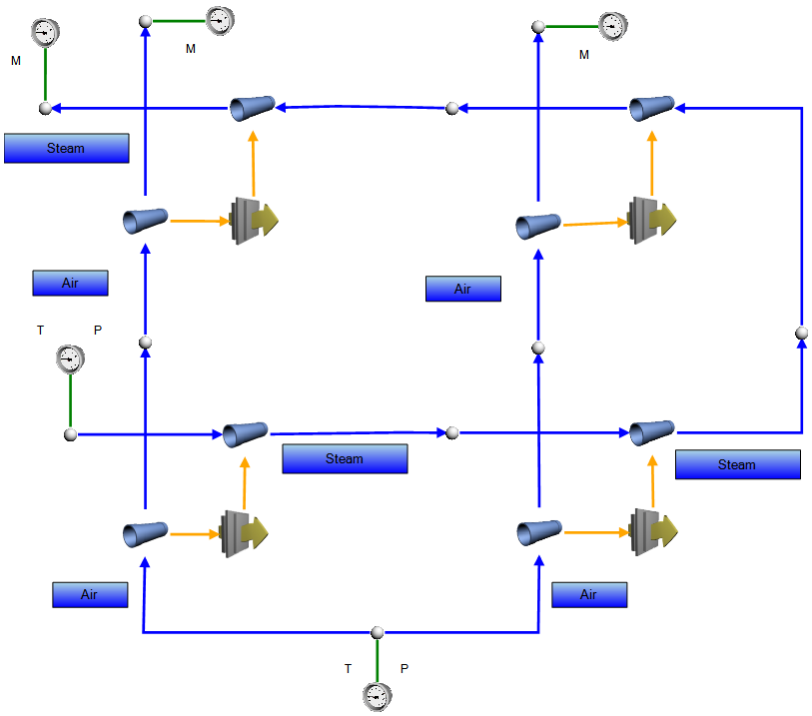

Figure 4-57. Flownex Representation of SIMPLIFICATION 3 shown in Figure 4-55.

Under steady state, the outlet steam temperature of each model was monitored and the results are presented in Figure 4-58. It is illustrated that the accuracy of the outlet steam temperature improves as the layout of the model approaches the real layout of the finite tube with two passes.

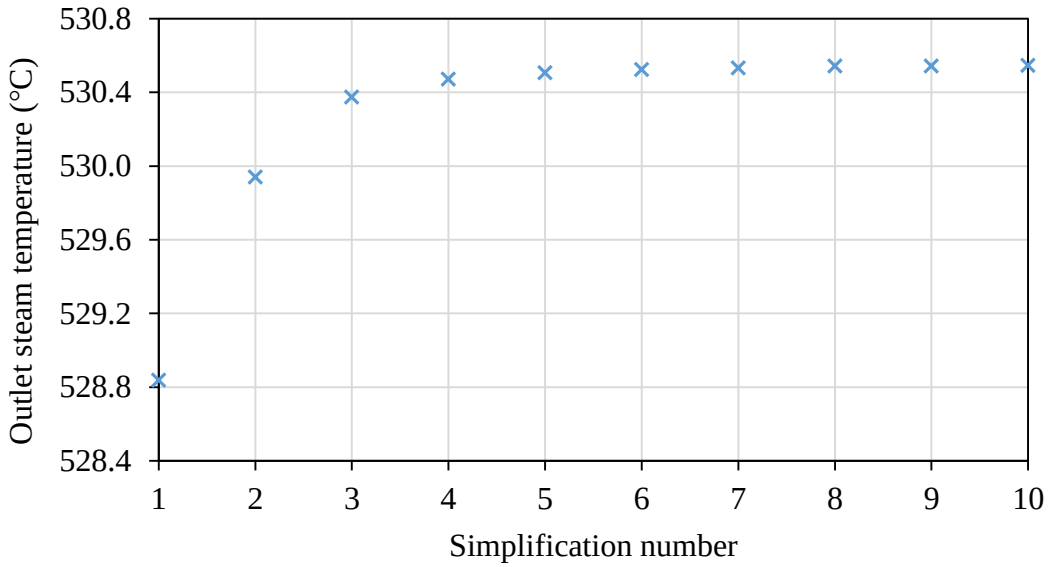

Figure 4-58. Sensitivity study of the effect of simplification on the outlet steam temperature under steady state.

The investigation of the effect of the layout simplification was further extended to transient simulations. The transients were introduced by a step change of the inlet air temperature from 1061 °C to 1200 °C at time t = 10s, keeping all other conditions the same for all the models. The time constants for the transient outlet steam temperature for each model were calculated and graphically presented in Figure 4-59. The figure illustrates that the time constant decreases as the model becomes a better approximation of the finite tube with two passes.

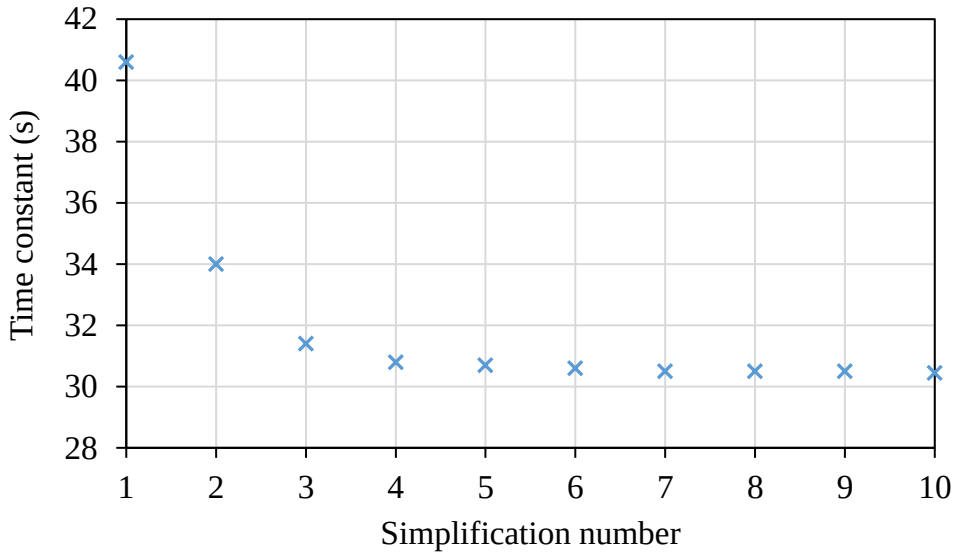

Figure 4-59. Time constant vs the simplification number for a transient simulation.

It can be seen that for this specific geometry, the results obtained at SIMPLIFICATION 3 are already close to those obtained at SIMPLIFICATION 10 either for the steady state outlet steam temperature or the time constant.

4.4.3.2 Time-wise discretisation

Since Flownex is a numerical solver, the numerical approximation of the governing equations that Flownex solves depends on the time step size for transient simulations, as explained in the section about the application of the finite volume numerical method in subsection 4.3.2. Thus, the selected time step size has an effect on the accuracy of the transient result.

In order to illustrate the effect of Flownex time step size on transient modelling in Flownex, SIMPLIFICATION 5 model from the layout simplification analyses in the subsection 4.4.3.1 above was used. This Flownex model is shown in Figure 4-60.

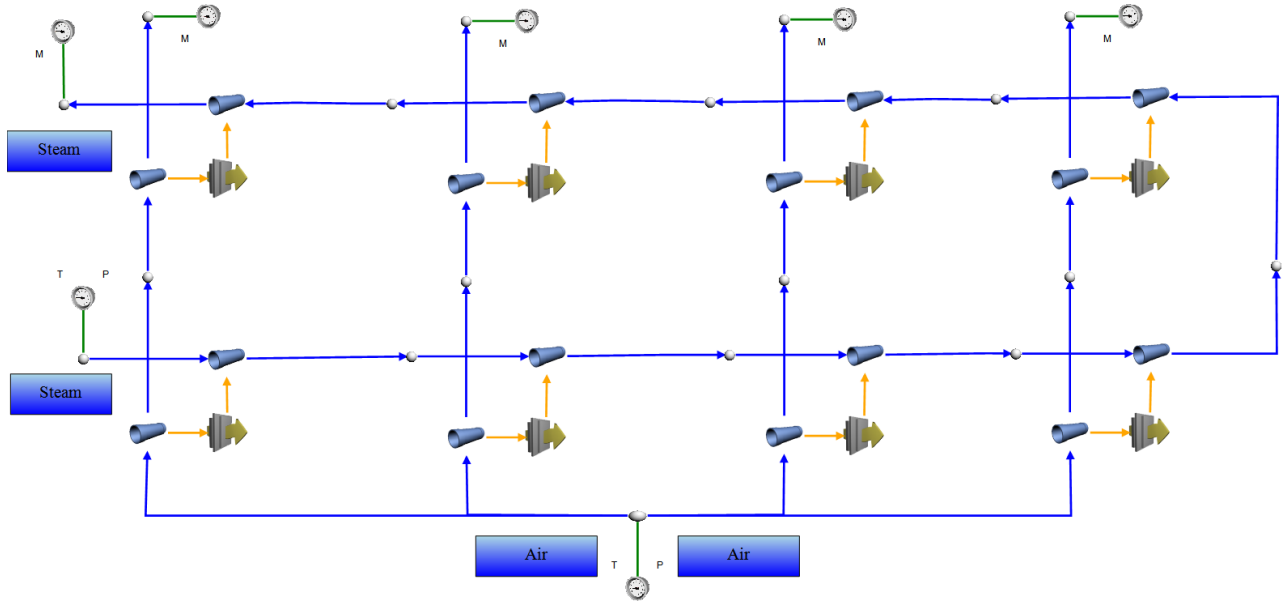

Figure 4-60. Flownex model for SIMPLIFICATION 5 model of the finite tube with two passes.

The transients were introduced by a step change of the inlet air temperature from 1061 °C to 1200 °C at time t = 10s, keeping all other conditions the same. The outlet steam temperature after 40 seconds from the initiation of the transient was monitored for different time step sizes and the results are presented in Figure 4-61.

The monitored outlet steam temperature was still in the unsteady stage of the process to ensure that the equations solved by Flownex were still dependent on the time step. The time step sizes considered were factors of 10 in order to capture the initiation of the transient step change at 10 seconds. Figure 4-61 illustrates that the time step size has an effect on the outlet steam temperature, with the accuracy increasing as the time step becomes smaller and smaller, as it was illustrated for the numerical methods in subsection 4.3.2. In addition, the time constant was calculated and illustrated in Figure 4-62, which further shows that the time steps has an influence on the transient simulations.

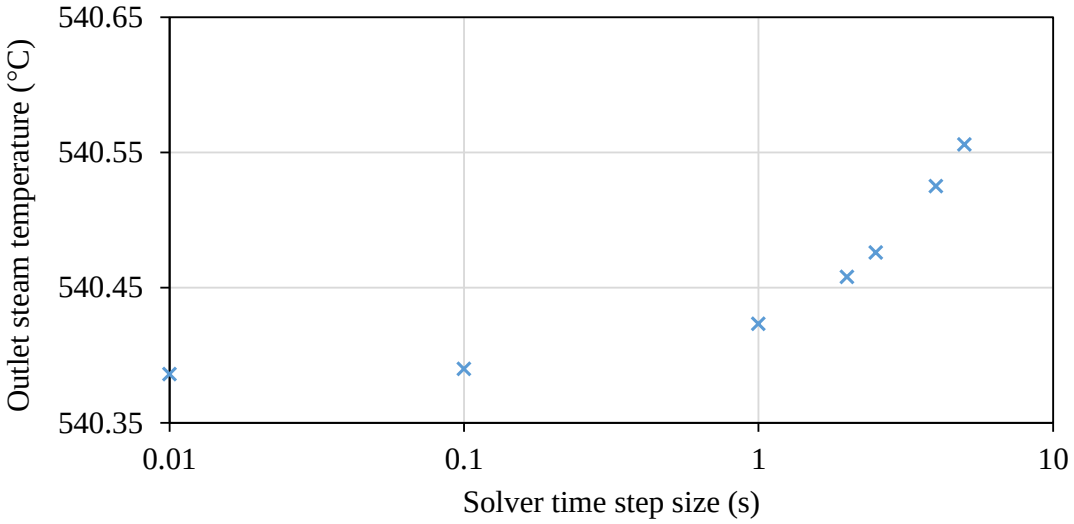

Figure 4-61. Outlet steam temperature vs the time step size after 40s from the initiation of the transient for SIMPLIFICATION 5.

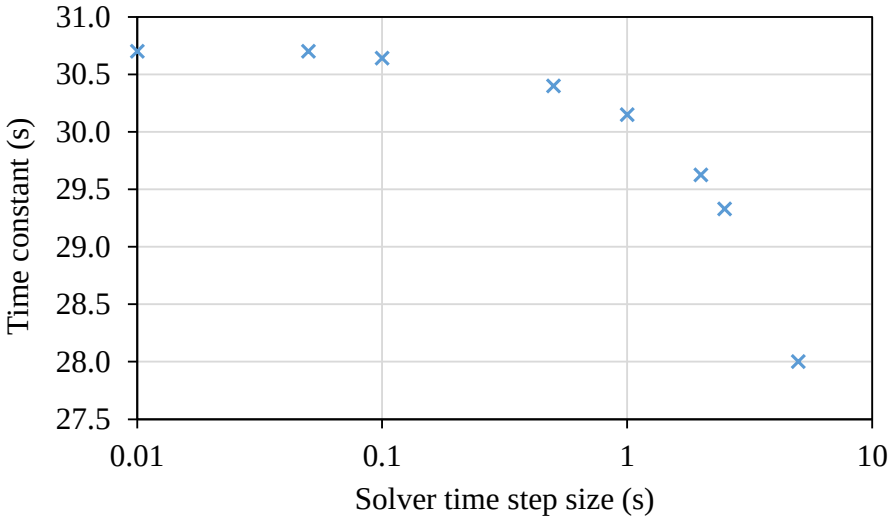

Figure 4-62. Time constant vs solver time step size for the outlet steam temperature for SIMPLIFICATION 5.

4.4.4 Heat exchanger bundle

A boiler heat exchanger is made of tube bundles, as it was introduced in chapter 2. An example of a typical boiler heat exchanger bundle is illustrated in Figure 4-63. This heat exchanger bundle can be modelled using the traditional tube by tube method with the respective discretisation schemes. However, this process is laborious and unrealistic for big heat exchangers. Thus, there is a need for a simple method to model a heat exchanger bundle on Flownex.

This subsection explores a possible method that can be used to simplify the modelling of a heat exchanger bundle on Flownex. This method is compared to the tube by tube method for a heat

exchanger bundle with four tubes. The bundle analysed in this section is described by Figure 4-63, Figure 4-64, Table 4-6, Table 4-7 and a pitch across depth of 70 mm.

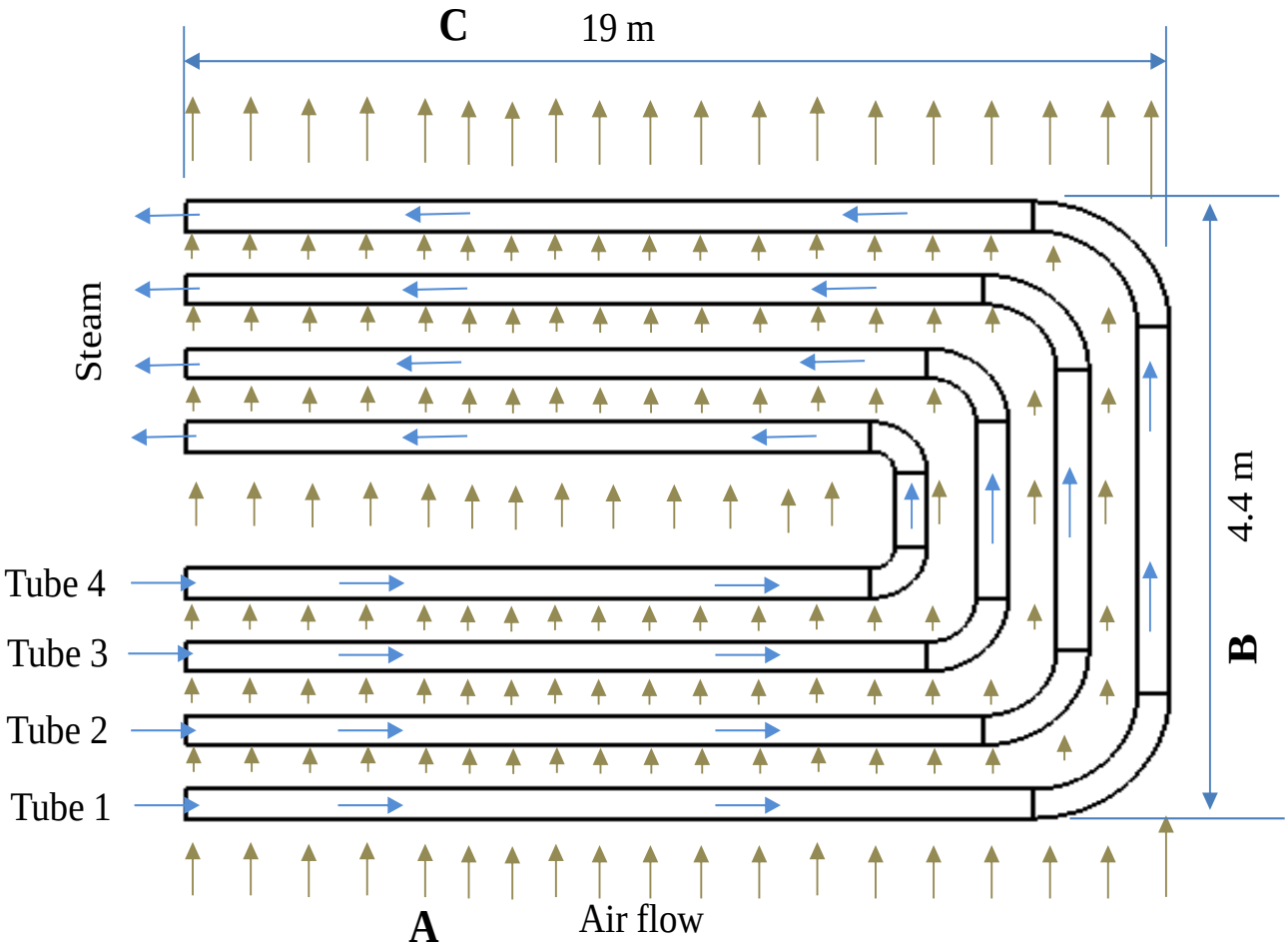

Figure 4-63. Four tubes (bundle) with two passes experiencing cross flow over their major lengths.

Table 4-6. Flow parameters for the case of a tube bundle with two passes.

Parameter	Units	Steam/tube	Air
Flow rate	kg/s	0.96	30
Inlet temperature	°C	480	1061
Inlet pressure	MPa	17.5	0.1
Heat transfer coefficients	$W/m^2°C$	4955	46.7

Table 4-7. Summary of the geometry for the heat exchanger bundle.

Parameter	Units	Tube 1	Tube 2	Tube 3	Tube 4
Inner diameter	mm	31.9	31.9	31.9	31.9
Tube thickness	mm	6.3	6.3	6.3	6.3
Length	m	42.4	42.19	41.98	41.77

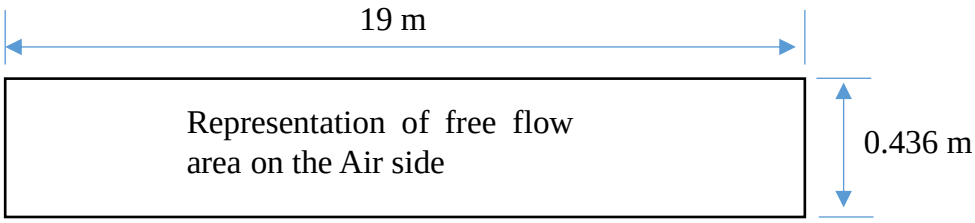

Figure 4-64. Representation of the free flow area on the air side for the heat exchanger bundle.

The analyses begins with the use of the traditional tube by tube modelling method, which serves as a reference case. As with subsection 4.4.3 above, the tubes of this heat exchanger bundle have two passes. Each of these tubes with two passes can be approximated by a tube with a single pass and without axial discretisation in the Flownex modelling as illustrated in Figure 4-65. These tubes can also be modelled on Flownex with two passes as illustrated in Figure 4-66. In Figure 4-66, the vertical part of each tube is divided into two, with one part included in the bottom length and the other in the top length as illustrated by the letters A, B and C on the schematics. Additionally, with the two pass model, the length of the tubes can also be axially discretised as shown in Figure 4-67. The length of the tubes in both passes can be axially discretised further until the desired outlet steam temperature accuracy is achieved.

For this tube by tube modelling method, the first case which is illustrated by Figure 4-65 was named REAL 1. The second model shown on Figure 4-66 was named REAL 2, and the model on Figure 4-67 was named REAL 3. Further models were constructed by axially discretising the length of the tubes on both passes as with the case from Figure 4-66 to Figure 4-67. These models were successively named REAL 2+i (with i being the number of axial building blocks added per tube and per pass).

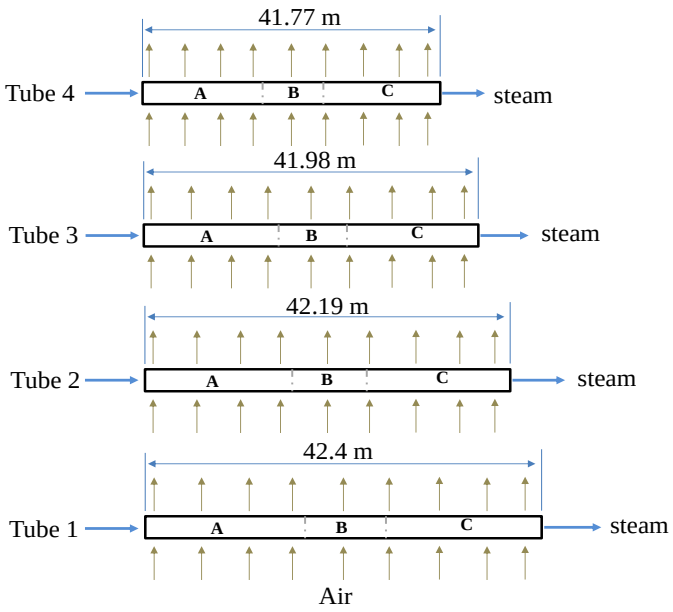

Figure 4-65. Heat exchanger bundle with two pass modelled as one pass, REAL 1.

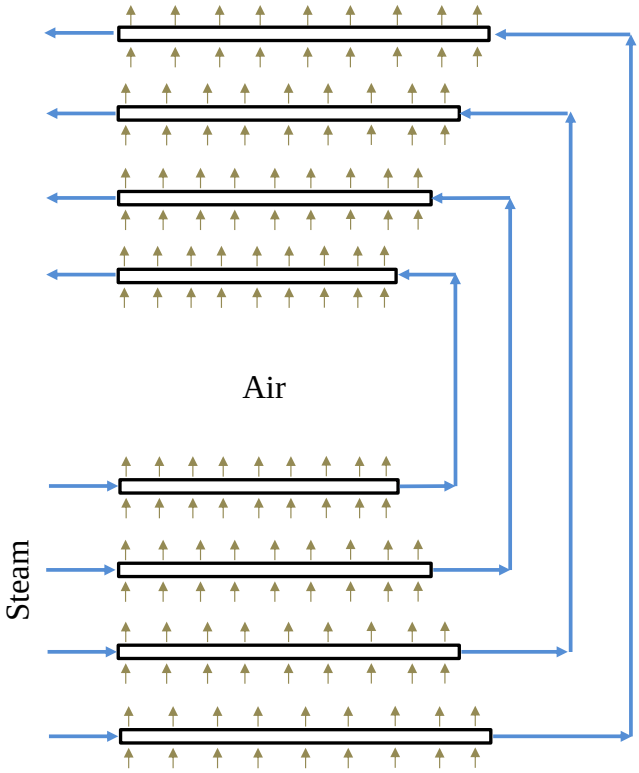

Figure 4-66. Heat exchanger bundle with two passes modelled as two passes without axial discretization, REAL 2.

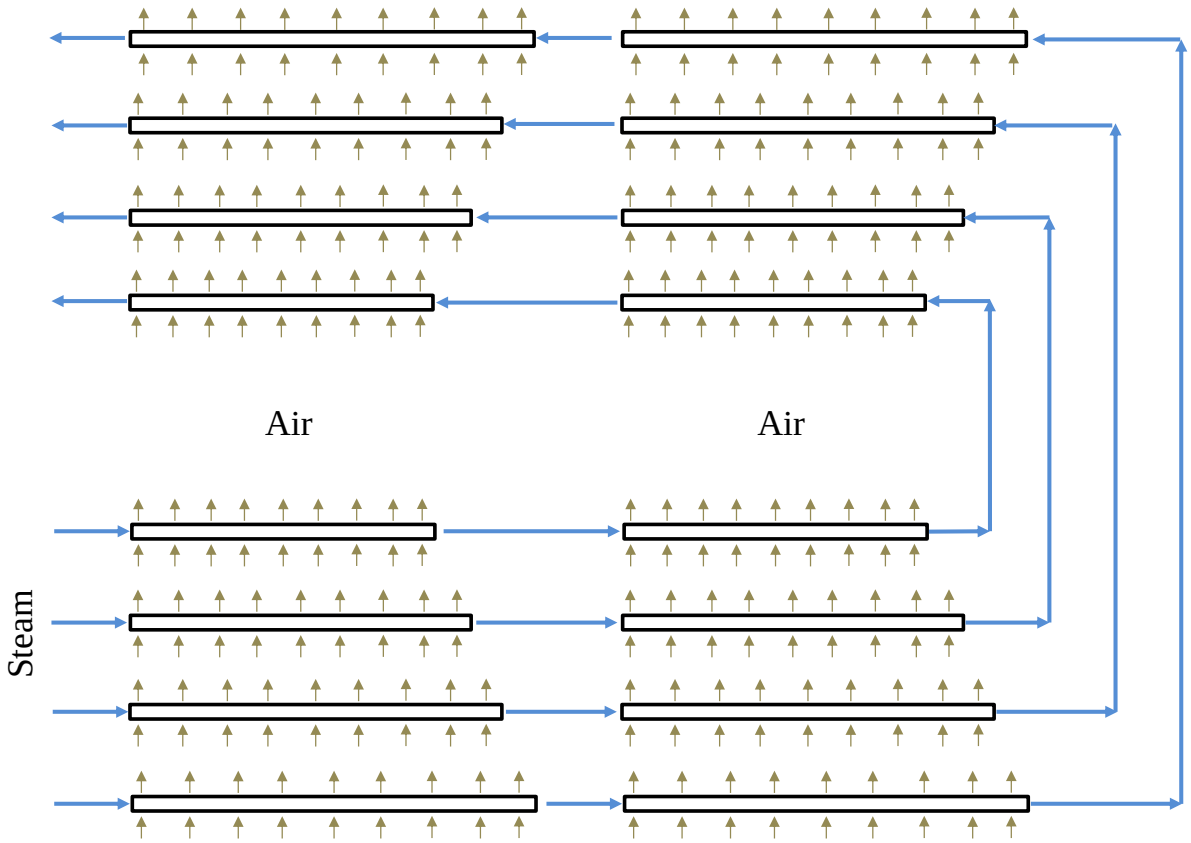

Figure 4-67. Heat exchanger bundle with two passes modelled as two passes with axial discretization, REAL 3.

For all the Flownex models, the outer diameter of each tube is maintained on the air stream through manipulating the inlet circumference of the tube for the air and keeping the inlet free flow area the same. This is achieved by using equation (4.22) which is given by:

$$P_{outer} = \frac{4A_{freeflow}}{OD_{tube}}$$

with P, A and OD the inlet perimeter, inlet area and outer diameter, respectively. The inlet area is shown on Figure 4-64. This results in a hydraulic diameter which is the same as the outer diameter of each tube.

The effect of radial discretisation on each tube is assumed to be negligible, thus all the tubes modelled on Flownex have no discretisation on the thickness.

Similarly to the cases in subsection 4.4.3, the temperature of the air stream over each tube is calculated as the average temperature of the inlet and the outlet temperatures on the Flownex models. For each successive model after REAL 2, the Flownex models do not allow mixing of the air stream from tube row to row and pass to pass due to the way the tubes are discretised on Flownex, as shown in Figure 4-68 for REAL 3. However, this assumption will still be investigated further in projects to follow.

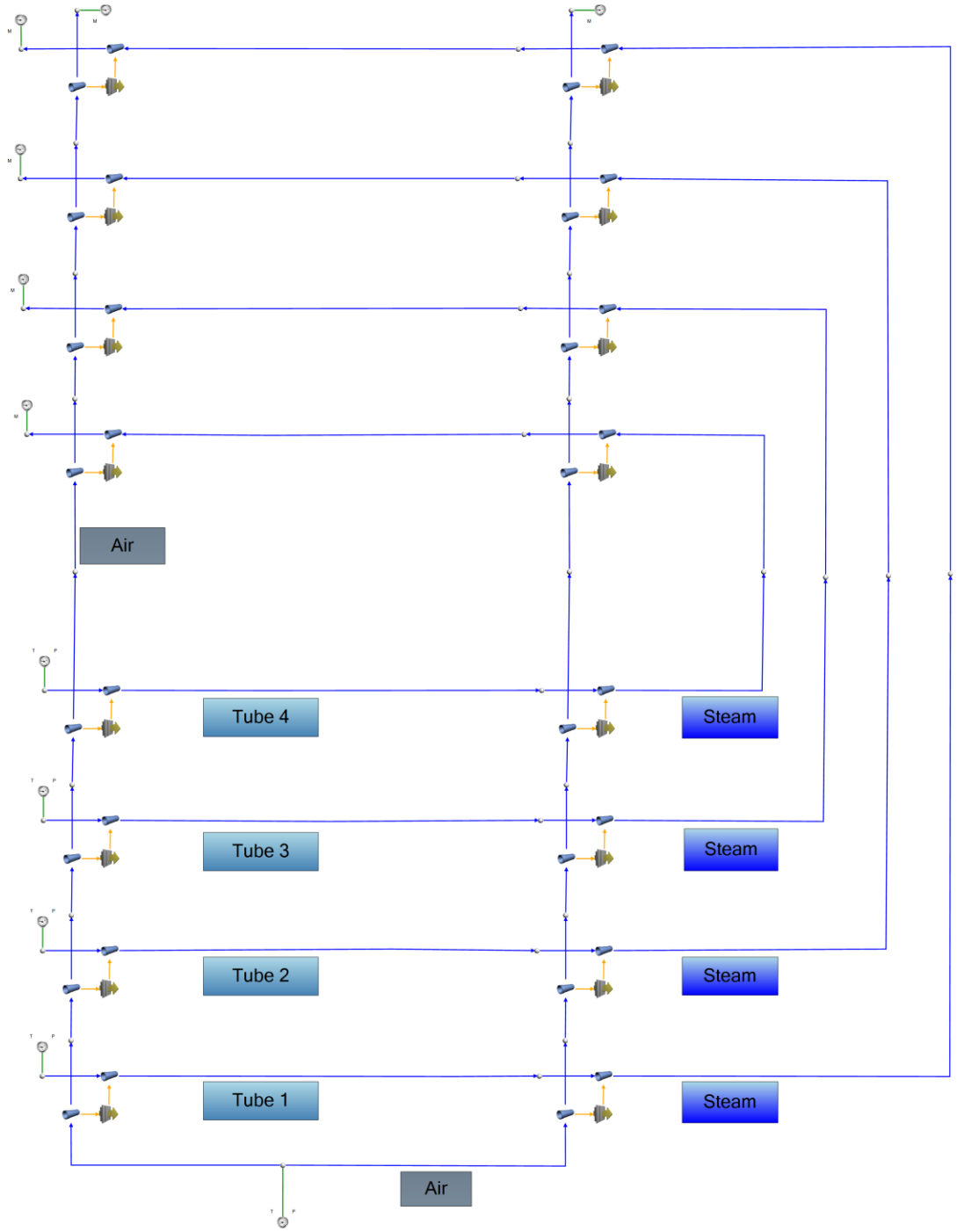

Figure 4-68. Flownex representation of REAL 3 which is schematically shown in Figure 4-67.

Now investigating the possibility of simplifying the modelling of a heat exchanger bundle. It is assumed that the tubes of the heat exchanger bundle can be combined and modelled as one tube on Flownex as shown in Figure 4-69.

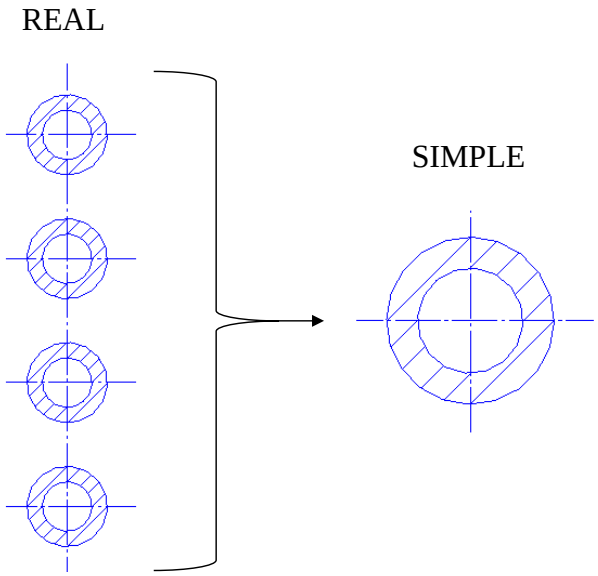

Figure 4-69. Schematic showing the desired simplification of the REAL model to a SIMPLE model.

With this simplification the average tube length of 42.085 m is used. In the modelling, the first case involves the approximation of the four tubes' two passes by one tube with a single pass and without axial discretisation as illustrated in Figure 4-70. The second case involves modelling these tubes as one tube with two passes as illustrated in Figure 4-71. In this case the vertical part of each tube is divided into two, with one part included in the bottom length and the other in the top length as illustrated by the letters A, B and C on the schematics. Additionally, with the two pass model, the length of the tube can also be axially discretised as shown in Figure 4-72. The length of the tube in both passes can be axially discretised further until the desired outlet steam temperature accuracy is achieved.

In this simplified modelling method, the first case which is illustrated on Figure 4-70 was named SIMPLE 1. The second case which is shown on Figure 4-71 was named SIMPLE 2, and the case illustrated on Figure 4-72 was named SIMPLE 3. Further models were done by axially discretising the length of the tubes on both passes as the case from Figure 4-71 to Figure 4-72. These models were successively named SIMPLE 2+i (with i being the number of axial building blocks added per tube).

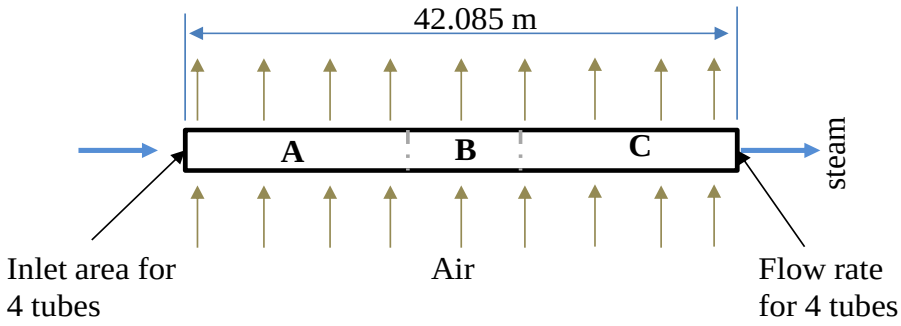

Figure 4-70. Heat exchanger bundle with two pass modelled as one pass with all four tubes combined into one tube, SIMPLE 1.

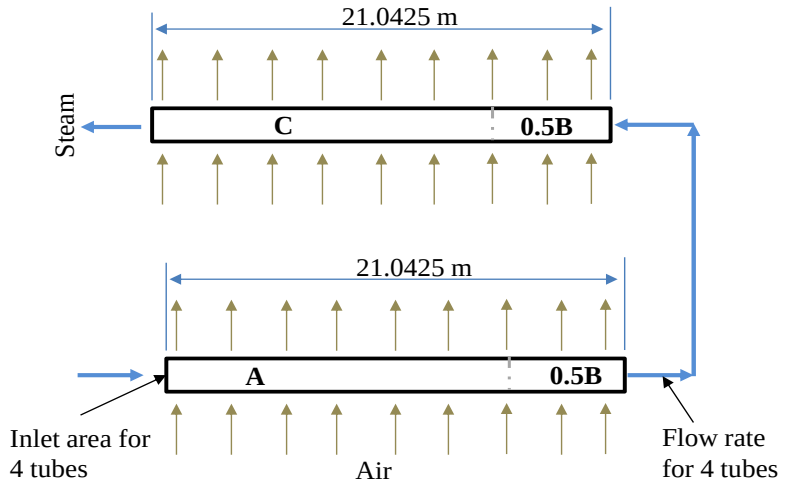

Figure 4-71. Heat exchanger bundle with two passes modelled as two passes without axial discretization with all the four tubes modelled as one tube, SIMPLE 2.

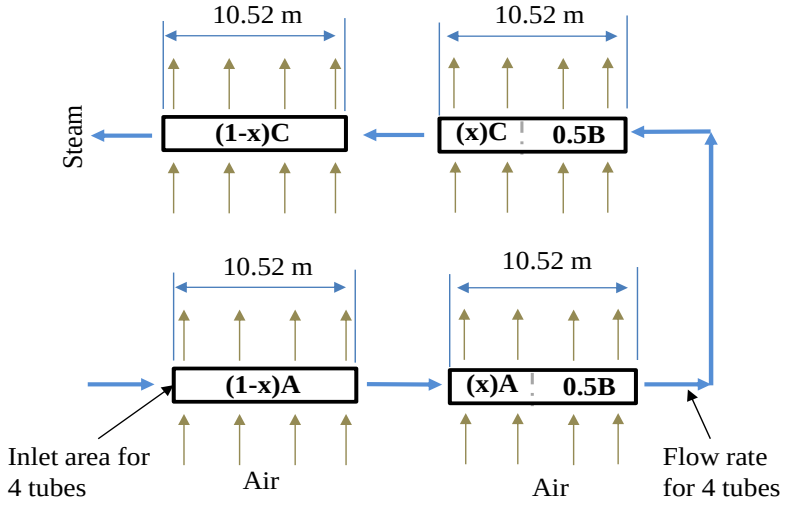

Figure 4-72. Heat exchanger bundle with two passes modelled as two passes with axial discretization and the four tubes are modelled as one tube, SIMPLE 3.

Similarly to the tube by tube modelling method, for the outside flow, the outer hydraulic diameter calculated by Flownex should be the same as the outer diameter for one tube. This is ensured by manipulating the inlet perimeter/circumference on the Flownex inputs using equation (4.22) written as:

$$P_{outer} = \frac{4A_{freeflow}}{OD_{tube}}$$

with P, A and OD the inlet perimeter, inlet area and outer diameter, respectively. The inlet area is shown on Figure 4-64. Despite the fact that the tubes are combined into one tube, the outer diameter used in the equation should be that of one tube in the bundle.

In addition, for this simplified method, the inner hydraulic diameter calculated by Flownex should be equivalent to the diameter of one tube in the bundle. This is done through manipulating the inlet perimeter/ circumference of the tube for the steam flow, using the following equation:

$$P_{inner} = \frac{4A_{combined}}{ID_{tube}} \tag{4.23}$$

with $A_{combined} = 4 \times A_{one.tube}$. Also, P, A and ID represent the inlet perimeter, inlet cross sectional area and inner diameter, respectively.

Ensuring that the inner and outer hydraulic diameter are the same as that for one tube is important in the calculation of the heat transfer coefficients for cases in which Flownex is instructed to calculate them. However, in the cases modelled here the heat transfer coefficients are fixed.

For this method as well, the effect of radial discretisation on the SIMPLE tube is assumed to be negligible, thus for all the Flownex models there is no discretisation on the thickness.

For this modelling method, the air stream temperature is the same for all the four tubes in a pass. This temperature is calculated as the average of the inlet and outlet temperature for that pass. For each successive model after SIMPLE 2, the Flownex models do not allow mixing of the air stream from tube pass to pass due to the way the tubes are discretised on Flownex, as shown in Figure 4-73 for SIMPLE 3. However, this assumption will still be investigated further in projects to follow.

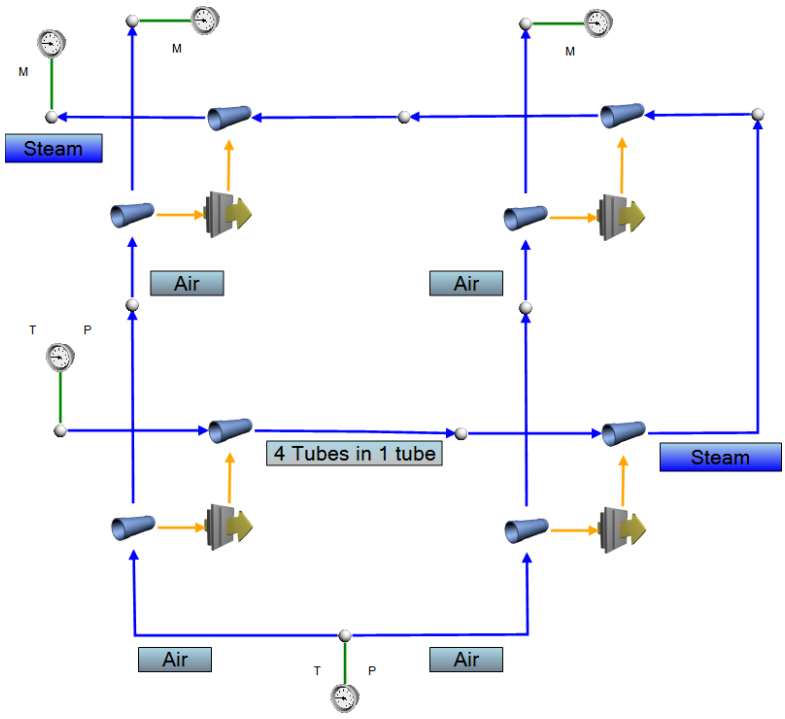

Figure 4-73. Flownex model representing the scenario presented by Figure 4-72, SIMPLE 3.

4.4.4.1 Steady state simulations

For steady state simulations on Flownex, the thermal resistance for both modelling methods must be calculated with extra caution. The equation used by Flownex to calculate the thermal resistance of a system as per the selected standard (average areas) area discretisation scheme is as follows:

$$R_{th} = \frac{1}{h_i \cdot SA_i} + \frac{x}{kA_{av}} + \frac{1}{h_o \cdot SA_o} \tag{4.24}$$

with $A_{av} = \frac{SA_i + SA_o}{2}$ for a case without thickness discretisation.

h, SA, k, x and L represent the heat transfer coefficient, surface area, thermal conductivity of the tube, the thickness of the tube and the length of the tube, respectively. Subscripts i and o stands for inside and outside of the tube, respectively.

For the tube by tube method, Flownex uses equation (4.24) to calculate the thermal resistance for each tube. However, for the simplified method, SIMPLE, the thermal resistance on the modelled tube should be calculated with extra caution. So, for correct calculations of the thermal resistance for the SIMPLE method, the thickness of the tube in the SIMPLE method should be the same as that of each tube in the REAL method. This ensures that the middle term in equation (4.24) is calculated correctly. Additionally, both the inner and outer surface areas should represent that of the four tubes combined, in order to capture the correct amounts of heat transferred. Furthermore, the flow rates for both fluid streams should be the same as that on four tubes. Thus, the steam flow is a combination of the steam flow for four tubes and the air flow is left unchanged.

For both modelling methods, REAL and SIMPLE, the steady state outlet steam temperature was monitored and recorded in Table 4-8.

Table 4-8. Steady state temperature results for both REAL and SIMPLE modelling methods.

Description	Steady state temperature (°C)				Description	Steady state temperature (°C)
	Tube 1	Tube 2	Tube 3	Tube 4		
REAL 1	528.837	528.247	527.665	527.089	SIMPLE 1	527.108
REAL 2	529.363	529.119	528.877	528.638	SIMPLE 2	528.110
REAL 3	529.788	529.538	529.289	529.041	SIMPLE 3	528.507
REAL 4	529.884	529.631	529.381	529.131	SIMPLE 4	528.594
REAL 5	529.916	529.665	529.414	529.164	SIMPLE 5	528.626

In Table 4-9, the average steady state temperature from the tubes of the REAL modelling method is compared to the temperature results from the SIMPLE modelling method, for each modelling stage. The percentage differences shows that at each modelling stage the results of the SIMPLE method are within 0.002% of the average results from the REAL method.

Table 4-9. Comparison of the average steady state temperatures of the REAL method to the temperature results of the SIMPLE method.

Description	REAL: Average Temperature (°C)	SIMPLE: Temperature (°C)	Temperature Difference (°C)	% Difference
Stage 1	527.960	527.108	0.851	0.00161
Stage 2	528.999	528.110	0.889	0.00168
Stage 3	529.414	528.507	0.907	0.00171
Stage 2	529.507	528.594	0.913	0.00172
Stage 5	529.540	528.626	0.914	0.00173

Table 4-10 shows the worst case scenario, where the maximum temperature from the REAL method is compared to the results of the SIMPLE method. For this comparison, the temperature difference when compared to the maximum temperature for each stage is within 0.004%.

Table 4-10. Comparison of the maximum steady state temperatures of the REAL method to the temperature results of the SIMPLE method.

Description	REAL: Maximum Temperature (°C)	SIMPLE: Temperature (°C)	Temperature Difference (°C)	% Difference
Stage 1	528.837	527.108	1.729	0.00327
Stage 2	529.363	528.110	1.253	0.00237
Stage 3	529.788	528.507	1.281	0.00242
Stage 2	529.884	528.594	1.290	0.00243
Stage 5	529.916	528.626	1.290	0.00243

4.4.4.2 Transient simulations

In addition to the caution in capturing the thermal resistance of the original case on the SIMPLE model, transient simulations also require special attention on the capturing of the thermal mass of the system.

For the fundamental understanding of the transient behaviour of the system, it is analysed through representing it using the electrical circuit network shown in Figure 4-74. This analyses was introduced in subsection 2.2.2.1 for the lumped capacity system. From this analyses, it can be depicted that for correct transient simulations:

$$\left(R_{th}C_{th}\right)_{SIMPLE} = \left(R_{th}C_{th}\right)_{REAL} \tag{4.25}$$

with R_{th} and C_{th} the thermal resistance and capacitance, respectively.

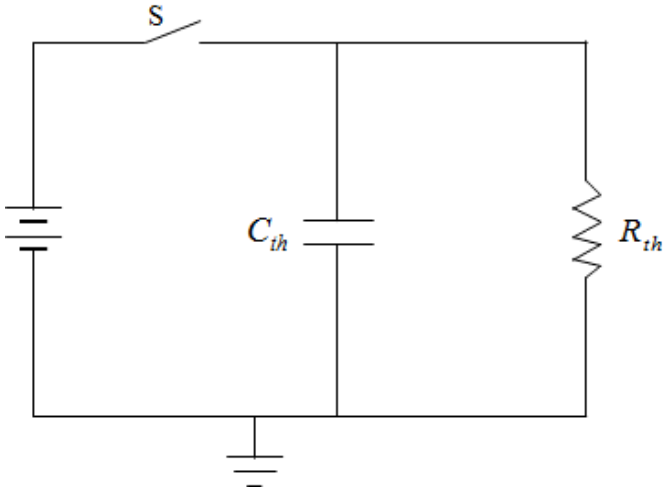

Figure 4-74. An electrical representation of the thermal system.

The thermal resistance, R_{th} for both the REAL and SIMPLE models is controlled by the steady state simulations as demonstrated in subsection 4.4.4.1 above. Due to the modifications on the steady state simulations, the sum of the thermal resistances for all the tubes in the REAL models is different from the thermal resistance of the SIMPLE models in each stage. This is summarised as:

$$R_{SIMPLE} \neq \left(\sum\left(R_{th}\right)\right)_{REAL}$$

This implies that only the thermal capacitance of the SIMPLE model can be altered to satisfy the transient simulations. The selected standard (average areas) area discretisation scheme allows Flownex to solve the 2D Cartesian form of the heat conduction equation without heat generation given by equation (2.10) in per unit volume as:

$$\frac{\partial}{\partial x}\left(k\frac{\partial T}{\partial x}\right)+\frac{\partial}{\partial y}\left(k\frac{\partial T}{\partial y}\right)=\rho c\frac{\partial T}{\partial t}$$

The thermal capacitance of a system is given by:

$$C_{th} = \rho c V$$

with ρ, c and V representing the density, the specific heat capacity and the volume of the solid material, respectively.

The volume of the material on Flownex is determined by the geometry modelled to satisfy the steady state. Thus the volume is controlled by the steady state simulations and cannot be altered for the transient simulations. However, the thermal capacitance per unit volume of the material given by:

$$\frac{C_{th}}{V} = \rho c$$

can be altered on Flownex for the transient simulations, since the steady state simulations do not depend on it.

In order to modify the thermal capacitance per unit volume for the SIMPLE model, a Microsoft excel model was built. In this model, the thermal resistance and capacitance for the system were calculated using both methods. Then, the $R_{th}C_{th}$ for both methods were calculated. The thermal capacitance per unit volume for the SIMPLE method was altered to force an equality for equation (4.25). The Microsoft excel model was customised for all five modelling stages. It was found that the capacitance per unit volume should be the same for all the models, given as:

$$\left(\frac{C_{th}}{V}\right)_{SIMPLE} = 14569380 \cdot \frac{J}{m^3 \cdot °C}$$

This implies that the SIMPLE modelling method is modelling a different material compared to the REAL method. The REAL method is modelling the steel with properties given in Table 4-1, thus the thermal capacitance per unit volume for each tube is:

$$\left(\frac{C_{th}}{V}\right)_{REAL} = 3642345 \cdot \frac{J}{m^3 \cdot °C}$$

For both REAL and SIMPLE modelling methods, transient simulations were done. For all the models, the transients were introduced by a step change of the inlet air temperature from 1061 °C to 1200 °C at time t = 10s, keeping all other conditions the same. The transient outlet steam temperature was monitored and plotted against time until equilibrium was reached for a solver time step size of 0.1s. The time constants were established from the transient temperature vs time graphs, and they are tabulated in Table 4-11.

Table 4-11. Time constants for both REAL and SIMPLE method for transient simulations.

Description	Time constant (s)				Description	Time constant (s)
	Tube 1	Tube 2	Tube 3	Tube 4		
Real 1	40.7	41.2	41.7	42.2	Simple 1	43.9
Real 2	34.2	33.9	33.7	33.5	Simple 2	37.3
Real 3	31.6	31.5	31.3	31.1	Simple 3	34.7
Real 4	31.1	30.9	30.7	30.6	Simple 4	34.1
Real 5	31.0	30.8	30.6	30.4	Simple 5	33.9

In Table 4-12 the average time constant for each stage of the REAL model results is compared to the SIMPLE model time constant result. The percentage difference at each stage is below 0.15%.

Table 4-12. Comparison of the average time constant of the REAL model with the time constant result from the SIMPLE model.

Description	REAL: Average time constant (s)	SIMPLE: Time constant (s)	Time constants difference (s)	% Difference
Stage 1	41.5	43.9	2.5	0.06
Stage 2	33.8	37.3	3.5	0.10
Stage 3	31.4	34.7	3.4	0.11
Stage 2	30.8	34.1	3.3	0.11
Stage 5	30.7	33.9	3.2	0.11

Table 4-13 shows the worst case scenario comparison, where the minimum or smallest time constant of the REAL model results at each stage is compared to the time constant for the SIMPLE model. The percentage difference for this comparison is also below 0.15% at each stage.

Table 4-13. Comparison of the minimum time constant of the REAL model with the time constant result from the SIMPLE model.

Description	REAL: Minimum time constant (s)	SIMPLE: Time constant (s)	Time constants difference (s)	% Difference
Stage 1	40.7	43.9	3.2	0.08
Stage 2	33.5	37.3	3.8	0.11
Stage 3	31.1	34.7	3.6	0.12
Stage 2	30.6	34.1	3.5	0.11
Stage 5	30.4	33.9	3.5	0.12

It should be noted that the analyses were only done on a heat exchanger bundle with four tubes, thus they are not generic. However, this analyses presents a way that can be used to quickly model a heat exchanger bundle.

4.4.4.3 Other modelling aspects of a tube bundle

In modelling such a tube bundle, there are some issues to be aware off. Firstly, since the tube bundle is connected to a header in a real PF plant heat exchanger, the steam mass flow rate in the different tubes might not be the same. Secondly, it should also be noted that the fluid properties of both the air and steam varies along the length of the tube. This variation is a result of the change in temperature along the length. This variation has an effect on the heat transfer coefficient for each stream, since this coefficient depends on these properties. The heat transfer coefficient is calculated using correlations that are available from literature. Capturing the heat transfer using more refined heat transfer coefficient calculations will improve the accuracy of the outlet steam temperature.

Additionally, the heat transfer coefficients outside the tubes might differ. For example, in a case where the pitch of the tubes in a bundle like Figure 4-63 is small, then only the first tube in the first pass and the first tube in the second pass will experience cross flow heat transfer from the outside fluid. The other tubes will experience a flow on the sides only, since the outside fluid will not be able to penetrate within the tubes in the bundle. Furthermore, certain heat exchangers in the boiler are exposed to radiation heat transfer that has to be taken into account in the modelling.

However, this modelling aspect will not be addressed in this project.

4.4.5 Summary

This section illustrated the application of Flownex in modelling a boiler heat exchanger. It started by illustrating that Flownex is capable of modelling conduction heat transfer within the thickness of a tube. It was also illustrated that radial discretisation has an effect on the radial temperature distribution especially for thick tubes, due to the average area discretisation scheme in Flownex and truncation errors. It was further demonstrated that Flownex is capable of modelling tubes with finite lengths. With the possibility of discretising the length through physically building the tube with small heat exchangers called the “building blocks”. Finite tubes with two passes have also been modelled. For the modelling of multi-passes, the building block approach was used.

A tube bundle was modelled with two methods; a tube by tube method and a combined tube method which were then compared for both steady and transient simulations. It was further demonstrated that Flownex transient simulation results also depend on time-wise discretisation.

It is very important to note that the results presented in this section are case dependent hence cannot be generalised for all cross flow heat exchangers but they do illustrate the important issues that needs to be addressed when modelling such heat exchangers.

Finally as a general conclusion, it can be said that the main aim for Flownex modelling is to keep the models as simple as possible so that they can be quickly created and run as well as to avoid modelling errors while keeping the accuracy in a known range. The present work serves as a first approach in this area that is focused on determining the most critical parameters that have to be taken into account in analysing this trade-off between “modelling easiness” and “accuracy” of results.

Chapter 5

5 Conclusions and Future work

This chapter presents the conclusions of this project and future work on modelling boiler heat exchangers.

5.1 Conclusions

It is well known that aging of the high pressure and temperature parts of the water-steam power plants is mainly due to creep and thermal fatigue. The level of temperature generate creep while temperature gradients within the solids generate thermal stresses and lead to thermal fatigue when these stresses are cycled. This fatigue also accelerates the creep and vice versa in a mechanism called creep-fatigue interaction. Thus, establishing an understanding of the level and gradient of temperature in high temperature components is important, these being generated by the fluids surrounding the heat exchanger, i.e. the flue gas on the hot side and the water or steam on the cold side.

In this project, an understanding of the aging mechanisms in boiler heat exchangers due to dynamic operation was established through explaining these mechanisms. In addition, modelling approaches to characterising the dynamic behaviour of a boiler heat exchanger were presented. The modelling approaches entailed a systematic presentation starting with the use of exact analytical solutions to characterise transient conduction heat transfer for simplified problems. Then, followed by the use of the finite volume numerical method. Finishing off with the use of Flownex to model a heat exchanger bundle with complex layouts. In each approach, certain issues that need to be addressed in modelling heat exchangers were illuminated.

The activities involved the characterisation of the transient temperature distribution within a carbon steel material using exact analytical solutions and numerical solutions to the heat conduction equation. The exact analytical solutions established an understanding of transient conduction heat transfer including the dependency of the solution on dimensionless Fourier and Biot number. The exact analytical solutions to simplified heat transfer problems were further used to calculate thermal stresses within the material demonstrating the relationship between the temperature gradients and the thermal stresses. Furthermore, these exact analytical solutions were used as reference cases for comparison with the finite volume numerical solutions.

The characterisation of the transient temperature distribution using the finite volume numerical method entailed developing and applying the numerical solution to heat transfer problems. It was established

that the numerical solution is dependent on physical space discretisation and time-wise discretisation for transient solutions. An infinitely long tube with an inner radius of 0.2 m and a thickness of 0.1 m was used to demonstrate this. The transient for this case was introduced by changing the original temperature of 30 °C to 50 °C for the inner boundary and 200 °C for the outer boundary at time t = 0s. A Two Norm developed from comparing the numerical results to the exact analytical solution results for time t = 5s and time step size of $\Delta t = 0.01$s showed that the accuracy of the numerical results improves when the number of nodes on the thickness discretisation increases. Another Two Norm developed at time t = 20s for a scenario with 61 nodes on the thickness demonstrated that an increase in the time step size for transient simulations reduces the accuracy of the numerical results.

The thermal-fluid software Flownex was then used to demonstrate its ability in modelling a boiler heat exchanger. For this purpose only the average area discretisation scheme option in Flownex was investigated. It was demonstrated that it is capable of characterising the transient temperature distribution within a solid material. This was verified against the developed numerical solution. It was illuminated that in using Flownex to characterise the temperature distribution within the material, the discretisation of the thickness of the material is important, especially for thick components. This was demonstrated on an infinitely long tube with an inner radius and thickness of 0.2 m and 0.1 m, respectively. A Two Norm was developed by comparing the Flownex results to the numerical results with a fine thickness discretisation and fine time step size. The Two Norm illustrated that the accuracy of the Flownex results improves as the number of nodes for thickness discretisation increases. Thus in modelling thick cylindrical shaped components the thickness should be finely discretised in order to capture the correct temperature profile. The inherent truncation errors adopted in the discretisation scheme in Flownex has an effect on this.

It was also shown that thickness discretisation has a negligible effect on the steady state outlet steam temperature and the time constant calculations for a single pass thin pipe in Flownex. Two tubes with inner diameter of 31.9 mm and 19 m long were used to demonstrate the effect of thickness discretisation on Flownex. One tube had a thickness of 6.3 mm which is a typical thickness for boiler heat exchanger tubes and the thickness of the other tube was 100 mm. For the thin tube, the effect of thickness discretisation on the steady state outlet steam temperature was negligible. However for the thick tube, there was variation on the steady state outlet steam temperature due to the change in the number of nodes on the thickness.

Also, Flownex has the capability of modelling tubes with finite lengths and also allowing for axial discretisation of tubes. It was shown how both heat transfer and time constant are affected by axial discretisation. The possibilities to model multi-passes heat exchangers that will serve at modelling real

tube bundles on Flownex were shown. A heat exchanger bundle was modelled using two methods: a tube by tube (REAL modelling method) and a combined tubes methods (SIMPLE modelling method). For each modelling method, the models' layout was axially discretised in stages in an attempt to capture the real layout of the bundle. For steady state simulation, the resistance of the system was captured with extra caution on the SIMPLE modelling method. The thickness of the combined tube was set to be the same as that of each tube in order to correctly calculate the resistance within the material. The steady state outlet steam temperature results for both modelling methods were compared. The percentage temperature difference from comparing the difference to the average temperature or the worst case scenario at each modelling stage was below 0.004%. For transient simulations, the product of the thermal resistance and the capacitance of the two methods had to be the same. That was ensured by altering the thermal capacitance per unit volume of the SIMPLE method. The time constants from the transient simulation on both modelling methods were compared. The percentage time constant difference from comparing the difference in time constant to the average time constant or the worst case scenario at each modelling stage was below 0.15%.

Finally, since Flownex is a numerical solver, the influence of time step size in modelling transient problems was also shown. This was demonstrated on a finite tube with two passes. Changing the solver's time step size had an effect on the transient outlet steam temperature and time constant.

5.2 Future work

The above described project serves as a starting point in modelling boiler heat exchangers and the complete boiler.

Future work will be aimed at modelling heat exchanger bundles on Flownex illustrating the different amount of flows in the tubes on the steam side as well as different flow and temperature profile on the cross flow flue gas side. Also, programming the properties of flue gas in Flownex will be necessary. It will also entail investigating the error introduced if a tube thickness is modelled using the standard (average areas) area discretisation scheme compared to the linear area change discretisation scheme. For this coming work, the use of appropriate heat transfer correlations in capturing both convection and radiation heat transfer on the flue gas side is fundamental and will be benchmarked with literature review as well as measurements in real boilers.

Future work will also attempt to make the simplified method of modelling cross flow heat exchangers generic. This has to be done in parallel with a tube by tube modelling method for a range of cross flow heat exchangers as well as comparing to experimental results.

Future work will also involve connecting the Flownex heat exchanger models to form a complete boiler model. This model should also include pressure loss analyses in the system. Ultimately this boiler model will be connected to the rest of the plant models that will also include the steam turbine, the condensing, re-generating and boiler feeding systems.

Chapter 6

6 List of References

[1] L. Jestin, M. Fawkes, B. Maccoll and M. Koko, “Eskom Power Plant Engineering Institute (EPPEI) 5-years research strategic plan,” in *POWER-GEN AFRICA CONFERENCE*, Cape Town, South Africa, 2014.

[2] J. B. Kitto and S. C. Stultz, Steam: its Generation and Use, Ohio, United States of America: The Babcock & Wicox Company, 2005.

[3] M. M. Koko, J. Musel and J.-P. Fouiloux, “The New Power Plant Projects of Eskom: An Overview of Medupi and Kusile Power Plants,” in *VGB PowerTech*, Lyon, France, 2009.

[4] B. Li, T. Chen and Y. Dong, “Energy Conversion and Management,” *DBSSP - A computer program for simulation of controlled circulation boiler and natural circulation boiler start up behaviour*, no. 46, pp. 533-549, 2005.

[5] F. P. de Mello and J. C. Westcott, “Power Technologies, Inc,” *Steam Plant Startup and Control in System Restoration,* vol. 9, no. 1, pp. 93-101, 1 February 1994.

[6] K. E. Heselton, Boiler operator's handbook, Lilburn: Fairmont Press, Inc., 2005.

[7] E. B. Woodruff, H. B. Lammers and T. F. Lammers, Steam Plant Operation, 8. Edition, Ed., McGraw-Hill Companies, 2004.

[8] T. J. Wardle, “Creep-Rupture assessment of superheater tubes using nondestructive oxide thickness measurements,” in *ICOLM (International conference on life management and life extension of power plant)*, Xi'an, P.R. China, 2000.

[9] K. Sankhala, Z. Gauri, P. Sharma and D. K. Jain, “Study of microstructural degradation of boiler tubes due to creep for remaining life analysis,” *International journal of engineering research and applications,* vol. 4, no. 7, pp. 93-99, 2014.

[10] D. N. French, “Creep and creep failures,” The national board of boiler and pressure vessel inspectors, Northborough, MA, 1991.

[11] A. Weronski and T. Hejwowski, Thermal fatigue of metals, New York: Marcel Dekker, Inc., 1991.

[12] Y. F. Balandin, “Thermal fatigue of metals,” *Metal science and heat treatment of metals,* vol. 3, no. 3-4, pp. 91-96, 1961.

[13] V. Radu, E. Paffumi and N. Taylor, "New Analytical Stress Formulae for Arbitrary Time Dependent Thermal Loads in Pipes," European Commission Joint Research Centre Institute for Energy, Netherlands, 2007.

[14] A. Lanin and I. Fedik, Thermal Stress Resistance of Materials, New York: Springer-Verlag Berlin Heidelberg, 2008.

[15] R. F. Barron and B. R. Barron, Design for Thermal Stresses, Hoboken, New Jersey: John Wiley & Sons, Inc., 2012.

[16] A. E. Segall, "Thermal Stresses in Vessels, Piping, and Components," in *Pressure Vessels and Piping Systems*, University Park, USA, UNESCO-EOLSS, pp. 1-6.

[17] L. Madureira and F. Q. Melo, "A hybrid formulation in the stress analysis of curved pipes," *Engineering Computations,* vol. 17, no. 8, pp. 970-980, 2000.

[18] Y. Takahashi, "Creep-fatigue interaction: Its mechanism and predictability," in *Asian Pacific Conference for Materials and Mechanics*, Yokohama, Japan, 2009.

[19] Verein Deutscher Ingenieure, VDI Heat Atlas, Verlag, Berlin & Heidelberg: Springer, 2010.

[20] J. P. Holman, Heat Transfer, Singapore: McGraw-Hill, 2010.

[21] B. Weigand, Analytical Methods for Heat Transfer and Fluid Flow Problems, Berlin, Germany: Springer, 2004.

[22] R. Haberman, Elementary Applied Partial Differential Equations with Fourier Series and Boundary Value Problems, New Jersey: Prentice-Hall, INC, 1983.

[23] N. M. Ozisik, Heat Conduction, New York: John Wiley & Sons, Inc, 1993.

[24] H. S. Carslaw and J. C. Jaeger, Conduction of Heat in Solids, London: Oxford University Press, 1959.

[25] F. Bowman, Introduction to Bessel Functions, New York: Dover Publications Inc., 1958.

[26] C. P. Kothandaraman, Fundamentals of heat and mass transfer, New Delhi: New Age International (P) Limited, Publishers, 2006.

[27] T. L. Bergman, A. S. Lavine, F. P. Incropera and D. P. Dewitt, Fundamentals of heat and mass transfer, United states of America: John Wiley & Sons, Inc., 2011.

[28] Y. A. Cengel, Heat Transfer: A practical Approach, New York: McGraw-Hill Higher Education, 2003.

[29] C. G. du Toit, "A Simple Tutorial on Finite Differences, Volumes and Elements at the Hand of an Example," in *Seventh South African Conference on Computational and Applied Mechanics*, Potchefstroom, North West Province, South Africa, 2010.

[30] K.-F. V. Wong, Intermediate Heat Transfer, New York, Basel: Marcel Dekker, Inc., 2003.

[31] A. Ilgevicius, "Analytical and numerical and simulation of heat transfer in electrical conductors and fuses," University of the German Federal Armed Forces, Munich, 2004.

[32] A. Faghri, Y. Zhang and J. Howell, Advanced Heat and Mass Transfer, Columbia, USA: Global Digital Press, 2010.

[33] S. V. Patankar, Numerical Heat Transfer and Fluid Flow, New York: Hemisphere Publishing Corperation, 1980.

[34] J. C. Olivier, "Network modelling of transient heat exchanger performance," Potchefstroom University for Christian Higher Education, Potchefstroom, 2005.

[35] A. Walter, A. Schulz and G. Lohnert, "Comparison of Two Models for a Pebble Bed Modular Reactor Core Coupled to a Brayton Cycle," in *2nd International Topical Meeting on High Temperature Reactor Technology*, Beijing, China, 2004.

[36] P. G. Rousseau and B. du Toit, Practical Thermal-Fluid System Simulation: Short Course, Potchefstroom, North West South Africa: M-Tech Industrial (Pty) Ltd, 2013.

[37] Y. A. Cengel and J. M. Cimbala, Fluid Mechanics: Fundamentals and Applications, New York: McGraw-Hill Companies, Inc, 2006.

[38] M-Tech Industrial, Flownex Library Manual, Potchefstroom, North West Province, South Africa: M-Tech Industrial, 2013.

[39] D. Gvozdenac, "Analytical solution of dynamic response of heat exchanger," in *Heat exchanger - basic design applications*, Rijeka, InTech, 2012, pp. 53-78.

[40] D. D. Gvozdenac, "Analytical solutions of the transient response of gas to gas cross flow heat exchanger with both fluids unmixed," *Journal of heat transfer*, vol. 108, no. 4, pp. 722-727, 1986.

[41] J. Yin and M. K. Jensen, "Analytical model for transient heat exchanger response," *International journal of heat and mass transfer*, pp. 3255-3264, 2003.

[42] M. A. Abdelghani-Idrissi, F. Bagui and L. Estel, "Analytical and experimental response time to flow rate step along a counter flow double pipe heat exchanger," *International journal of heat and mass transfer*, pp. 3721-3730, 2001.

[43] K. S. Chang, Y. C. Kweon and S. R. Jin, "A numerical analysis on the transient heat transfer in a heat exchanger pipe flow," *Journal of the Korean Nuclear Society*, vol. 32, no. 1, pp. 46-56, 2000.

[44] S. Bracco, I. Faccioli and M. Troilo, "A numerical discretization method for the dynamic simulation of a double-pipe heat exchanger," *International journal of energy*, vol. 1, no. 3, pp. 47-58, 2007.

[45] W. Roetzel and Y. Xuan, "Transient behaviour of multipass shell-and-tube heat exchangers," *International journal of heat and mass transfer,* vol. 35, no. 3, pp. 703-710, 1992.

[46] M. R. Ansari and V. Mortazavi, "Simulation of dynamical response of a countercurrent heat exchanger to inlet temperature or mass flow rate change," *Applied thermal engineering,* pp. 2401-2408, 2006.

[47] J. L. M. Hensen and A. E. Nakhi, "Fourier and Biot numbers and the accuracy of conduction modelling," in *BEPAC Conference '94,* University of York, 1994.

[48] J. R. Waters and A. J. Wright, "Criteria for the distribution of nodes in multilayer walls in finite-difference thermal modelling," *Building and Environment,* vol. 20, no. 3, pp. 151-162, 1985.

[49] T. P., K. Piira and M. Vuolle, "A rational method for the distribution of nodes in modelling of transient heat conduction in slabs," *Building and Environment,* vol. 35, pp. 397-406, 2000.

[50] R. Holopainen, P. Tuomaala and J. Piippo, "Uneven gridding of thermal nodal networks in floor heating simulations," *Energy and Buildings,* vol. 39, pp. 1107-1114, 2007.

[51] A. V. Luikov, Analytical Heat Diffusion Theory, New York & London: Academic Press, 1968.

[52] L. R. Ingersoll, O. J. Zobel and A. C. Ingersoll, Heat Conduction with Engineering, Geological, and Other Applications, London: Thames and Hudson, 1955.

[53] D. W. Mackowski, "Conduction Heat Transfer: Notes for MECH 7210," Mechanical Engineering Department, Auburn University.

[54] E. Gutierrez-Miravete, "Conduction Heat Transfer," 11 January 2006. [Online]. Available: http://www.ewp.rpi.edu/hartford/~ernesto/S2006/CHT/Notes/ch03.pdf. [Accessed 22 September 2013].

Appendix A

A. Exact solution derivation for an infinite plate

If an infinite plate, which is at an equilibrium condition is suddenly subjected to a change in the surrounding environment, sometime must be allowed to pass before a new equilibrium temperature condition is established [20]. The analysis of the change of temperature with time as a new equilibrium is being established is called the transient analysis.

Considering an infinite plate as shown on Figure 2-8b (without heat generation) and Figure 4-2, mathematically the transient temperature can be given in Cartesian coordinates as

$$\frac{\partial^2 T}{\partial x^2} = \frac{1}{\kappa}\frac{\partial T}{\partial t} \tag{7.1}$$

with $\kappa = k/\rho c$, the thermal diffusivity of the material, with the assumption that the thermo-physical properties do not vary with x.

If originally $(t < 0)$ the temperature distribution in the plate and the surroundings is given by a constant T_{or} as shown in Figure 4-2a. Then, if at time $t = 0$ a temperature T_L is instantaneously imposed at both boundaries of the plate, as shown in Figure 4-2b for $T_L = 0.$ Then, the initial and boundary conditions can be summarised as

$$T(x,0) = T_i, \quad t = 0 \quad \text{initial condition} \tag{7.2}$$

$$T(\pm L, t) = 0, \quad t > 0 \quad \text{boundary condition} \tag{7.3}$$

Due to the symmetry of this case, it is deduced that

$$\frac{\partial T(0,t)}{\partial x} = 0 \tag{7.4}$$

Thus only the positive x direction can be considered. In using the separation of variables method, let

$$T(x,t) = u(x).v(t) \tag{7.5}$$

Differentiating the equation leads to

$$\frac{dT}{dx} = u'v, \quad \frac{d^2T}{dx^2} = u''v, \quad \frac{dT}{dt} = uv'$$

Thus, equation (7.1) can be written as

$$u''v = \frac{1}{\kappa} uv'$$

$$\frac{u''}{u} = \frac{v'}{\kappa v} \tag{7.6}$$

The left hand side of equation (7.6) is a function of x only and the right hand side a function of t only. This two side of the equation can only be possible if both sides are equal to a constant, called the constant of separation. Letting the constant of separation be $-\lambda^2$, then equation (7.6) produces two ordinary differential equations which are

$$v' + \kappa\lambda^2 v = 0 \tag{7.7}$$

$$u'' + \lambda^2 u = 0 \tag{7.8}$$

A typical solution to equation (7.7) is

$$v(t) = A_1 e^{-\kappa\lambda^2 t} \tag{7.9}$$

and a typical solution to equation (7.8) is

$$u(x) = A_2 \cos(\lambda x) + A_3 \sin(\lambda x) \tag{7.10}$$

where A_1, A_2 and A_3 are arbitrary constants. Substituting equations (7.9) and (7.10) into equation (7.5) results to a typical solution for equation (7.1) given by

$$T(x,t) = \left(A_4 \cos(\lambda x) + A_5 \sin(\lambda x)\right) e^{-\kappa\lambda^2 t} \tag{7.11}$$

where A_4 and A_5 are arbitrary constants. Differentiating equation (7.11) results to

$$\frac{\partial T(x,t)}{\partial x} = \left(\lambda A_5 \cos(\lambda x) - \lambda A_4 \sin(\lambda x)\right) e^{-\kappa\lambda^2 t} \tag{7.12}$$

According Luikov [51], due to the symmetry of the problem given by equation (7.4),

$$\frac{\partial T(0,t)}{\partial x} = \lim_{x\to 0} \left(\lambda A_5 \cos(\lambda x) - \lambda A_4 \sin(\lambda x)\right) e^{-\kappa\lambda^2 t} = \lambda A_5 e^{-\kappa\lambda^2 t} = 0$$

Thus $A_5 = 0$ for $0 < t < \infty$. So the particular solution becomes

$$T(x,t) = A_4 \cos(\lambda x) e^{-\kappa\lambda^2 t} \tag{7.13}$$

Assuming that $T_L = 0$ and applying the boundary condition (equation (7.3)) then

$$T(L,t) = A_4 \cos(\lambda L) e^{-\kappa\lambda^2 t} = 0$$

resulting to

$$\cos(\lambda L) = 0 \tag{7.14}$$

where λ has infinite many real solutions. Thus from the principle of superposition, which states that the sum of a particular solution to a differential equation is a solution, the general solution can be given as

$$T(x,t) = \sum_{n=1}^{\infty} A_n \cos(\lambda_n x) e^{-\kappa\lambda_n^2 t} \tag{7.15}$$

If the initial condition is given by a function $f(x)$ then at time, $t = 0$

$$f(x) = \sum_{n=1}^{\infty} A_n \cos(\lambda_n x) \tag{7.16}$$

which is a Fourier series [51]. Multiplying both sides of equation (7.16) and integrating from 0 to L results to

$$\int_0^L f(\mathrm{x}) \cos(\lambda_m x)\, \mathrm{dx} = \sum_{n=1}^{\infty} A_n \int_0^L \cos(\lambda_n x) \cos(\lambda_m x) dx \tag{7.17}$$

which is the orthogonality property of the series. Since this is a Sturm-Lioville problem, then according to Ozisik [23]

$$\int_0^L \cos(\lambda_n x) \cos(\lambda_m x) dx = \begin{cases} 0 & \text{for } n \neq m \\ N(\lambda_n) & \text{for } n = m \end{cases}$$

Thus the constants A_n can be found from

$$A_n = \frac{1}{N(\lambda_n)} \int_0^L f(x) \cos(\lambda_n x) dx \tag{7.18}$$

According to Ozisik [23], for the boundary condition of $T_L = 0$

$$N(\lambda_n) = \frac{L}{2}$$

Thus,

$$A_n = \frac{2}{L}\int_0^L f(x)\cos(\lambda_n x)dx \tag{7.19}$$

From the initial condition given by equation (7.2), $f(x) = T_i$, then

$$A_n = \frac{2}{L}\int_0^L T_i \cos(\lambda_n x)dx = \frac{2T_i}{L\lambda_n}\sin(\lambda_n x)\Big|_0^L = \frac{2T_i}{L\lambda_n}\sin(\lambda_n L)$$

Therefore, the solution for this case becomes

$$T(x,t) = 2T_i\sum_{n=1}^{\infty}\frac{1}{L\lambda_n}\sin(\lambda_n L)\cos(\lambda_n x)e^{-\kappa\lambda_n^2 t} \tag{7.20}$$

Appendix B

B. Introduction to the Bessel functions

This section introduces the Bessel functions, especially those that are applied in the analysis of transient heat transfer on cylindrical components using exact analytical solutions.

I. Bessel's function of zero order

According to Bowman [25], the Bessel's function of zero order, which is denoted by $J_0(x)$, is a function that is defined by the infinite power series that is given by equation (8.1) as

$$J_0(x) = 1 - \frac{x^2}{2^2} + \frac{x^2}{2^2 \cdot 4^2} - \frac{x^6}{2^2 \cdot 4^2 \cdot 6^2} + \ldots \tag{8.1}$$

This series converges for all values of x. Since $J_0(x)$ is a power series, then all its derivatives are continuous for all values of x, regardless of whether x is real or complex [25]. Figure B-1 show a graphical representation of the Bessel's function of zero order.

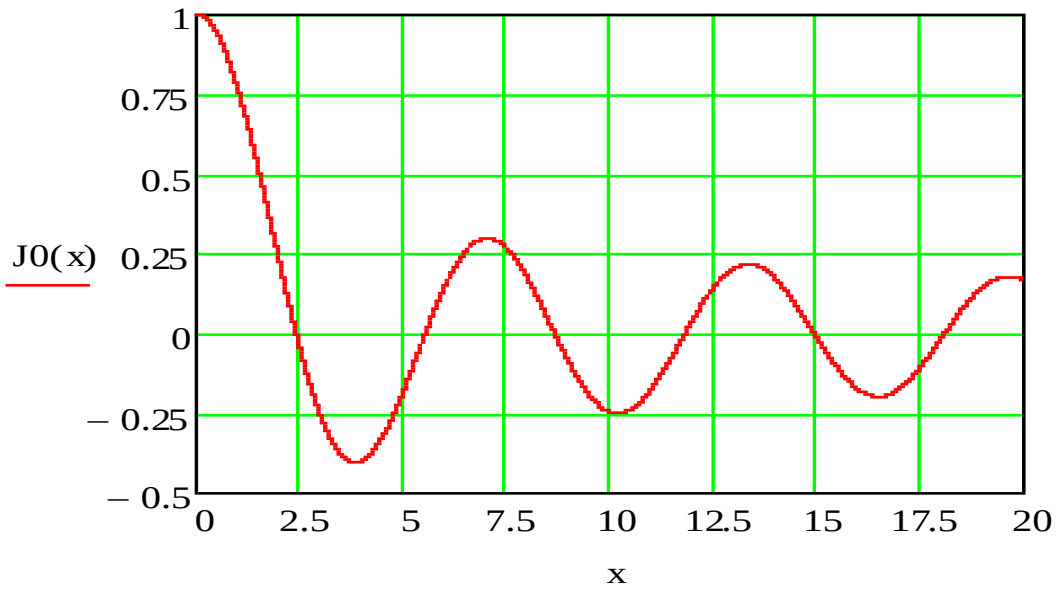

Figure B-1. Bessel's function of zero order.

II. Bessel's function of order n

A Bessel's function of order n, denoted by $J_n(x)$, is defined by an infinite power series shown in equation (8.2), if n is a positive integer. This series is also convergent for all values of x, whether x

is real or complex [25]. It can be seen from the series that if n is even, the function is even and if n is odd, the function is odd, as shown in Figure B-2.

$$J_n(x) = \frac{x^n}{2^n n!}\left(1 - \frac{x^2}{2\cdot 2n+2} + \frac{x^4}{2\cdot 4\cdot 2n+2\cdot 2n+4} - \ldots\right) \tag{8.2}$$

Of particular interest because of its application to physical problems is the Bessel's function of order one which is given by equation (8.3) as

$$J_1(x) = \frac{x}{2} - \frac{x^3}{2^2\cdot 4} + \frac{x^5}{2^2\cdot 4^2\cdot 6} - \frac{x^7}{2^2\cdot 4^2\cdot 6^2\cdot 8} + \ldots \tag{8.3}$$

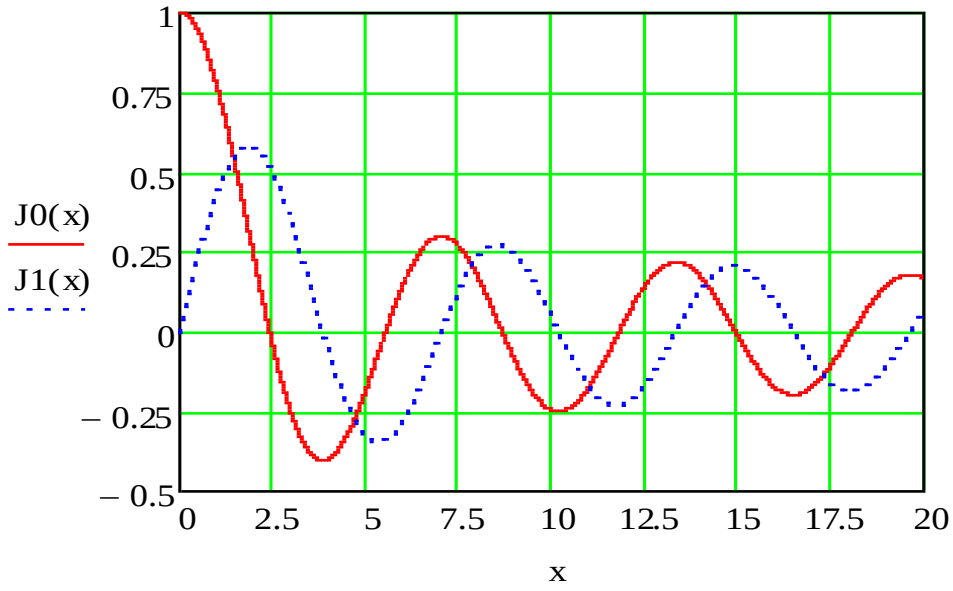

Figure B-2. Bessel's functions $J_0(x)$ and $J_1(x)$

III. Bessel's equation of zero order

According to Bowman [25], differentiating the series for the Bessel's function of the zero order, results into a series that is the negative of the Bessel's function of the first order [25], thus

$$\frac{dJ_0(x)}{dx} = -J_1(x) \tag{8.4}$$

Also, multiplying the series for $J_1(x)$ by x and differentiating it [25], it resulted on equation (8.5).

$$\frac{d}{dx}\left(xJ_1(x)\right) = xJ_0(x) \tag{8.5}$$

Using equation (8.4), equation (8.5) can be rewritten as

$$\frac{d}{dx}\left(x\frac{dJ_0(x)}{dx}\right)+xJ_0(x)=0 \tag{8.6}$$

which can also be written as

$$x\frac{d^2J_0(x)}{dx^2}+\frac{dJ_0(x)}{dx}+xJ_0(x)=0 \tag{8.7}$$

Equation (8.7) is a second order linear differential equation. Letting $y=J_0(x),$ then equation (8.7) can be written as

$$\frac{d^2y}{dx^2}+\frac{1}{x}\frac{dy}{dx}+y=0 \tag{8.8}$$

Equation (8.8) is known as the *Bessel's equation of zero order.*

IV. Bessel function of the second kind of zero order

There is another solution to the Bessel's equation which is not a numerical multiple of the Bessel Function of zero order, $J_0(x),$ but derived from it. This solution is called a *Bessel function of second kind* [25]. Its derivation is presented in Bowman chapter 1 [25].

Here, the Bessel function of second kind, also known as *Neumann's Bessel function of the second kind of order zero,* denoted as $Y_0(x)$ is given because of its application to physical problems. This function is given by equation (8.9) as

$$Y_0(x)=J_0(x)\log(x)+\frac{x^2}{4}-\frac{3x^4}{128}+... \tag{8.9}$$

Figure B-3 compares the graphs of $J_0(x)$ and $Y_0(x)$

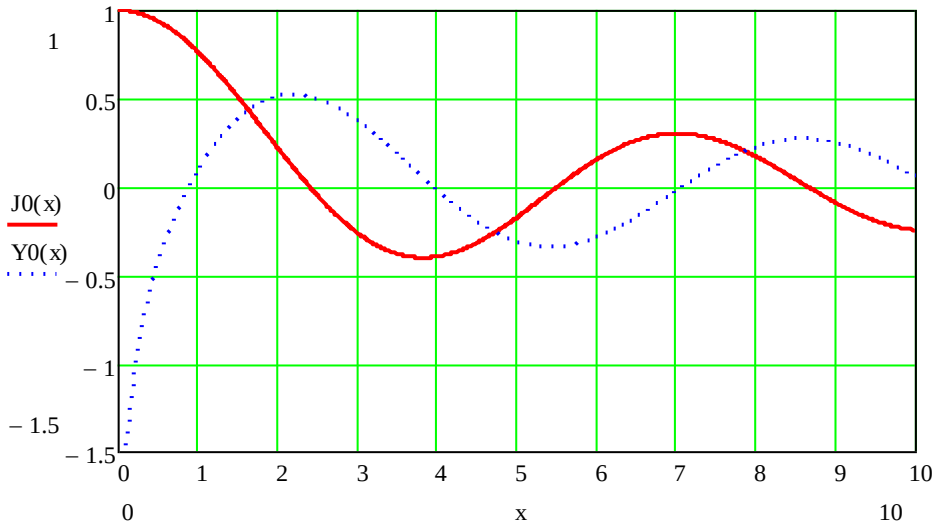

Figure B-3. Graphs of the Bessel function $J_0(x)$ and $Y_0(x)$.

V. General solution for the Bessel's equation of zero order

However as mentioned above, $J_0(x)$ and $Y_0(x)$ are independent solutions for the Bessel's equation of zero order given by equation (8.10) as

$$\frac{d^2y}{dx^2}+\frac{1}{x}\frac{dy}{dx}+y=0 \tag{8.10}$$

Thus a general solution to the equation can be written as

$$y=AJ_0(x)+BY_0(x) \tag{8.11}$$

where A and B are arbitrary constants and $x>0$ for $Y_0(x)$ to be real.

On the other hand, if x is replaced by kx, where k is a constant [25], then equation (8.8) becomes

$$\frac{1}{k^2}\frac{d^2y}{dx^2}+\frac{1}{kx}\frac{dy}{dx}+y=0 \tag{8.12}$$

Multiplying by k^2 throughout result to

$$\frac{d^2y}{dx^2}+\frac{1}{x}\frac{dy}{dx}+k^2y=0 \tag{8.13}$$

The general solutions for equation (8.13) is given by

$$y=AJ_0(kx)+BY_0(kx) \tag{8.14}$$

subject to $k>0$ for $Y_0(kx)$ to be real when $x>0$.

Appendix C

C. Exact solution for an infinitely long cylindrical rod

For an infinitely long cylindrical rod, the heat transfer along the length is negligible compared to the radial flow. Thus the temperature can be represented as a function of the radius, r and the time t only, provided that temperature variation with the angle theta, θ along its radius is negligible as well.

Thus the conduction heat equation is given by [24] in cylindrical coordinates as follows:

$$\frac{\partial T}{\partial t} = \kappa\left(\frac{\partial^2 T}{\partial r^2} + \frac{1}{r}\frac{\partial T}{\partial r}\right) \tag{9.1}$$

for a range of radius, as $0 < r < a$ and $\kappa = k/\rho c$.

In order to derive a specific solution from the generic heat equation given by equation (9.1), initial and boundary conditions for the specific scenario has to be imposed in the derivation. Consider the initial and boundary conditions that are given by

$$T(r,0) = f(r), \quad t = 0 \quad \text{initial condition} \tag{9.2}$$

$$T(a,t) = 0, \quad t > 0 \qquad \text{boundary condition} \tag{9.3}$$

In solving a differential equation like equation (9.1), the method of separation of variables is useful [22, 53]. Let,

$$T(r,t) = u(r)\cdot v(t) \tag{9.4}$$

where u is a function of r only and v a function of t only. Differentiating equation (9.4) leads to

$$\frac{\partial T}{\partial t} = u \cdot v' \tag{9.5}$$

$$\frac{\partial T}{\partial r} = v \cdot u' \tag{9.6}$$

$$\frac{\partial^2 T}{\partial r^2} = v \cdot u'' \tag{9.7}$$

Substituting equations (9.5), (9.6) and (9.7) into (9.1) results into

$$uv' = \kappa\left(vu' + \frac{1}{r}vu''\right) \tag{9.8}$$

which can be rearranged to

$$\frac{v'}{v\kappa} = \frac{1}{u}\left(u'' + \frac{1}{r}u'\right) \tag{9.9}$$

From equation (9.9), it can be seen that the left hand side is a function of t only and the other a function of r only. Since r and t are independent variables, such an equation is impossible unless each side is equal to the same constant [25]. Putting each side of equation (9.9) equal to a constant, μ, it result to the following equations:

$$\frac{v'}{vk} = \mu \tag{9.10}$$

and

$$\frac{1}{\mu}\left(u'' + \frac{1}{r}u'\right) = \mu \tag{9.11}$$

Considering equation (9.10) and rearranging it, it result to

$$v' - \mu vk = 0 \tag{9.12}$$

which is an ordinary differential equation (ODE). This ODE has a solution of the form

$$v = A_b e^{\mu\kappa t} \tag{9.13}$$

where A_b is an arbitrary constant. However, accounting for the condition that $T(r,t) \to 0$ as $t \to 0$, it can be seen that that is only possible if μ is negative. Thus put $\mu = -\lambda^2$, which gives

$$v = A_b e^{-\lambda^2\kappa t} \tag{9.14}$$

After rearranging equation (9.11) becomes

$$u'' + \frac{1}{r}u' + \lambda^2 u = 0 \tag{9.15}$$

which is a Bessel's equation of order zero, as seen in Appendix B.

Deducing from equation (8.13) and (8.14) the only solution to equation (9.15) that has a physical meaning since the radius range includes $r = 0$, is given by [25, 54] as

$$u(r) = A_c J_0(\lambda r) \tag{9.16}$$

where A_c is an arbitrary constant.

Since equation (9.14), is never zero at any particular point, then applying the condition given by equation (9.3), implies that

$$u(a) = 0 \tag{9.17}$$

which requires that

$$J_0(\lambda a) = 0 \tag{9.18}$$

which further defines the eigenvalues and eigenfunction for this problem. Thus the eigenvalues are given as the roots of

$$J_0(\mathrm{a}\,\lambda_n) = 0 \tag{9.19}$$

Deducing from the series of the Bessel's function of zero order, given by equation (8.1) it can be stated that equation (9.19) has no complex or repeated roots. Instead, it has an infinite number of real positive roots [24],which can be written as

$$\lambda_1, \lambda_2, \lambda_3, \lambda_4, \ldots$$

Substituting equations (9.14) and (9.16) into (9.4) gives

$$T_n(r,t) = u_n(r) \cdot v(t) = A_n J_0(\lambda_n r) e^{-\lambda_n^2 \kappa t} \tag{9.20}$$

where $A_n = A_b A_c$ and $n = 1, 2, 3, \ldots$

Equation (9.20) is a particular solution for equation (9.1). Since the equation is composed of two linear differential equations, mathematically for a linear equation the sum of the particular solutions is still a solution. Thus,

$$T(r,t) = \sum_{n=1}^{\infty} A_n J_0(\lambda_n r) e^{-\lambda_n^2 \kappa t} \tag{9.21}$$

This solution also satisfy the condition for $f(r)$ being an expanded series [24] given by

$$f(r) = A_1 J_0(\lambda_1 r) + A_2 J_0(\lambda_2 r) + A_3 J_0(\lambda_3 r) + \ldots \tag{9.22}$$

Subjecting the initial condition given by equation (9.2) to equation (9.21) gives

$$T(r,0) = f(r) = \sum_{n=1}^{\infty} A_n J_0(\lambda_n r) \tag{9.23}$$

which is a Fourier-Bessel series representation of the series $f(r)$ given by equation (9.22) [54]. Thus, the orthogonality property of eigenfunctions apply [54]. However, before applying the orthogonality property, some integrals that will be used with the property. These integrals are derived, first by multiply both sides of equation (9.22) by $rJ_0(\lambda_n r),$ and integrating the resulting equation from 0 to a, which result to

$$\int_0^a rJ_0(\lambda_m r) J_0(\lambda_n r) dr = 0 \quad \text{for } m \neq n \tag{9.24}$$

and

$$\int_0^a r\left(J_0(\lambda_n r)\right)^2 dr = \frac{1}{2}a^2\left(J_0'(a\lambda_n)\right)^2 = \frac{1}{2}a^2 J_1^2(a\lambda_n) \quad \text{for } m \neq n \tag{9.25}$$

Noticing that $J_0'(x) = -J_1(x)$ as given in appendix B.

Now applying the orthogonality property of eigenfunctions with the use of equations (9.19), (9.24) and (9.25), then

$$\begin{aligned}\int_0^a rJ_0(\lambda_m r) f(r) dr &= \sum_{n=1}^{\infty} A_n \int_0^a rJ_0(\lambda_m r) J_0(\lambda_n r) dr \\ &= A_n \int_0^a rJ_0^2(\lambda_m r) dr \\ &= \frac{a^2 A_m}{2}\left(J_0^2(\lambda_m a) + J_1^2(\lambda_m a)\right) \\ &= \frac{a^2 A_m}{2} J_1^2(\lambda_m a)\end{aligned}$$

Therefore,

$$A_m = \frac{2}{a^2 J_1^2(a\lambda_n)} \int_0^a rf(r) J_0(\lambda_n r) dr \tag{9.26}$$

Rewriting equation (9.21) by including equation (9.26) it becomes

$$T(r,t) = \frac{2}{a^2} \sum_{n=1}^{\infty} e^{-\lambda_n^2 \kappa t} \frac{J_0(\lambda_n r)}{J_1^2(a\lambda_n)} \int_0^a rf(r) J_0(\lambda_n r) dr \tag{9.27}$$

The solution is completed by considering different cases of the initial temperature condition $f(r)$.

Case 1:

If the initial temperature is constant, T_i, then

$$f(r) = T_i \tag{9.28}$$

So the integral on equation (9.27), becomes

$$\int_0^a rT_i J_0(\lambda_n r)dr = \frac{T_i r J_1(\lambda_n r)}{\lambda_n} \tag{9.29}$$

from [24], given that

$$\int_0^r r^{n+1} J_n(\lambda_n r)dr = \frac{1}{\lambda} r^{n+1} J_{n+1}(\lambda r) \tag{9.30}$$

Thus from equation (9.27) and (9.29) the solution becomes

$$T(r,t) = \frac{2T_i}{a} \sum_{n=1}^{\infty} \frac{J_0(\lambda_n r)}{\lambda_n J_1(a\lambda_n)} e^{-\lambda_n^2 \kappa t} \tag{9.31}$$

Case 2:

This case considers the scenario where the initial temperature is zero, $f(r) = 0$, and the surface is maintained at T_s for $t > 0$. This conditions are an opposite of the first case above, thus the solution is obtained by subtracting equation (9.31), from T_s [24] as follows:

$$T(r,t) = T_s - \frac{2T_s}{a} \sum_{n=1}^{\infty} \frac{J_0(\lambda_n r)}{\lambda_n J_1(a\lambda_n)} e^{-\lambda_n^2 \kappa t} \tag{9.32}$$

If the above equation is evaluated using dimensionless variables, one way would be to let

$$\beta_n = a\lambda_n \quad \text{and} \quad \tau = \frac{\kappa t}{a^2}$$

For $\beta_n, n = 1, 2, 3, \ldots$ roots of

$$J_0(\beta) = 0 \tag{9.33}$$

Appendix D

D. Numerical analysis of heat transfer problems

In the previous sections analytical solutions to simplified transient heat transfer problems with simplified geometry were presented. These solutions cannot be extended to complex geometries and boundary conditions. Thus, numerical methods to heat transfer problems are developed. Analytical solutions are presented as temperature distribution expressions, yet numerical solutions give results at discrete points. Also, the numerical solution involves the following stages: firstly, the discretisation of the computational domain, secondly the discretisation of the governing equations, and lastly, solving the algebraic equations [32].

I. A tube or rod heat transfer problem

1. Discretisation of the computational domain

The discretisation of a computational domain involves dividing the domain into small control volumes [32, 33]. Figure D-1 shows the discretisation of the computational domain into control volumes for a two – dimensional axially symmetric cylinder. These control volumes cover the whole body of the solid material. The dashed lines represent the faces of the subdomains and the physical properties of each cell are defined on the grid points [32].

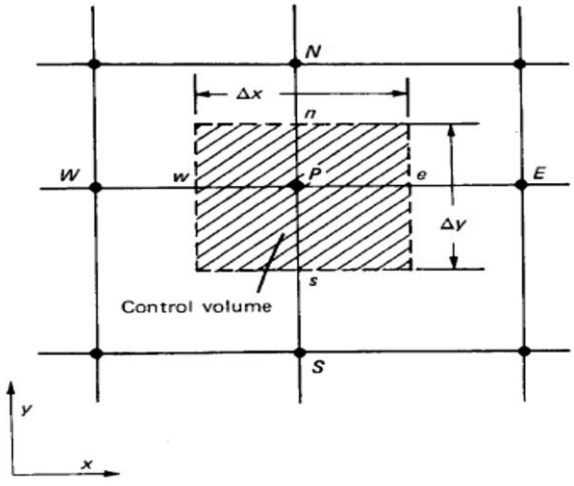

Figure D-1. Computational grid and control volume definition for a two - dimensional axially symmetric approximation for a cylinder [33].

2. Discretisation of the governing equations

The methods that are used to discretise the governing partial differential equations either use a local or point-wise representation of the equation. These methods include the finite difference method (FDM), finite element method (FEM) and the finite volume method (FVM) amongst others. The FVM involves the integration of the governing partial differential equation over the control volume which guarantees integral conservation of quantities such a mass, energy and momentum over that control volume [32, 33]. In this project the FVM is preferred.

From chapter 2, the unsteady energy balance for the infinitesimal cylindrical control volume with volume $rdrd\theta dz$ can be written as

$$\rho c\frac{\partial T}{\partial t}rdrd\theta dz=-\frac{\partial q_r}{\partial r}dr-\frac{\partial q_\theta}{\partial \theta}d\theta-\frac{\partial q_z}{\partial z}dz+\dot{q}rdrd\theta dz \tag{10.1}$$

with q_r, q_θ and q_z being the heat transfer rates [W] in the respective directions and $\dot{q}$ being the volumetric heat source [W/m^3].

If the heat transfer rates are written in term of heat fluxes, i.e. heat transfer rate per unit area, then equation (10.1) becomes

$$\rho c\frac{\partial T}{\partial t}rdrd\theta dz=-\frac{\partial}{\partial r}\left(\varphi_r rd\theta dz\right)dr-\frac{\partial}{\partial \theta}\left(\varphi_\theta drdz\right)d\theta-\frac{\partial}{\partial z}\left(\varphi_z rdrd\theta\right)dz+\dot{q}rdrd\theta dz \tag{10.2}$$

with $\varphi_r, \varphi_\theta$ and φ_z the heat fluxes [W/m^2] in the respective coordinates directions.

This unsteady energy balance equation can be written in a unit volume basis through dividing equation (10.2) by $rdrd\theta dz$ to get the unsteady heat transfer partial differential equation

$$\rho c\frac{\partial T}{\partial t}=-\frac{1}{r}\frac{\partial}{\partial r}\left(r\varphi_r\right)-\frac{\partial \varphi_\theta}{\partial \theta}-\frac{\partial \varphi_z}{\partial z}+\dot{q} \tag{10.3}$$

For a two dimensional axially symmetric control volume $\frac{\partial T}{\partial \theta}=0$ and for no heat generation $\dot{q}=0,$ therefore equation (10.3) becomes

$$\rho c\frac{\partial T}{\partial t}=-\frac{1}{r}\frac{\partial}{\partial r}\left(r\varphi_r\right)-\frac{\partial \varphi_z}{\partial z} \tag{10.4}$$

Applying the FVM will result in a set of simultaneous algebraic equation that are solved in order to get the temperatures at the nodes in the computational grid shown in Figure D-1. The FVM entails the

integration of the partial differential equation over the control volume defined around a grid point. Thus integrating equation (10.4) leads to

$$\int_{z_s}^{z_n}\int_0^{2\pi}\int_{r_w}^{r_e}\rho c\frac{\partial T_P}{\partial t}rdrd\theta dz=-\int_{z_s}^{z_n}\int_0^{2\pi}\int_{r_w}^{r_e}\frac{\partial}{\partial r}(r\varphi_r)drd\theta dz-\int_{z_s}^{z_n}\int_0^{2\pi}\int_{r_w}^{r_e}\frac{\partial\varphi_z}{\partial z}rdrd\theta dz \qquad (10.5)$$

Assuming that the properties of the solid material are homogeneous within the given control volume and constant over the duration of the time step, then equation (10.5) can be evaluated to be

$$2\pi(z_n-z_s)\left(\frac{r_e^2-r_w^2}{2}\right)\rho c\frac{\partial T_P}{\partial t}=-2\pi(z_n-z_s)\int_{r_w}^{r_e}\frac{\partial}{\partial r}(r\varphi_r)dr-2\pi\left(\frac{r_e^2-r_w^2}{2}\right)\int_{z_s}^{z_n}\frac{\partial\varphi_z}{\partial z}dz \qquad (10.6)$$

Simplifying equation (10.6) and writing it on a unit radian basis by dividing with 2π radians, leads to

$$\rho c\frac{\partial T_P}{\partial t}=-\left(\frac{2}{r_e^2-r_w^2}\right)\int_{r_w}^{r_e}\frac{\partial}{\partial r}(r\varphi_r)dr-\left(\frac{1}{z_n-z_s}\right)\int_{z_s}^{z_n}\frac{\partial\varphi_z}{\partial z}dz \qquad (10.7)$$

Applying the fundamental theorem of calculus to the integrals in equation (10.7) leads to

$$\rho c\frac{\partial T_P}{\partial t}=-\left(\frac{2}{r_e^2-r_w^2}\right)(r_e\varphi_{re}-r_w\varphi_{rw})-\left(\frac{1}{z_n-z_s}\right)(\varphi_{zn}-\varphi_{zs}) \qquad (10.8)$$

However, for further evaluation the heat fluxes over the control volume boundaries at e, w, n and s must be known.

2.1. Heat fluxes

Different heat fluxes can be present at the boundaries of the control volume. These includes conduction and/or convection and/or specific value heat fluxes.

2.1.1. Conduction heat transfer

In chapter 2, the incremental heat transfer for conduction in three directions in cylindrical coordinates was given as

$$q_r=-krd\theta dz\frac{\partial T}{\partial r},\quad q_\theta=-kdrdz\frac{1}{r}\frac{\partial T}{\partial\theta}\quad\text{and}\quad q_z=-krdrd\theta\frac{\partial T}{\partial z} \qquad (10.9)$$

Thus, the conduction incremental heat fluxes in the positive cylindrical coordinates direction can be given as

$$\varphi_r=-k\frac{\partial T}{\partial r},\quad \varphi_\theta=-k\frac{1}{r}\frac{\partial T}{\partial\theta}\quad\text{and}\quad \varphi_z=-k\frac{\partial T}{\partial z} \qquad (10.10)$$

2.1.2. Convection heat transfer

The incremental heat transfer for convection in the positive cylindrical coordinates' direction is given by

$$q_r = -hrd\theta dz\Delta T_{fs}, \quad q_\theta = -hdrdz\Delta T_{fs} \quad \text{and} \quad q_z = -hrdrd\theta\Delta T_{fs} \tag{10.11}$$

h is the local convective heat transfer coefficient and ΔT_{fs} the temperature difference between the fluid and the solid surface across the boundary.

Thus, the convective incremental heat fluxes in the positive cylindrical coordinates' direction can be given as

$$q_r = -h\Delta T_{fs}, \quad q_\theta = -h\Delta T_{fs} \quad \text{and} \quad q_z = -h\Delta T_{fs} \tag{10.12}$$

3. Algebraic equations

Since the heat fluxes have been determined, the algebraic equations for the different grid points and different types of boundary conditions can be derived from equation (10.8).

3.1. Internal body nodes

A node surrounded by four nodes within the solid material will have conduction heat fluxes across the four boundaries of the control volume. Thus equation (10.8) becomes

$$\rho c\frac{\partial T_P}{\partial t} = \left(\frac{2}{r_e^2 - r_w^2}\right)\left(r_e k_e\left(\frac{\partial T}{\partial r}\right)_e - r_w k_w\left(\frac{\partial T}{\partial r}\right)_w\right) + \left(\frac{1}{z_n - z_s}\right)\left(k_n\left(\frac{\partial T}{\partial z}\right)_n - k_s\left(\frac{\partial T}{\partial z}\right)_s\right) \tag{10.13}$$

The temperature differentials at the boundaries maybe approximated via the discrete temperature gradients expressed in terms of the nodal temperature. Assuming that the thermal conductivity of the material is constant, then equation (10.13) maybe written as

$$\frac{\partial T_P}{\partial t} \approx \frac{k}{\rho c}\left[\begin{array}{l}\left(\frac{2}{r_e^2 - r_w^2}\right)\left[r_e\left(\frac{T_E - T_P}{r_E - r_P}\right) - r_w\left(\frac{T_P - T_W}{r_E - r_W}\right)\right] \\ +\left(\frac{1}{z_n - z_s}\right)\left[\left(\frac{T_N - T_P}{z_N - z_P}\right) - \left(\frac{T_P - T_S}{z_P - z_S}\right)\right]\end{array}\right] \tag{10.14}$$

Rearranging equation (10.14) leads to

$$\frac{\partial T_P}{\partial t} \approx \frac{k}{\rho c}\left(\begin{array}{l}\left(\frac{2}{r_e^2 - r_w^2}\right)\left(\frac{r_e}{r_E - r_P}\right)T_E + \left(\frac{2}{r_e^2 - r_w^2}\right)\left(\frac{r_w}{r_P - r_W}\right)T_W \\ \\ +\left(\frac{1}{z_n - z_s}\right)\left(\frac{1}{z_N - z_P}\right)T_N + \left(\frac{1}{z_n - z_s}\right)\left(\frac{1}{z_P - z_S}\right)T_S \\ \\ -\left(\begin{array}{l}\left(\frac{2}{r_e^2 - r_w^2}\right)\left(\left(\frac{r_e}{r_E - r_P}\right)+\left(\frac{r_w}{r_P - r_W}\right)\right) \\ \\ +\left(\frac{1}{z_n - z_s}\right)\left(\left(\frac{1}{z_N - z_P}\right)+\left(\frac{1}{z_P - z_S}\right)\right)\end{array}\right)T_P\end{array}\right) \tag{10.15}$$

For simplicity, let

$$\frac{\partial T_P}{\partial t} \approx a_E T_E + a_W T_W + a_N T_N + a_S T_S - a_P T_P \tag{10.16}$$

with

$$\begin{aligned} a_E &= \frac{2\kappa r_e}{\left(r_e^2 - r_w^2\right)\left(r_E - r_P\right)} \\ a_W &= \frac{2\kappa r_w}{\left(r_e^2 - r_w^2\right)\left(r_P - r_W\right)} \\ a_N &= \frac{\kappa}{\left(z_n - z_s\right)\left(z_N - z_P\right)} \\ a_S &= \frac{\kappa}{\left(z_n - z_s\right)\left(z_P - z_S\right)} \\ a_P &= a_E + a_W + a_N + a_S \end{aligned}$$

and with $\kappa = \frac{k}{\rho c}$ the thermal diffusivity of the material [m^2/s].

For a one-dimensional, infinitely long cylindrical rod or infinitely long tube, $a_N = 0$ and $a_S = 0$. In addition, for the infinitely long cylindrical rod the radius at node position r_P as well as the radius of the western node r_W would be zero.

3.2. Fixed temperature boundary nodes

If the inner and outer surface temperatures for a tube are known (boundary condition of the first kind), the known temperatures are simply assigned to the inner and outer node temperatures. In addition, these temperatures will be the same for all time steps [23, 28, 32]. Thus,

$$T_0 = T_a, \qquad T_M = T_b \tag{10.17}$$

3.3. Convection heat transfer on the inner surface

On the other hand, if the inner surface of the tube is exposed to a convection heat transfer with the surrounding fluid, then equation (10.8) becomes

$$\rho c \frac{\partial T_P}{\partial t} = \left(\frac{2}{r_e^2 - r_w^2}\right)\left(r_e k_e \left(\frac{\partial T}{\partial r}\right)_e - r_w h_w \left(\Delta T_{fs}\right)_w\right) + \left(\frac{1}{z_n - z_s}\right)\left(k_n \left(\frac{\partial T}{\partial z}\right)_n - k_s \left(\frac{\partial T}{\partial z}\right)_s\right) \tag{10.18}$$

Approximating the temperature differentials on the boundaries using the discrete temperature gradients based on the temperature of the surrounding nodes of the solid and the fluid stream leads to

$$\rho c \frac{\partial T_P}{\partial t} \approx \left[\begin{array}{l} \left(\frac{2}{r_e^2 - r_w^2}\right)\left[r_e k_e \left(\frac{T_E - T_P}{r_E - r_P}\right) - r_w h_w \left(T_P - T_{\infty,W}\right)\right] \\ + \left(\frac{1}{z_n - z_s}\right)\left[k_n \left(\frac{T_N - T_P}{z_N - z_P}\right) - k_s \left(\frac{T_P - T_S}{z_P - z_S}\right)\right] \end{array}\right] \tag{10.19}$$

Assuming the thermal conductivity of the material is constant and rearranging results to

$$\frac{\partial T_P}{\partial t} \approx \frac{k}{\rho c}\left(\begin{array}{l} \left(\frac{2}{r_e^2 - r_w^2}\right)\left(\frac{r_e}{r_E - r_P}\right) T_E + \left(\frac{2}{r_e^2 - r_w^2}\right)\left(\frac{r_w h_w}{k}\right) T_{\infty,W} \\ + \left(\frac{1}{z_n - z_s}\right)\left(\frac{1}{z_N - z_P}\right) T_N + \left(\frac{1}{z_n - z_s}\right)\left(\frac{1}{z_P - z_S}\right) T_S \\ - \left(\begin{array}{l} \left(\frac{2}{r_e^2 - r_w^2}\right)\left(\left(\frac{r_e}{r_E - r_P}\right) + \left(\frac{r_w}{r_P - r_W}\right)\right) \\ + \left(\frac{1}{z_n - z_s}\right)\left(\left(\frac{1}{z_N - z_P}\right) + \left(\frac{1}{z_P - z_S}\right)\right) \end{array}\right) T_P \end{array}\right) \tag{10.20}$$

For simplicity, let

$$\frac{\partial T_P}{\partial t} \approx a_E T_E + a_W T_W + a_N T_N + a_S T_S - a_P T_P \tag{10.21}$$

with

$$a_E = \frac{2\kappa r_e}{\left(r_e^2 - r_w^2\right)\left(r_E - r_P\right)}$$
$$a_W = \frac{2\kappa Bi_w}{\left(r_e^2 - r_w^2\right)}$$
$$a_N = \frac{\kappa}{\left(z_n - z_s\right)\left(z_N - z_P\right)}$$
$$a_S = \frac{\kappa}{\left(z_n - z_s\right)\left(z_P - z_S\right)}$$
$$a_P = a_E + a_W + a_N + a_S$$

and $Bi = \frac{hr}{k}$ the local Biot number.

3.4. Convection heat transfer on the outer surface

If the convection heat flux is now applied on the outer boundary, the same manipulation of equation (10.8) as in the subsection above for a convection heat flux at the inner boundary. The simplified resulting equation is given by

$$\frac{\partial T_P}{\partial t} \approx a_E T_E + a_W T_W + a_N T_N + a_S T_S - a_P T_P \tag{10.22}$$

with

$$a_E = \frac{2\kappa Bi_e}{\left(r_e^2 - r_w^2\right)}$$
$$a_W = \frac{2\kappa r_w}{\left(r_e^2 - r_w^2\right)\left(r_P - r_W\right)}$$
$$a_N = \frac{\kappa}{\left(z_n - z_s\right)\left(z_N - z_P\right)}$$
$$a_S = \frac{\kappa}{\left(z_n - z_s\right)\left(z_P - z_S\right)}$$
$$a_P = a_E + a_W + a_N + a_S$$

II. One dimensional heat conduction

As mentioned above for an infinitely long tube, the heat conduction is one dimensional hence there is no variation with the z axis. Since numerical solutions are generated using a computer, the control volumes has to be generated using a discretised mesh of nodes in radius r_j with $j = 0,1,\ldots,\mathrm{M}$ and a spacing size Δr as shown on Figure D-2b.

Thus from Figure D-2, equation (10.16) can be written as

$$\frac{\partial T_j}{\partial t} \approx a_{j+1}T_{j+1} + a_{j-1}T_{j-1} - a_j T_j \tag{10.23}$$

with

$$a_{j+1} = a_E \quad a_{j-1} = a_W \quad and \; a_j = a_P$$

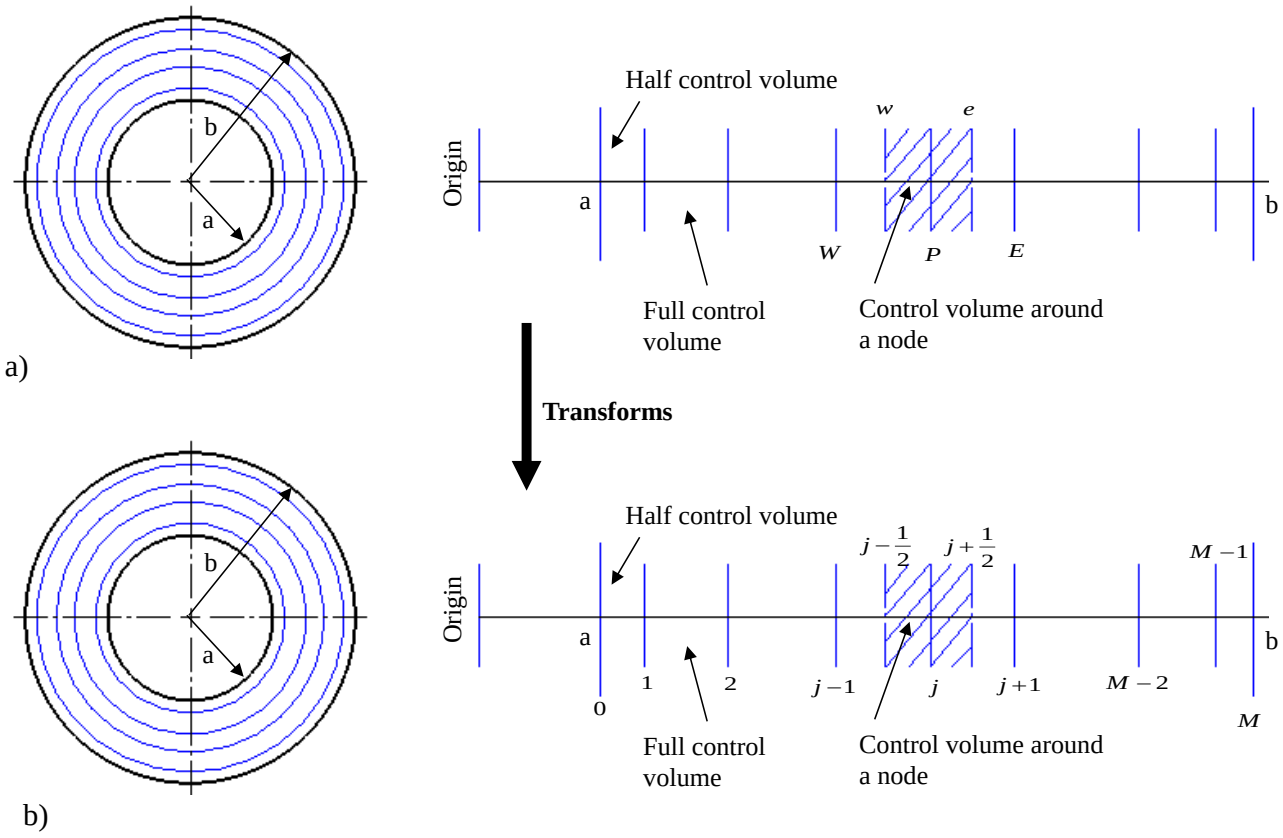

Figure D-2. One dimensional computation domain and control volume a) General setup b) computational domain with defined grid points for the whole domain.

III. Time-wise integration

Since equation (10.16) varies with time, it can be defined by the time dependent source term given as

$$S_P(t) = a_E T_E + a_W T_W + a_N T_N + a_S T_S - a_P T_P \tag{10.24}$$

Integrating equation (10.24) over a discrete time step given by Δt such that

$$\int_t^{t+\Delta t} \frac{\partial T_P}{\partial t} dt \approx \int_t^{t+\Delta t} S_P(t)\, dt \tag{10.25}$$

The source term is an unknown function that varies with time. However, it can be approximated as a weighted average of the source term between the old time step and the new time step. Thus, after integration it result to

$$T_P \approx T_P^0 + \left(\alpha S_P + (1-\alpha) S_P^0\right)\Delta t \tag{10.26}$$

If the time computational domain is discretised to a mesh of nodes in time t_i with $i = 0,1,2,\ldots$ and a spacing size of Δt. And if the time *i* domain and the radius *j* domain are used equation(10.26), it becomes

$$T_j^{i+1} \approx T_j^i + \left(\alpha S_j^{i+1} + (1-\alpha) S_j^i\right)\Delta t \tag{10.27}$$

If the constant α is selected to be zero $(\alpha = 0)$, then the solution will use the known temperatures of the previous time step, resulting to an *explicit solution*. If on the other hand $(\alpha = 1)$, then the solution will be based on the unknown temperature at the new time, which requires iterations in order to find the solution. That solution is called a *fully implicit solution*. However, if $(0 < \alpha < 1)$, then the solution will consist of both known and unknown temperatures as shown in equation (10.27), hence referred to as a *semi-implicit solution*. A special case of the semi-implicit solution for $\alpha = 0.5$, is the average between the new and old temperatures and it is called the *Crank-Nicholson solution*.